THE COMPARISON OF MICROSTRUCTURE AND MECHANICAL
PROPERTIES OF A LOW CARBON BAINITIC FORGING STEEL AFTER
ISOTHERMAL TRANSFORMATION AND DIRECT COOLING

A THESIS SUBMITTED TO
THE GRADUATE SCHOOL OF NATURAL AND APPLIED SCIENCES
OF
MIDDLE EAST TECHNICAL UNIVERSITY

BY

MUHAMMED MUSTAFA BALCILAR

IN PARTIAL FULFILLMENT OF THE REQUIREMENTS
FOR
THE DEGREE OF MASTER OF SCIENCE
IN
METALLURGICAL AND MATERIALS ENGINEERING

APRIL 2022

Approval of the thesis:

THE COMPARISON OF MICROSTRUCTURE AND MECHANICAL PROPERTIES OF A LOW CARBON BAINITIC FORGING STEEL AFTER ISOTHERMAL TRANSFORMATION AND DIRECT COOLING

submitted by **MUHAMMED MUSTAFA BALCILAR** in partial fulfillment of the requirements for the degree of **Master of Science** in **Metallurgical and Materials Engineering, Middle East Technical University** by,

Prof. Dr. Halil Kalıpçılar
Dean, Graduate School of **Natural and Applied Sciences**   _____

Prof. Dr. Cemil Hakan Gür
Head of the Department, **Met. and Mat. Eng.**   _____

Prof. Dr. Bilgehan Ögel
Supervisor, **Met. and Mat. Eng., METU**   _____

Examining Committee Members:

Prof. Dr. Rıza Gürbüz
Metallurgical and Materials Eng, METU   _____

Prof. Dr. Bilgehan Ögel
Metallurgical and Materials Eng, METU   _____

Prof. Dr. Ender Keskinkılıç
Metallurgical and Materials Eng, Atılım University   _____

Assist. Prof. Dr. Eda Aydoğan Güngör
Metallurgical and Materials Eng., METU.   _____

Assist. Prof. Dr. Irmak Sargın
Metallurgical and Materials Eng., METU   _____

Date: 27.04.2022

I hereby declare that all information in this document has been obtained and presented in accordance with academic rules and ethical conduct. I also declare that, as required by these rules and conduct, I have fully cited and referenced all material and results that are not original to this work.

Name Last name : Muhammed Mustafa Balcılar

Signature :

ABSTRACT

THE COMPARISON OF MICROSTRUCTURE AND MECHANICAL PROPERTIES OF A LOW CARBON BAINITIC FORGING STEEL AFTER ISOTHERMAL TRANSFORMATION AND DIRECT COOLING

Balcılar, Muhammed Mustafa
Master of Science, Metallurgical and Materials Engineering
Supervisor : Prof. Dr. Bilgehan Ögel

April 2022, 137 pages

Bainitic forging steels have emerged in recent decades as an alternative to Quench and Temper steels due to their low cost and energy requirements and optimum combination of strength, ductility, and toughness. Although effect of continuous cooling on bainitic forging steels have been studied, the effect of isothermal transformation on microstructure and mechanical properties of microalloyed bainitic forging steels is an open field. A low carbon microalloyed bainitic forging steel is examined in this study, with a composition of 0.2C-1.3Si-1.5Mn-1.45(Cr+Mo), microalloyed with V-Ti-Nb. The steel is isothermally transformed at various temperatures and continuously cooled and compared in terms of microstructural features by optical microscopy and scanning electron microscopy, phase analysis by XRD measurements, and mechanical properties. Effect of isothermal holding time is also studied at each isothermal transformation temperature, varying from 15 minutes to 30 hours. Isothermal transformation just above Ms gives the maximum amount of bainite with the smallest lath thickness, which is proven by microstructural characterization. Retained austenite measurements demonstrated that in all samples,

similar amounts of austenite remain in the system. Hardness measurements show that bainitic samples are similar in terms of hardness, but the specimen transformed at the lowest temperature gave the hardest microstructure ranging from 391-420 HV. The bainitic microstructure hardness values for other specimens range from 378HV to 421HV. The isothermal transformation just above the M_s temperature has given the most ductile and toughest steel, with an elongation of 17% and a UTS of 1264 MPa. The results show that isothermally transformed specimens have superior mechanical properties and isothermal transformation heat treatment routes should be designed to obtain materials with the best performance.

ÖZ

DÜŞÜK KARBONLU BEYNİTİK DÖVME ÇELİĞİNİN İZOTERMAL DÖNÜŞÜM VE DOĞRUDAN SOĞUTMA SONRASI MİKROYAPI VE MEKANİK ÖZELLİKLERİNİN KARŞILAŞTIRILMASI

Balcılar, Muhammed Mustafa
Yüksek Lisans, Metalurji ve Malzeme Mühendisliği
Tez Yöneticisi: Prof. Dr. Bilgehan Ögel

Nisan 2022, 137 sayfa

Beynitik dövme çelikleri son yıllarda düşük maliyetleri ve enerji gereksimlerinden ve en uygun dayanç, süneklik, ve tokluk bileşimilerinden dolayı temperleme çeliklerine alternatif olarak ortaya çıkmıştır. Her ne kadar sürekli soğumanın beynitik dövme çeliklerine olan etkisi çalışılmışsa da, izotermal dönüşümün mikroalaşımlı beynitik dövme çeliklerinin mikroyapı ve mekanik özelliklerine etkisi hala açık bir alandır. Bu çalışmada 0.2C-1.3Si-1.5Mn-1.45(Cr+Mo) kompozisyonlu, V-Ti-Nb ile mikroalaşımlanmış, düşük karbonlu mikroalaşımlı beynitik bir dövme çeliği incelenmiştir. Çelik çeşitli sıcaklıklarda izotermal olarak dönüştürülmüş ve sürekli soğumaya bırakılmş, mikroyapısal nitelikleri optik miroskopi ve taramalı elektron mikroskopi ile, faz analizi için XRD ölçümleri ile, ve mekanik özellikleriyle kıyaslanmıştır. İzotermal dönüşüm süresinin etkisi de, 15 dakikadan başlayarak 30 saate kadar, her izotermal dönüşüm sıcaklığında incelenmiştir. Mikroyapısal karakterizasyon M_s sıcaklığının hemen üstünde yapılan izotermal dönüşümün en küçük iğne boyutlu ve maksimum beynit miktarının verdiğini göstermiştir. Kalıntı östenit ölçümleri bütün numunelerde sistem içinde benzer miktarda östenit kaldığını göstermiştir. Sertlik ölçümleri beynitik numune sertliklerinin benzer olduğunu ama en düşük sıcaklıkta dönüşen numunenin en sert

mikroyapıyı verdiğini göstermiştir, sertlik aralığı 391-420HV'dir. Diğer numunelerin beynitik mikroyapı sertlik değerleri 378HV'den 421HV'ye kadar değişmektedir. M_s sıcaklığının hemen üstündeki izotermal dönüşüm %17 uzama ve 1264 MPa çekme dayancı ile en sünek ve tok çeliği oluşturmuştur. Sonuçlar izotermal dönüşümle elde edilen numunelerin üstün mekanik özelliklere sahip olduğunu göstermiştir ve en iyi performansa sahip malzemeler elde etmek için izotermal dönüşüm ısıl işlem yöntemleri tasarlanmalıdır.

Anahtar Kelimeler: Beynitik Çelik, Çelik, Beynit, Kalıntı Östenit, Beynitik Dövme Çeliği, İzotermal Dönüşüm

To my friends and family

ACKNOWLEDGMENTS

TABLE OF CONTENTS

LIST OF TABLES

TABLES

LIST OF FIGURES

FIGURES

LIST OF ABBREVIATIONS

ABBREVIATIONS

%EL: Percent elongation

%RA: Percent reduction in area

ASTM: American Society for Testing and Materials

B: Bainite

B_s: Bainite start temperature

CCT: Continuous cooling transformation

GB: Granular bainite

HV: Vickers Hardness

HV: Vickers Hardness

ITT: Isothermal Transformation Temperature

LB: Lower Bainite

M/A: Martensite/Austenite

M_{90}: 90% Martensite Formation Temperature

M_s: Martensite start temperature

NB: Needle bainite

Q&T: Quench and Temper

RA: Retained Austenite

SEM: Scanning Electron Microscopy

TEM: Transmission Electron Microscopy

TRIP: Transformation induced plasticity

TTT: Time-Temperature-Transformation

UTS: Ultimate Tensile Strength

Wt%: Weight percent

XRD: X-Ray Diffraction

YS: Yield Strength

LIST OF SYMBOLS

SYMBOLS

γ: Austenite

α: Ferrite

λ: Wavelength of X-Ray radiation

θ: Angle of diffraction

Ø: Diameter

CHAPTER 1

INTRODUCTION

In recent years, high safety demands from automotive, aerospace, and defense industries and stringent energy and environment regulations have driven the steel industry to develop products with superior mechanical properties and lower energy consumption from its predecessors such as conventional ferritic-pearlitic steel. Improvements in yield strength, ultimate tensile strength, impact toughness, fracture toughness, fatigue resistance, machinability and weldability are now a must for the steel sector and ferritic-pearlitic steels, even with microalloying, fall short when it comes to these demands [1-3]. To meet these demands, quench and temper (Q&T) process is employed [3]. However, Q&T process is costly and time-consuming, which in turn increases the cost and carbon footprint of steel products [4, 5]. Hence, bainitic forging steels were developed in 1980s to replace the previous materials and processes [6].

Bainitic microstructures can be obtained by applying either continuous cooling or isothermal transformation. Bainitic forging steels, with or without microalloying, are usually continuously cooled to obtain bainitic microstructures. However, continuous cooling control is difficult, and reliability of cooling systems is an issue [6]. On the other hand, obtaining bainite by isothermal transformation is proven to give the best mechanical properties [3, 6, 7].

In addition to producing a homogeneous bainitic microstructure with relative ease, carbide precipitation should be suppressed to obtain better mechanical properties since carbides, especially cementite, acts as a nucleation site for void and cracks, which reduce mechanical properties like fatigue resistance and fracture toughness drastically [8].

Retained austenite content is also a major factor in improvement of mechanical properties. Excessive amounts of retained austenite may lead to higher ductility at the expense of strength, due to transformation induced plasticity (TRIP) effect [9]. Although bainitic forging steels without microalloying subjected to continuous cooling and isothermal transformations have been studied, the effect of isothermal transformation on microalloyed bainitic forging steels is still to be investigated.

In this study, a forging steel microalloyed with V, Ti, and Nb is subjected to isothermal transformations at various temperatures to obtain the carbide free bainite mentioned. The aim of this study is to compare the isothermally heat-treated and continuously cooled structures in terms of microstructure, bainite morphology, carbide formation, volume fraction of phases, and mechanical properties. Two different parameters are studied in this work: the isothermal transformation temperature and isothermal holding time. Several characterization and tests such as optical and scanning electron microscopy, X-Ray Diffraction (XRD) Analysis, hardness measurements and tensile tests were employed to achieve this goal.

CHAPTER 2

LITERATURE REVIEW

2.1   Bainite

Bainite is a phase mixture, formed by decomposition of high temperature austenite (γ) phase of steel into ferrite (α) and cementite (Fe_3C). It was first discovered in 1930 by Davenport and Bain as they were studying isothermal transformation of austenite between martensite-forming and pearlite-forming temperatures [10]. The properties of this new phase were unknown at the time but later works described it as having similar levels of hardness as tempered martensite, but higher levels of toughness [11]. The microstructure was described as "acicular, dark etching aggregate", and it was significantly different from the familiar lamellar pearlitic structures, as seen in Figure 2.1. After the first works presented by Davenport and Bain, this new type of steel generated quite an attention and generated a significant amount of research, such that bainitic steels are a discipline on its own.

Bainite is usually obtained by applying isothermal transformation to the steel of interest. Isothermal transformation refers to holding the steel at a constant temperature for the transformation to occur, hence the term isothermal. Formation of bainite is achieved by decomposition of austenite into ferrite and cementite, so enough time must be given to the transformation for completion. The temperature of the transformation has upper and lower limits: namely, the bainite start (B_s) and martensite start (M_s) temperatures [12]. B_s is the temperature at which bainitic microstructures start to form when steel is cooled down and held at that temperature. Above this temperature, the bainite microstructure is not observed anymore and reconstructive growth of ferrite and cementite takes place, which leads to the pearlite microstructure [13]. M_s is the temperature at which martensite starts to form by diffusionless shear or displacive transformation [14]. The isothermal transformation

limits and resultant microstructures are usually visualized as Time-Temperature-Transformation (TTT) diagrams. Figure 2.2 shows a TTT diagram for two different steels, a steel of eutectoid composition and an alloyed steel, and the range of temperature in which bainite can be formed are highlighted in red [15]. The addition of alloying elements has a significant influence on bainite and pearlite formation kinetics, hence the shape of the TTT diagram changes drastically.

2.2   Microstructure and Morphology of Bainite

Depending on the shape of bainitic ferrite, and the arrangement of ferrite and cementite inside the microstructure, bainite has several classifications. Conventionally, bainite is classified as upper bainite and lower bainite [10, 15]. However, several studies show that different morphologies such as granular bainite or degenerated bainite can be observed in forging steels [1, 9].

2.2.1   Upper and Lower Bainite

Upper bainite is formed by isothermally heat-treating steels at high temperatures, close to B_s, whereas lower bainite is formed by isothermally heat-treating steels at low temperatures, close to M_s. Although both structures consist of ferrite laths or sheaves, and cementite, along with retained austenite and/or martensite, the difference arises from the precipitation of carbides in the structure. In upper bainite, the ferrite sheaves or plates are parallel to each other, and they are separated by layers of carbides, either in continuous or semicontinuous form. In lower bainite, the ferrite laths are again separated with carbide layers, but carbide precipitation also takes place in the bainitic ferrite in discontinuous form, usually at an angle of 55-60º to the direction of ferrite lath [10, 16, 17]. Figure 2.3 shows how upper and lower bainite forms from the high temperature austenite phase [10] and Figure 2.4 illustrates and gives the microstructures of upper and lower bainite [18].

4
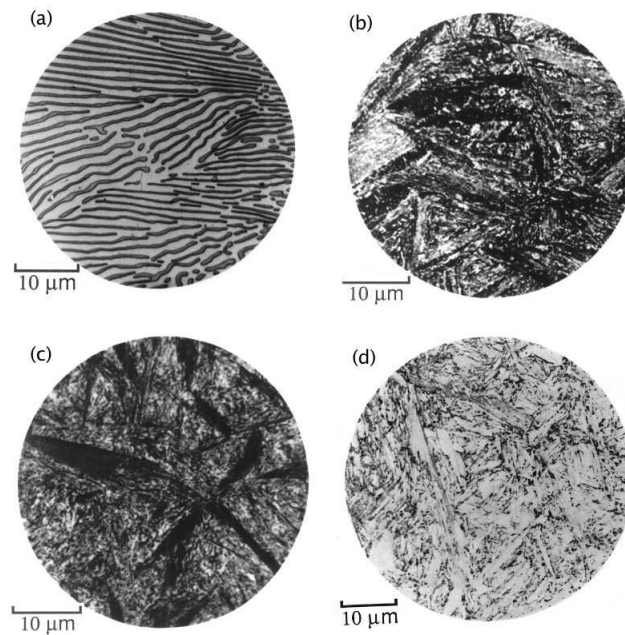
Figure 2.1. Microstructures of a steel of eutectoid composition. (a) Pearlitic structure resulting at 720°C, (b) bainitic structure obtained after an isothermal transformation at 290°C, (c) bainitic structure obtained after an isothermal transformation at 180°C, (d) martensite of the steel [10].
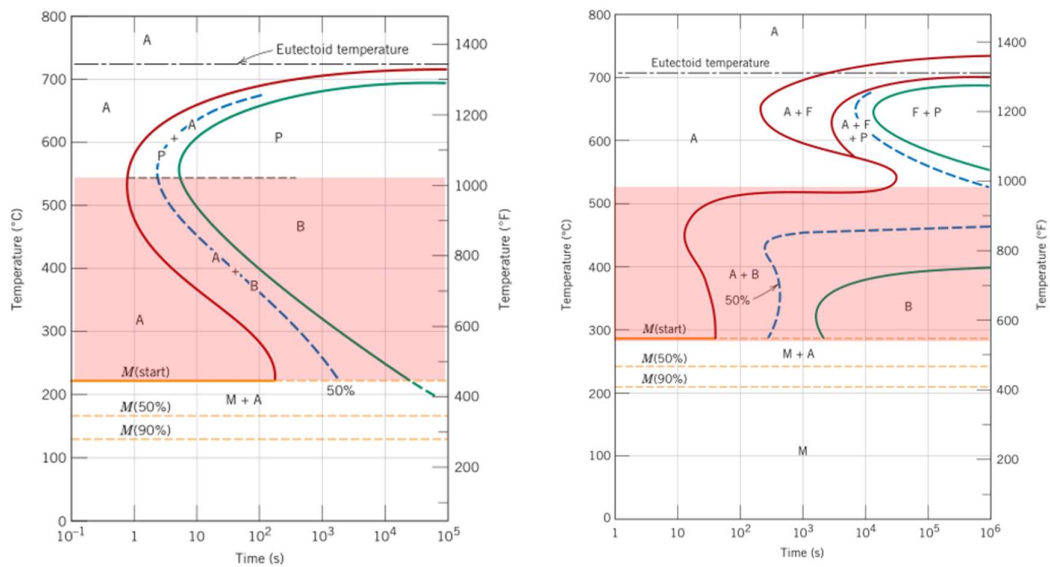
Figure 2.2. TTT diagrams of a steel of eutectoid composition (left) and of an alloy steel (4340, right) [15]. A: austenite, B: bainite, P: pearlite, F: primary ferrite, M: martensite. M_s temperature is the orange line, B_s temperature is the dashed on the left, for 4340 steel bainite nose is separate. Bainite forming temperature range is highlighted in red.

5
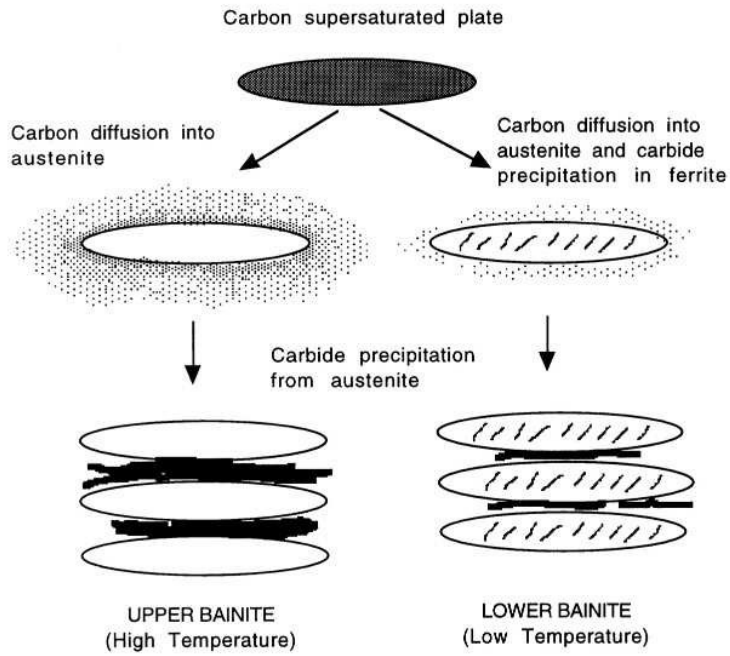
Figure 2.3. Upper to lower bainite transition, illustrated schematically [10].
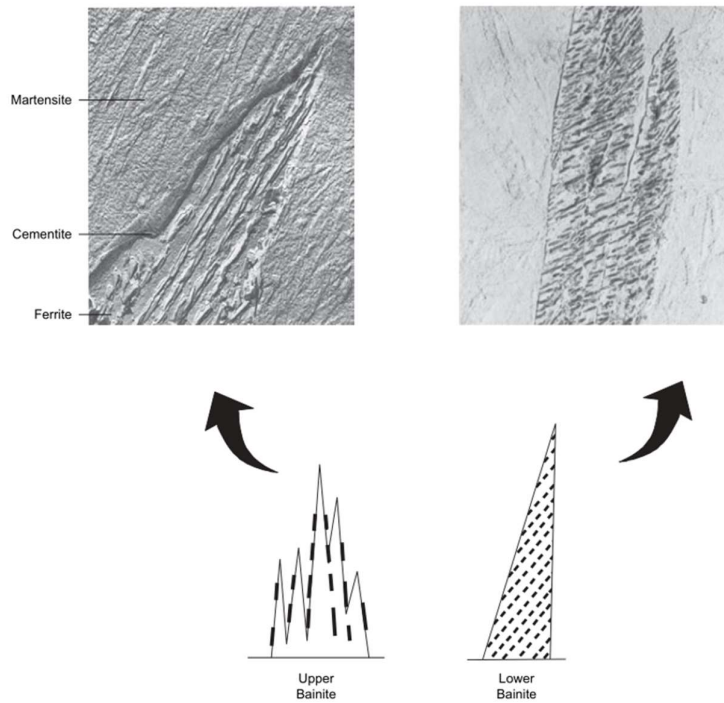
Figure 2.4. Upper and lower bainite SEM microstructures (top) and illlustrations (bottom) [18].

Aside from the carbide precipitation, an important difference between the upper and lower bainite morphologies is the ferrite plate thickness. The studies by Huang et al. (2013), and Yoozbashi, et al. (2015) suggest that the bainitic ferrite plate thickness is influenced by the transformation temperature, as the temperature decreases, plate thickness get finer [19, 20]. However, studies by Garcia-Mateo, et al., Cornide et al., indicate that although transformation temperature influences the plate thickness, main factors at play are the strength of austenite at the transformation temperature, the dislocation density in austenite, and the free energy change as the result of bainite transformation; all these factors increase as transformation temperature is reduced, which in turn decreases the plate thickness [12, 21].

The difference in carbide precipitation of upper and lower bainite influences the resulting mechanical properties. It has been reported that due to fine precipitation of carbides, a finer microstructure and higher dislocation density in lower bainite results in superior mechanical properties, compared to upper bainite [17, 22].

2.2.2 Carbide-free Bainite and Granular Bainite

In recent years, carbide-free bainite also generated quite a bit of interest. In carbide-free bainite, the carbide precipitation is suppressed by the addition of alloying elements such as silicon or aluminium [4, 7-9, 22]. The elimination of carbides and cementite, which are hard, brittle phases that are nucleation sites for voids and cracks, results in a bainite with an optimum combination of strength, ductility, toughness, and resistance to crack propagation [7-9]. The suppression of cementite formation by Si or Al alloying causes carbon to be partitioned between bainitic ferrite and untransformed austenite and when the structure is cooled down, the austenite transforms into martensite and residual austenite, also known as retainted austenite. The retained austenite is stabilized down to room temperature due to high local concentration of carbon and it also gives a TRIP effect to the steel [7-9, 22-24]. The regions of retained austenite and martensite are also known as blocky M/A islands. The formation of carbide-free bainitic steels in term of kinetics and growth is still an

intensely debated topic [24]. Figure 2.5 shows a TEM image of a carbide-free bainite obtained in an alloy steel [23].
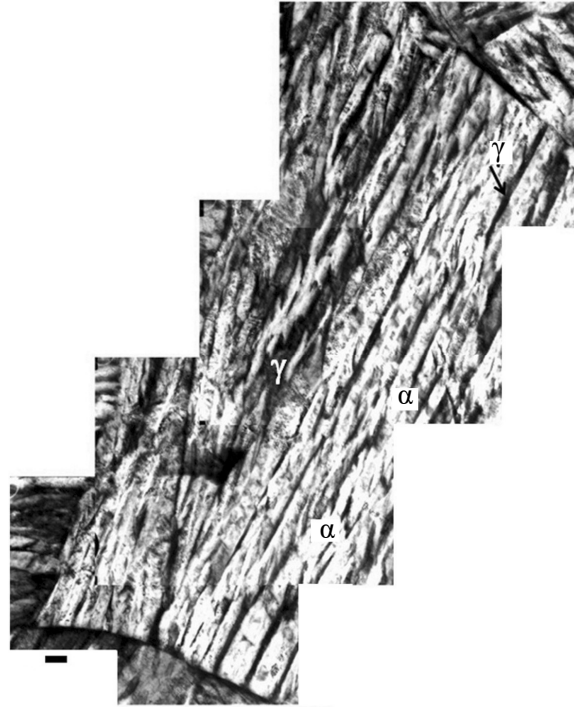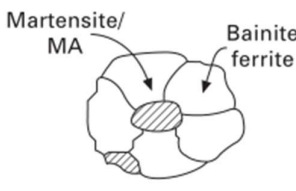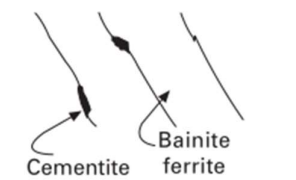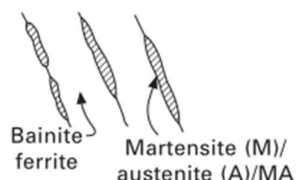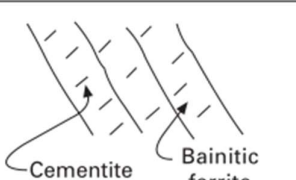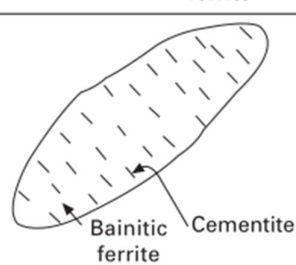
Figure 2.5. Transmission electron microscopy image of a Fe-0.30C-1.50Si-3.50Ni-1.44Cr-0.25Mo wt% steel with carbide-free bainite, forged and air cooled, α is bainitic ferrite, γ is austenite [23]

The investigations in carbide-free bainite also resulted in newer classifications of bainite morphologies, namely granular bainite, cementite-free lath-like bainite, degenerated upper bainite [1, 4, 16, 22, 23]. Table 2.1 shows the illustrations of these structures [22]. Of these, granular bainite garnered the most interest since it forms not by isothermal treatments, but by continuous cooling [10], where this method is employed for cooling forging steels. In addition to continuous cooling, the carbon content of the steel must be low [10]. Although there is not any crystallographic difference from regular accustomed bainitic structures, the morphology of granular bainite is quite different under optical microscope and SEM, where the ferrite appears to be in coarse, rounded shapes. But TEM studies reveal that, the granular bainite is still composed of bainite sheaves, just the sheave scale is very fine, and instead of cementite, retained austenite films are present between parallel laths. This

8

observation also confirms that formation kinetics of granular bainite is still the same, where carbon is partitioned between phases and austenite is stabilized as films instead of larger blocks or chunks [10, 22]. Figure 2.6 shows the optical and TEM micrographs of a granular bainitic microstructure [10].

Table 2.1 Morphology classifications of bainite and their representative illustrations that would be observed under optical microscope or SEM [23]

Bainite	Morphology	Bainite description
Granular bainite	Irregular ferrite with M/A	Martensite/MA — Bainite ferrite
Lath-like upper bainite	Lath-like ferrite with cementite on lath boundaries	Cementite — Bainite ferrite
Cementite-free lath-like bainite	Lath-like ferrite with M/A on lath boundaries	Bainite ferrite — Martensite (M)/austenite (A)/MA
Lath-like lower bainite	Lath-like ferrite with cementite inside the ferrite laths	Cementite — Bainitic ferrite
Plate-like lower bainite	Plate-like ferrite with cementite inside the ferrite plates	Bainitic ferrite — Cementite
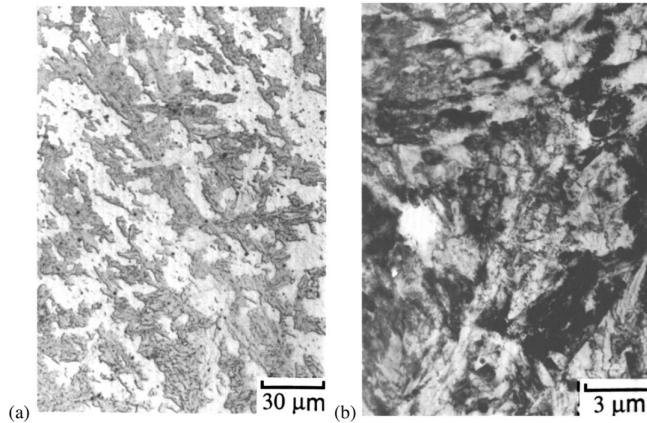
Figure 2.6. Fe-0.15C-2.25Cr-0.5Mo wt% steel with granular bainitic microstructure, (a) Optical microscopy, (b) Transmission electron microscopy [10]

The work done by Spanos, et al. characterized the change in bainitic microstructures with respect to the carbon content and transformation temperature in a Fe-C-2Mn ternary alloy [25]. In their work, the granular bainite was observed in hypereutectoid composition [25]. However, it can also be formed in hypoeutectoid compositions in the presence of other alloying elements [4, 10]. Figure 2.7 shows the phase diagram of the Fe-C system with bainite morphologies that can be obtained in Fe-C-2Mn alloy [25].
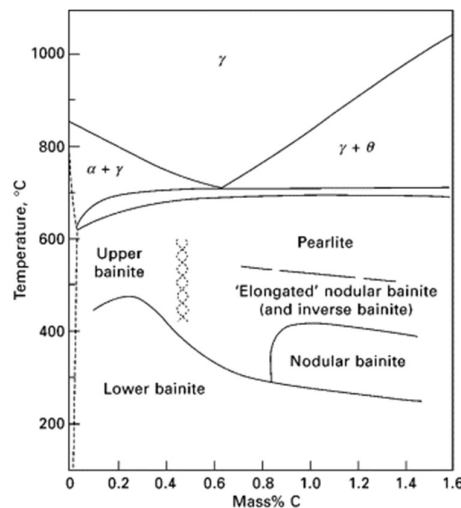
Figure 2.7. Morphologies of bainite with varying carbon content and transformation temperature in a Fe-C-2Mn ternary alloy [25].

10

2.3 Transformation Mechanism and Kinetics of Bainite

Since the discovery of bainite, development of a grounded theory of formation of bainite is attempted. From the works of various scholars and groups, two schools of thought have emerged. One of them considers that growth and kinetics of bainite are dominated by a diffusional mechanism whilst the other theory is based on a diffusionless, displacive, shear mechanism [10, 16, 26-28]. In literature, the diffusional theory, or reconstructive mechanism, is suitable for the underlying mechanism in growth of pearlite, whereas displacive theory is used to explain martensitic transformation [13, 14, 26].

2.3.1 Diffusion-Controlled Mechanism

The diffusion-controlled approach was first proposed by Hultgren in 1947 and was later supported by Hillert's work [28-30]. The main argument for the diffusion-controlled mechanism arises from the edgewise growth of the ferrite plates during bainitic transformation, which is considered to be as same as Widmanstatten ferrite growth [28-30]. This theory states that bainitic ferrite nucleates at the grain boundaries of austenite and starts to grow with a velocity determined by carbon diffusivity [29]. As the nucleated ferrite grows in one direction, it also expands towards to edges and at the α/γ interface, cementite may form and this further accelerates the ferrite growth [30], an illustration of this in given in Figure 2.8. The diffusive theory states that the reconstructive mechanism is further supported by observations such as similarities of bainitic microstructures with other diffusion-controlled growth structures and slow growth rates with a continuous characteristic and the accuracy of quantitative models developed to calculate the carbon content of bainitic ferrite and its growth kinetics [27]. Hillert further argued that experimental growth velocities indicate that growth of bainitic ferrite and Widmanstatten ferrite are driven by the same phenomenon, that there is no certain evidence bainitic ferrite is supersaturated whilst growing, martensitic growth rates are not observed in

bainitic ferrite, interface characteristics of martensite and bainite are not similar, and even if it is, this does not indicate that bainite growth is not rapid nor occurs with supersaturation [31]. Although the diffusional theory is ambitious to explain the bainitic growth via its own theory, it has some shortcomings such as quantitatively not being able to take into account the effect of carbide forming alloying elements [27], and recently, and more importantly, the formation of bainite at sub-M_s temperatures and the Zener-Hillert model not being able to accurately predict the growth rate of bainite [26].
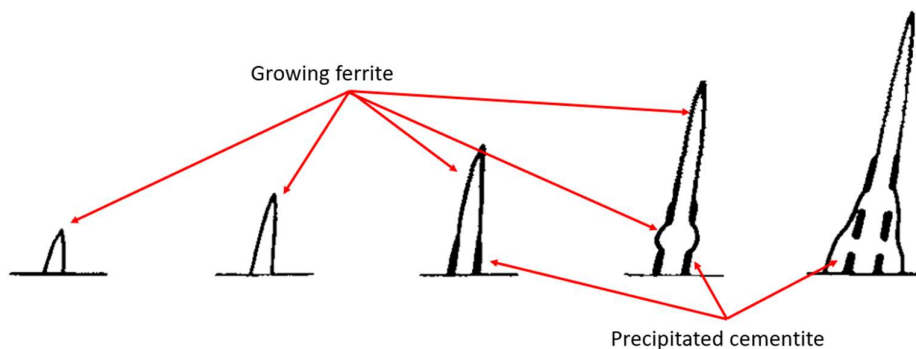
Figure 2.8. Illustration of nucleation and growth of bainite, based on diffusion theory [30]

2.3.2 Displacive Mechanism

The displacive or diffusionless approach to bainite formation goes back to works of Zener in 1946 [29], where he worked on the effect of alloying elements on pearlite, bainite, and martensite transformations. He realized that some of these elements effected the bainite transformation in the same way as the martensite transformation, which caused him to conclude that these two transformations must be closely related [27]. The theory developed by Zener focused on the free energy available for the bainite transformation, supplied by the alloying elements present in the system. From this model the famous T_0 concept arose. The T_0 temperature is defined as the temperature at which austenite and ferrite of the same composition have the same free energy. The locus of T_0 temperatures plotted on a phase diagram will give the

T_0 line which shows the limit of the bainite transformation. For a fixed composition, T_0 is the maximum temperature for bainite transformation. For a fixed temperature, T_0 shows degree of transformation [27]. The displacive nature of transformation also brings an additional stored energy in ferrite due to transformation strains, and when that additional strain energy is included, the line is known as T_0' [32, 33]. The work put forth by Bhadeshia also supports this view [29, 32]. Figure 2.9 illustrates the T_0 line for Fe-C system [27].
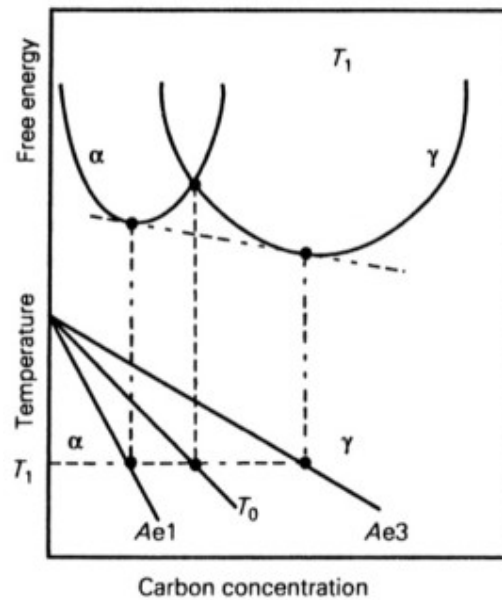
Figure 2.9. T_0 line for Fe-C system, Ae1 and Ae3 lines are boundaries of the α+γ region on the phase diagram [27]

The difussionless growth of bainite is possible only below the carbon concentration indicated by this T_0' line. The diffusionless growth of bainite occurs in form small plates known as sub-units. These plates are supersaturated with carbon and their size and shape are dictated by the microscale plastic deformation that can be accommodated by the system. The sub-unit forms on the austenite grain boundary and almost instantaneously grows into the grain and stops at the next grain. The supersaturated ferrite rejects carbon into austenite and depending on the composition and transformation temperature this may lead to carbide formation between ferrite

plates, carbide precipitation inside the plate, or stabilization of the residual austenite, also known as retained austenite. After initial sub-unit nucleation, the bainite growth occurs via autocatalytic nucleation, where new sub-units form again in a displacive manner [26, 27, 29, 32, 33]. The nature of this displacive growth and the T_0 curve also explains the incomplete transformation phenomenon [27] where the transformation continues more carbon is rejected into austenite and free energy available falls until T_0 is reached. The austenite will no longer transform to bainite. Another approach to explain the incomplete transformation phenomenon comes from the solute drag-like effect [3, 16, 27] where presence of alloying elements hinders the diffusion of carbon, causing the transformation to fail to reach completion, due to segregation of alloying elements.

The work of Samanta et al. demonstrated a peculiar behavior of bainite, it formed even under M_s temperatures, which is unexpected from a diffusional point of view. By crystallographic analyses they have demonstrated that the product obtained below M_s was indeed bainite and the analysis shows that the bainite formation takes place in a displacive manner [26]. Recently, the model for bainite growth developed by Wei et al. showed a significant agreement with the experimental data. The model they developed was based on a displacive approach [34]. The experimental observations such as high sub-unit growth rates, retained austenite measurements by XRD analysis that match T_0 curve, synchrotron experiments where carbon partitioning is observed, and atom probe measurements which show the carbon supersaturation in bainite transformation clearly and strongly support the displacive theory [27,34]. The application of displacive theory to design and production of bainitic steels also resulted in products with superior properties [27], all of which indicate that the displacive theory seems to be the correct one that established how bainite transforms. However, the diffusional theory cannot be ignored since the evidence gathered by them is not insignificant [27, 30, 31].

2.3.3 Kinetics

The two schools of thought in bainite kinetics, reconstructive/diffusional and displacive/diffusionless separately tried to develop their models that can fit to experimental data and can be used to predict the kinetics in different conditions. The diffusional mechanism models are based on the diffusivity of carbon and the reconstructive growth ferrite and carbide by the so-called "ledge" mechanism [34]. Whereas the displacive theory states that the nucleation of ferrite laths is instant, and it is supersaturated with carbon, partitioning of carbon occurs afterwards and growth of bainite is by shear [34]. Recent works have shown that the bainite formation is also autocatalytic and is quite complex [34, 35, 36]. The models developed by Ravi et al. [35, 36] show that previous models did not take the autocatalytic nucleation into account which caused a discrepancy between the experimental results and this issue was resolved by them. However, the issue of incomplete transformation phenomenon persists. The incomplete transformation phenomenon refers to the observations that bainitic transformation does not reach to its completion because carbon is partitioned or rejected into austenite from ferrite, which in turn stabilizes the retained austenite in the system. The displacive models explain this phenomenon by the T_0 concept. When the concentration of austenite hits the T_0 curve at a given ITT, the transformation thermodynamically cannot proceed, hence the transformation is incomplete [4, 7, 8, 9, 10, 16, 22, 24, 34]. The remaining austenite transforms into martensite upon cooling with some amount of retained austenite [9]. The reconstructive theories explain this phenomenon by the solute drag-like effect [3, 16, 29], where substitutional alloying elements segregate along austenite grain boundaries, causing the carbon diffusion and ferrite growth to be sluggish and in return transformation does not reach completion [3, 8, 16, 29].

The experimental evidence shows that displacive models fit the best to the data and Figure 2.10 shows the model developed by Wei et al., [34] which is expanded on the model of Ravi et al, [35, 36] and the experimental data obtained at several isothermal transformation temperatures.
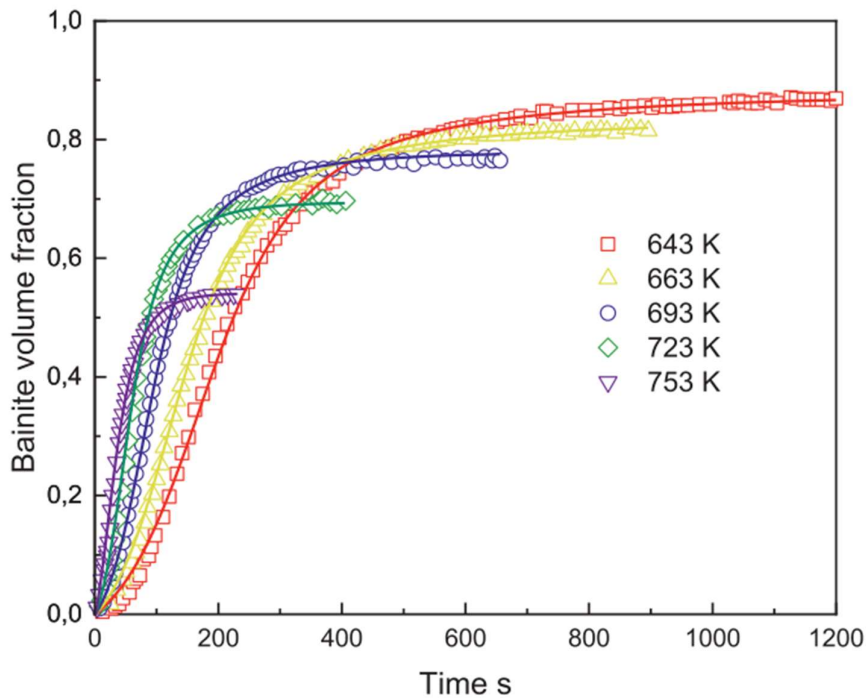
Figure 2.10. Kinetic data for a C-Si-Mn steel. Markers are experimental observations, solid lines are model fit developed by Wei et al. [34]

2.4 Heat Treatment of Bainite

The heat treatment to obtain bainite is a relatively simple process, with three steps: austenitization, quenching to bainite transformation temperature, and cooling by air, oil, or water. The steel of concern must be austenitized at the temperature of interest since bainite forms by decomposition of austenite and kept at that temperature for enough time for full homogenization, then the steel is either quenched to the isothermal transformation temperature and kept there until transformation finishes, or the steel is cooled continuously to room temperature with either at a fixed rate or freely [37].

With any type of process, there are advantages and disadvantages associated with isothermal transformation and continuous cooling heat treatments. The continuous cooling is attractive due to its simplicity and low cost since no further equipment is

required to form bainite and it is easier to perform, compared to isothermal transformation [37, 38]. But the main drawback of continuous cooling is the lack of microstructure control [39]. If the cooling rate cannot be controlled or adjusted with care, then there is the risk of forming regions of unwanted phases, such as ferrite and pearlite, in the microstructure, which in turn causes poorer mechanical properties [38].

Whereas with isothermal transformation, the control of microstructure can be much more precise, and the degree of transformation can be predictable. Although the energy consumption and cost for isothermal process is higher, the positives of this treatment overcome its negatives, and if the alloying of the steel is adequate, the transformation finish time is within reasonable durations. The transformation finish here does not necessarily mean 100% bainite formation due to incomplete transformation phenomenon and it should always be considered for this approach, since partitioning of carbon in austenite stabilizes residual austenite in the structure [7, 9]. Figure 2.11 shows schematic representation of isothermal heat treatment and continuous cooling schedules [6].

The isothermal transformation that takes place above the M_s and below the B_s temperature is known as austempering. Austempering results in fully bainitic microstructure and compared to other traditional heat treatments, it has the advantage to produce a product with increased ductility, toughness, and strength. Figure 2.12 shows the typical heat treatment route for austempering [18].
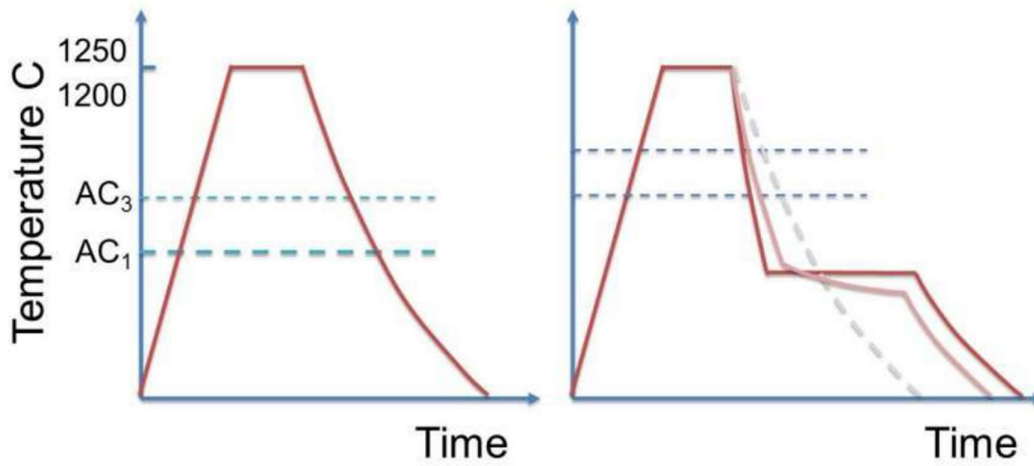
Figure 2.11. Schematic graphs of continuous/air cooling (left) and isothermal transformation (right).
On the right: red solid line is an ideal isothermal heat treatment schedule, conducted via salt baths.
The pink solid line represents a transformation in a heated tunnel [6].
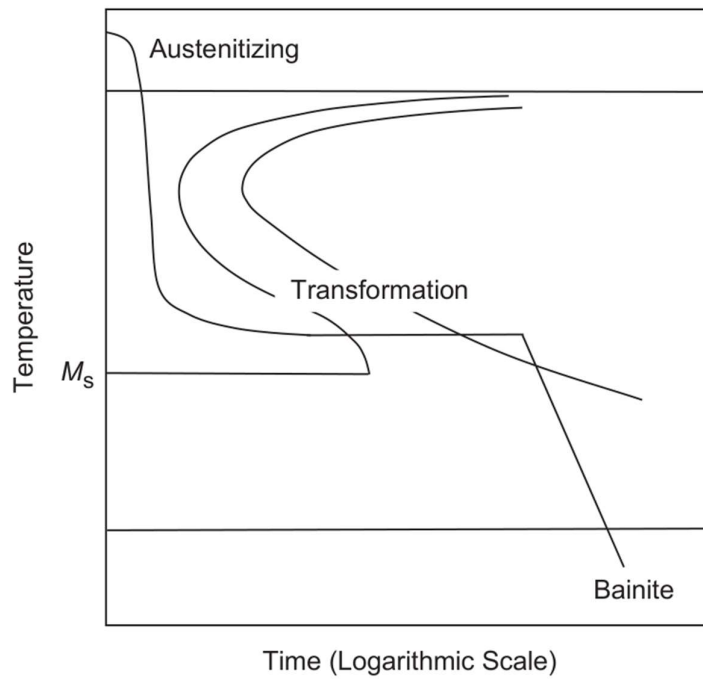
Figure 2.12. Schematic illustration of austempering heat treatment, superimposed on a hypothetical
TTT diagram [18]

2.5   Mechanical Properties of Bainite

The mechanical properties of any material are influenced by its processing history because that also affects its microstructure, all of which determine its performance under service conditions.   For bainitic steels, the enhancement of mechanical properties come from fine tuning the bainitic ferrite size so that an optimal balance of strength, toughness, and ductility is obtained.   As the bainitic ferrite lath size is reduced, there are more obstacles to dislocation motion, which results in an increase in strength. Recent studies show that when this lath size goes into nanoscale, the UTS values shoot up to values of 2 GPa with a ductility above 10%. The reduction in bainitic ferrite size is achieved by reducing the transformation temperature so finer laths grow in the structure and by addition of alloying elements such as Mn, Si, Ni, etc. The decrease in lath size not only causes obstacles to dislocation motion but an increase in dislocation density in the structure, causing an additional strengthening of the steel. The presence of alloying elements also causes solid solution strengthening and increase the carbon partitioning, all of which in turn increase the yield and ultimate tensile strengths. The enhancement in ductility is obtained by suppressing cementite formation by silicon alloying, so that hard and brittle phases do not form, and crack nucleation is retarded, and with the stabilization of retained austenite. The retained austenite in the structure results in what's known as TRIP effect. The transformation of austenite to martensite due to strain energy supplied to the system results in higher deformation ability [6, 7, 9, 10, 12, 40-45].

Research shows that decreasing the transformation temperature results in better mechanical properties, provided that carbide-free structures are formed, and example is given in Figure 2.13 [45]. But the reduction of transformation rate should be taken into consideration for low temperature transformation.

Table 2.2 gives a summary of previous work on bainitic steels in terms of mechanical properties [40, 46].
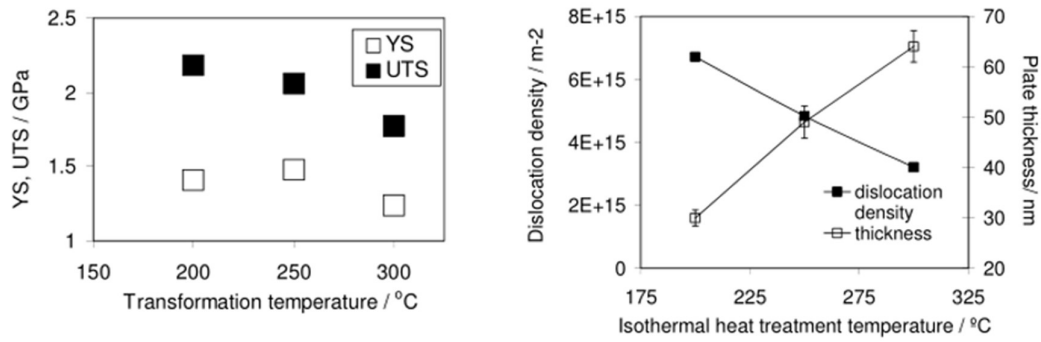
Figure 2.13. Effect of transformation temperature on yield and ultimate tensile strengths (YS, UTS) (left), and on bainitc ferrite plate thickness and dislocation density (right) [45]

Table 2.2 Mechanical properties of selected bainitic alloys, reported by Soliman et al., and, Kumar et al. [40,46]. (CC: Continuous cooling)

Alloy	C	Si	Mn	Al	Cr	Mo	Co	V/W/Ni/ Cu/Ti	T(ºC)/ t(h)	YS/ UTS	%EL
A	0.69	1.92	1.38	0.75	1.39	0.24	0.14	-/-/-/-/-	300/8	-/ 1600	32
B	0.79	1.55	1.00	-	1.01	0.25	-	0.1/-/-/-/-	250/8	1673/ 2098	4.3
C	0.26	1.42	1.70	-	1.10	0.24	-	0.1/- /1.10/0.94/-	340/4	880/ 1428	15
D	0.21	1.8	3.0	-	0.85	0.21	-	-/-/3/-/-	300/1	1062/ 1753	14.9
E	0.21	1.53	1.92	-	0.03	0.30	-	0.1/-/-/-/-	CC	955/ 1020	19
F	0.42	1.72	2.15	-	0.47	-	-	-	360/2	1218/ 1505	21.2

2.6   Retained Austenite

During formation of bainitic ferrite, the carbon is rejected to the austenite phase. If carbide suppressing elements such as silicon or aluminium are not present [7, 46], then carbide precipitation is observed. With adequate Si alloying the carbide precipitation and cementite formation is suppressed and the austenite in the system transforms into martensite upon cooling below Ms. If the carbon content of the remaining austenite is high enough, residual austenite is also present in the system since high carbon contents may lower the Ms temperature to cryogenic levels. This is known as retained austenite (RA). The mixture of martensite and retained austenite is also known as martensite/austenite or M/A. There are two different morhpologies of this M/A: blocky and film-like. Blocky M/A is observed in the microstructure as large chunks, whereas film-like M/A is extremely fine in size, such that usually TEM study is required to observe it. The enhancement of mechanical properties of bainitic steels, such as TRIP effect, usually arise from this latter morphology whereas high amounts of blocky M/A are shown to be detrimental to ductility and toughness [47, 48]. But other studies show that blocky M/A formation, in moderation, enhances the mechanical properties again due to TRIP effect [9, 48]. Retained austenite also plays a role in crack blunting [49] and retardation of crack nucleation and propagation [50], leading to better fracture toughness and fatigue properties. Figure 2.14 shows the schematic illustration of how retained austenite films form between bainitic ferrite sheaves [34].
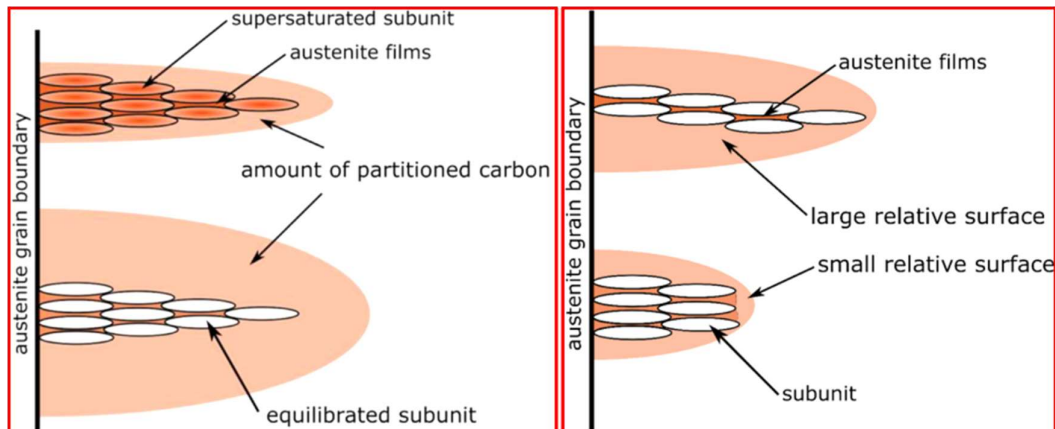
Figure 2.14. Left: effect of carbon content of bainitic ferrite on austenite carbon content and morphology. Right: effect of bainitic ferrite geometric arrangement on austenite morphology. Film of retained austenite form between the ferrite laths, the rest of the austenite (shaded in orange) may transform to blocky M/A [34]

The amount and type of retained austenite in the structure depends on multiple parameters such as carbon and alloying content, isothermal transformation temperature and holding time, or the cooling rate. These factors are affective in terms of stability of austenite, both mechanically and thermokinetically [51].

Girault et al. investigated the effect of silicon and aluminium in stabilization of retained austenite and have found that both silicon and aluminium suppress carbide formation, leading to a carbon-rich austenite that gives TRIP effect to the steel. They have also investigated the holding time at a constant temperature and observed after a certain period, martensite disappears from the system [52]. The work of Sugimoto et al. also has shown that the isothermal transformation temperature and holding time influence amount of RA and the carbon entrapped in RA [53, 54]. The studies have shown that the transformation temperature determines the initial carbon content of retained austenite instead of the amount of austenite in a TRIP-type bainitic C-Si-Mn steel [53], and in Al-added steel, the maximum amount of RA and maximum carbon concentration in RA are observed at different austempering temperatures [54]. The study conducted by Grajcar et al. also show that for a medium-Mn steel with Nb microalloying, the RA content increases and then decreases afterwards, with

respect to both isothermal transformation temperature and isothermal holding time. The effect of Nb microalloying was not observed to be as significant as temperature, time, or Mn content [51].

The stability of retained austenite can be examined in terms of internal and external factors as well. The internal factors, as the name explains, are related with the internal properties of the system such as alloying and carbon content, austenite morphology and grain size, and the neighboring structures in the system. The external factors refer to the process and service parameters that are applied externally to the system such as stress levels, strain rate, and deformation temperature [55].

2.7   Effect of Alloying Elements

The primary alloying element of steel is carbon but in addition silicon, manganese, chromium, molybdenum, vanadium, titanium, niobium, nickel, copper, cobalt, aluminium, boron, sulphur, and nitrogen are regularly used for different purposes. Each element causes a different type of strengthening when used in correct concentration, and they also influence the thermodynamics and kinetics of the system. Hence, they directly influence bainite formation in one way or another: they may accelerate or retard the kinetics, they may cause additional strengthening, increase hardenability, suppress formation of carbides, or may supply additional nucleation sites by forming carbides and/or nitrides [46]. The alloying elements also act as austenite or ferrite stabilizers, or carbide formers [56, 57].

Carbon, the main alloying element in steel, is austenite stabilizer during bainitic growth [7, 9]. If the cementite formation is suppressed by means of other alloying elements, then increase in carbon content will result in a lower M_s temperature, which enables the bainite transformation temperature to be lowered [46]. But the drawback in increasing the carbon content is the reduced transformation rates and deterioration of mechanical properties and weldability, excessive carbon alloying will cause precipitation of cementite in absence of carbide suppressors, and low

transformation temperature will cause lowered transformation rates [12]. Increasing the carbon content will also lead to lowering the B_s temperature [8, 58]. Effect of carbon on B_s and M_s is shown in Figure 2.15 for a Fe-Si-Mn-C steel [58].
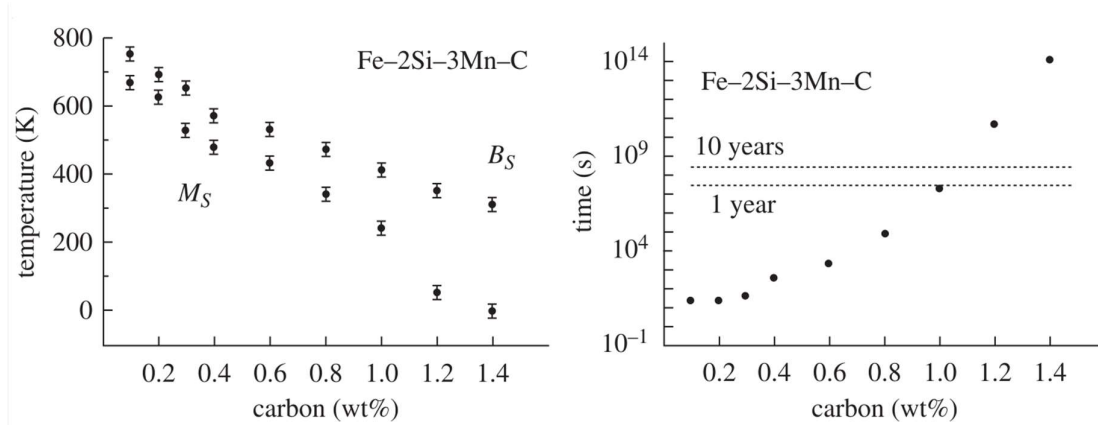
Figure 2.15. Effect of carbon content on B_s and M_s temperatures (left) and on transformation completion time (right) for a Fe-Si-Mn-C steel [58]

Silicon also behaves as an austenite stabilizer by stabilizing the retained austenite in the structure by means of suppressing the cementite formation. The suppression of cementite and carbides cause the carbon in the system to be trapped and partitioned between austenite and ferrite and increased carbon content in austenite leads to stabilization, i.e., formation of retained austenite. The cementite suppression is due to low solubility of silicon in cementite [4, 7, 9, 46].

Manganese is used to increase the hardenability and lower the B_s and M_s temperature, but it also retards the bainite formation kinetics by shifting TTT and CCT diagrams to the right and may also segregate, causing martensite formation, which deteriorates mechanical properties [4, 44, 46, 59]. It also gives the TRIP ability to steels [51].

Molybdenum is used for hardenability and to prevent temper embrittlement [46]. It also acts as a carbide former and causes carbide precipitation at austenite-ferrite phase boundary [16].

Vanadium increases the hardenability and, if used in microalloy concentrations, acts as a grain refiner by forming carbides and nitrides in the structure and pinning the

grain boundaries. The V(C,N) precipitates also act as nucleation sites for bainitic ferrite, which leads to acicular ferrite formation and they also give precipitation strengthening to steels [38, 59, 60, 61].

Titanium is used as a grain refiner and forms carbides and nitrides, strengthening the steel by precipitation hardening. Ti is also used to decrease the formation of boron nitride by forming TiN because BN is detrimental to mechanical properties of the steel. However, excessive Ti alloying will cause large TiN inclusions, which are also harmful to steels in terms of toughness [4, 38, 61, 62].

Niobium is used as a grain refiner and forms precipitates, causing precipitation strengthening in steels. Nb also increases the flow stress and retards pearlite transformation [38, 59, 60].

Aluminium is used as a deoxidation agent and it has high affinity for nitrogen [4, 59]. Al also has the effect of accelerating bainite kinetics and suppress carbide formation [46].

Chromium is used to increase the hardenability and it is a strong carbide former [29, 46]

A visual summary of effect of alloying elements on pearlite and bainite formation kinetics is given in Figure 2.16 [63].
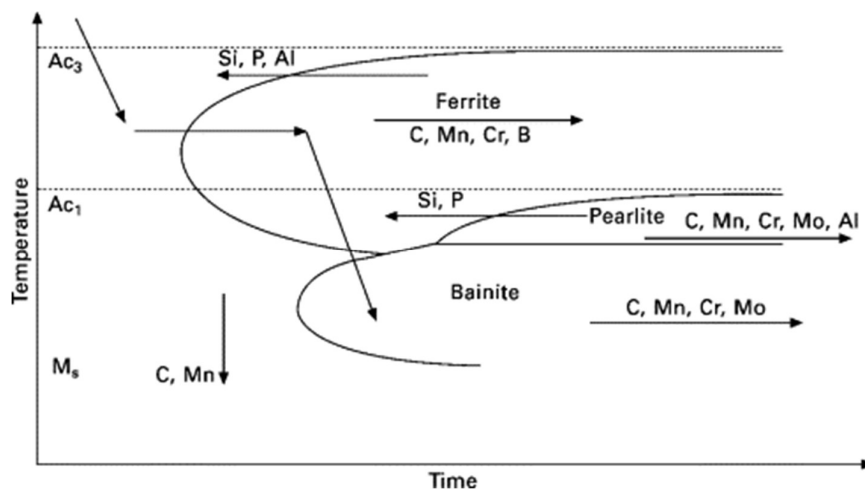
Figure 2.16. Schematic diagram of effect of alloying elements on a hypothetical TTT diagram [63]

2.8 Effect of Isothermal Transformation Temperature and Isothermal Holding Time

As stated in previous sections, the effect of isothermal transformation temperature and holding time influence both bainite morphology and the constituents of the microstructure. These factors ultimately determine the mechanical properties and performance of the component under service [3, 4, 6, 7, 8, 9, 12].

It has been reported in literature that isothermal transformation results in enhanced mechanical properties, such as elevated yield and tensile strength, and desired microstructure can be obtained with more precision [3, 6, 12]. The best mechanical properties are obtained at low transformation temperatures, where lower bainite, or finer nanobainite, structures can be formed [7, 9, 19, 20, 58]. As the transformation temperature is reduced, the bainitic ferrite sheave thickness decreases, which increases the area of interphase boundaries, an obstacle to dislocation motion. Hence, the strength increases [6, 7, 9, 10, 12, 40-45]. Increasing the transformation temperature results in poorer mechanical properties due to thickening of bainitic ferrite and the possibility of forming martensite upon cooling, due to incomplete transformation phenomenon [7].

The transformation temperature also influences the stability and morphology of retained austenite, which again influence mechanical properties. The increase in transformation temperature causes retained austenite amount to increase but after a certain point volume fraction decreases, possibly due to formation of martensite. The isothermal transformation temperature also decides on the amount of carbon rejected to austenite and it has been reported that at lower austempering temperature levels, carbon content of austenite increases, which increases the stability of austenite. A lower transformation temperature is also effective in forming film-like RA instead of the unwanted blocky M/A [64-66]. Figure 2.17 and Figure 2.18 show the effect of isothermal transformation temperature on volume fraction of retained austenite for a bainitic high-silicon steel and steels with different silicon content, respectively [65, 67].

The effect of isothermal holding time is also studied and it has been understood that as the holding time is increased, the retained austenite levels increase to a maximum and decrease afterwards. The increase in volume fraction can be explained due to stabilization of retained austenite [51, 53]. However, as the transformation duration is prolonged, the austenite size gets larger and possibility to form martensite increases. Figure 2.19 shows the change in retained austenite content and carbon concentration in a microalloyed manganese steel with respect to austempering time and Figure 2.20 shows the retained austenite volume fraction and carbon content change for a TRIP-type steel with respect to austempering time, respectively [51, 53].
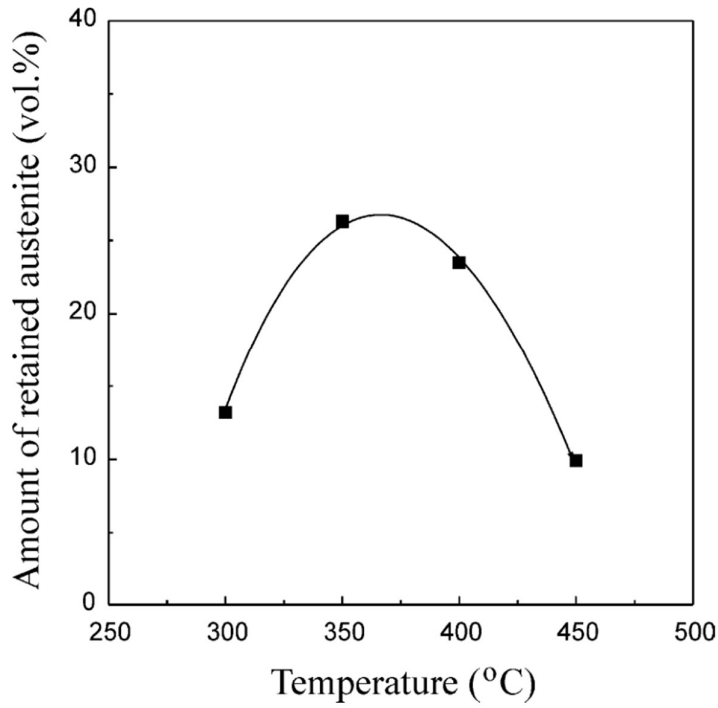
Figure 2.17. Retained austenite content change with respect to austempering temperature in a Fe-0.45C-3Si steel [65]
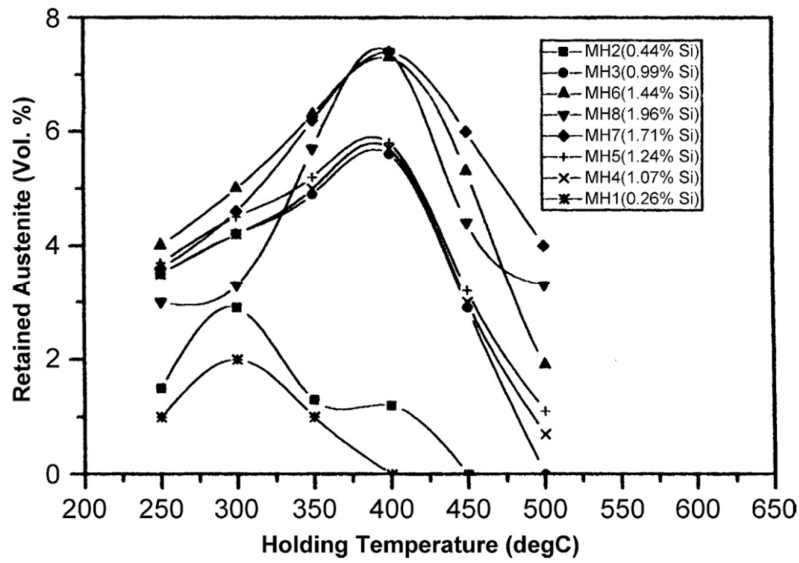
Figure 2.18. Effect of isothermal transformation temperature on volume fraction of retained austenite for steels with different silicon content [67]
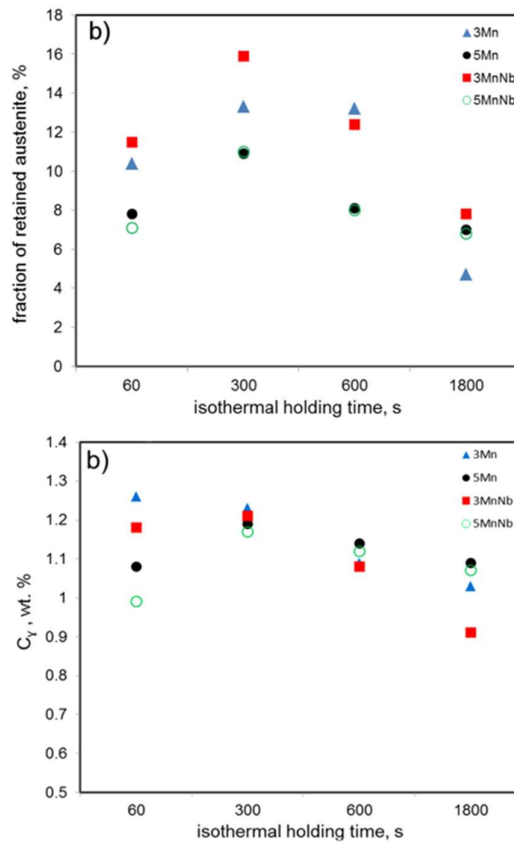
Figure 2.19. Effect of isothermal holding time on a microalloyed manganese steel isothermally transformed at 450ºC, top: volume fraction of RA, bottom: carbon content in austenite [51]
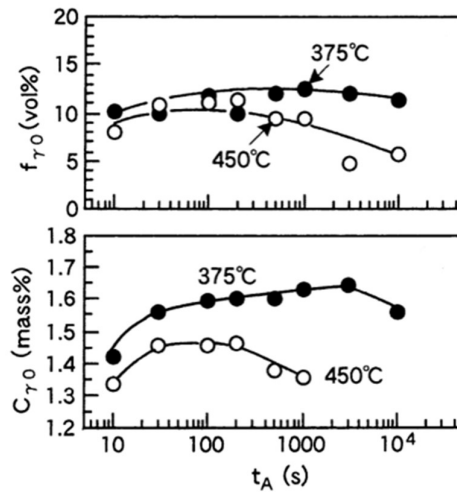
Figure 2.20. Effect of isothermal holding time on a TRIP-type bainitie steel isothermally transformed at 375 & 450ºC, top: volume fraction of RA, bottom: carbon content in austenite [53]

2.9   Bainitic Forging Steels

Bainitic forging steels emerged in 1980s as an alternative to quench and temper (Q&T) and precipitation hardenable or age hardenable ferritic-pearlitic (PHFP or AFP) steels. Although Q&T steels have high strength and reasonable ductility, their low production rate and high energy consumption is making them more costly and thus less desirable. Heat treatment of PHFP is not as energy demanding as Q&T steels but the mechanical properties of PHFP such as yield strength and toughness are inferior to Q&T steels. So, a need for high strength, tough, and ductile steel with low-cost production was present and as a cost cutting measure, forging steels that can produce bainitic structures upon continuous cooling or isothermal transformation were developed, since the process route of bainitic steels is similar to PHFP steels and strength and ductility values are high enough for most applications. In addition to adequate mechanical properties, the phase transformation temperatures are lower for bainitic steels, therefore energy consumption is lower. Figure 2.21 shows typical heat treatment routes for Q&T and PHFP steels and Figure 2.22 shows UTS vs Transformation Temperature diagram for steels in use [3, 4].
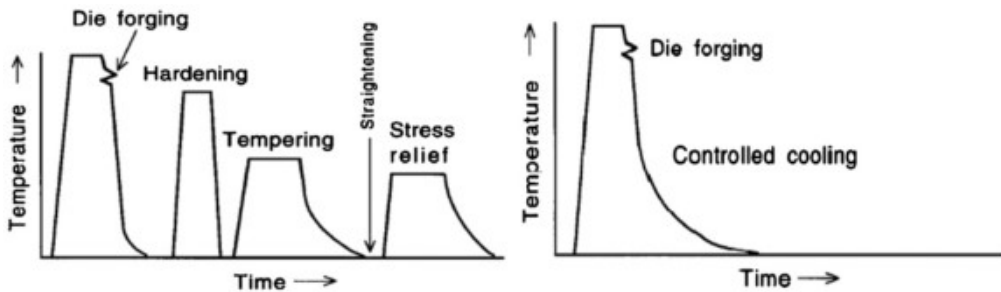
Figure 2.21. Processing schedules for Q&T (left) and PHFP (right) steels [3]
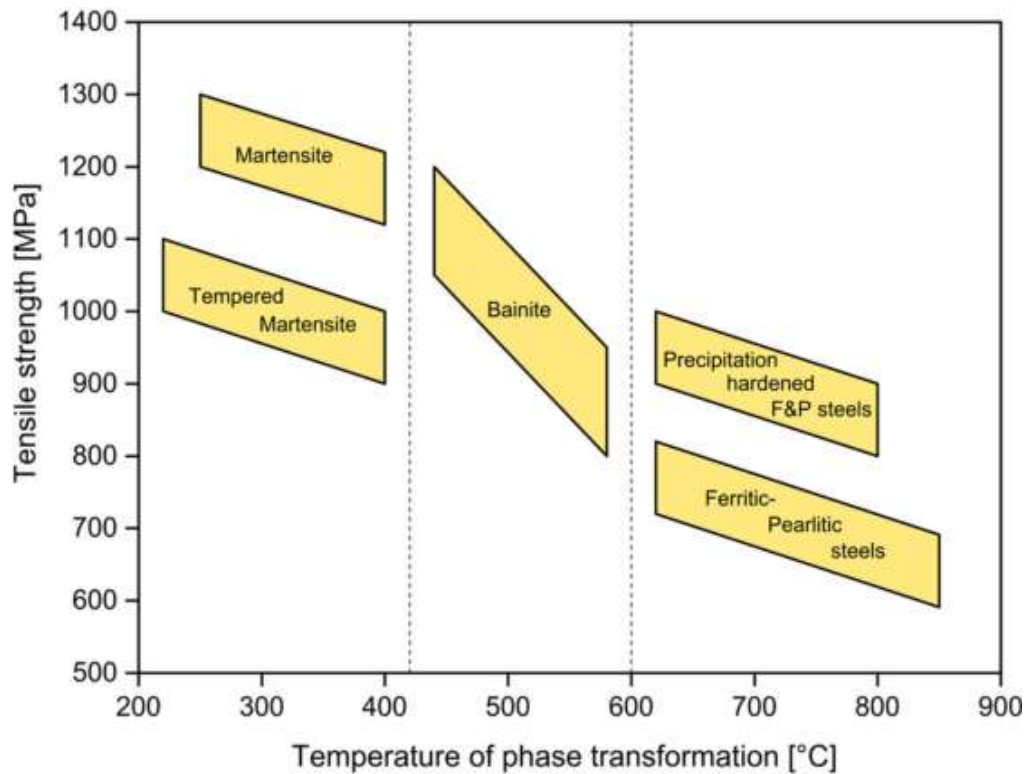
Figure 2.22. UTS vs Transformation Temperature for different steel types [4]

The optimum combination of strength, ductility, and toughness, better fatigue properties have made bainitic steels desirable, compared to regular Q&T or PHFP steels. In addition, microalloying was introduced to bainitic forging steels to further improve mechanical properties by means of solid solution strengthening, grain refining and precipitation strengthening by forming very fine V(C,N) or Nb(C,N) particles. If the silicon content is high enough, carbide or cementite precipitation is not observed and retained austenite becomes stabilized instead. Stabilization of RA is crucial in improving the ductility and toughness of forging steels since it provides the TRIP-effect. Strengthening of bainitic structures are further improved by limiting bainitic ferrite growth [68-76].

Table 2.3 lists some of the compositions of bainitic forging steels that have been studied previously.

Table 2.3 Chemical composition and mechanical properties of selected bainitic forging steels, HDB: High Ductility Bainite [3, 4].

Steel grade	%C	%Si	%Mn	%Cr	%Mo	Others	YS (MPa)	UTS (MPa)
20MnCrMo7	0.22	0.49	1.72	1.6	-	-	860	1250
HDB	0.17	1.46	1.52	1.32	-	-	782	1167
Solam B1100 18MnCr5-3	0.2	-	1.9	1.5	-	-	700	1100
Metasco MC 25MnCrSiVB6	0.25	0.9	1.3	0.8	-	-	700	1000
Unknown grade	0.27	0.5	1.7	1.3	0.5	Ni, V, Ti, Nb	820	1388

Bainitic forging steels are usually subject to ausforming, a type of thermomechanical process, where the steel is austenitized at high temperatures and deformed at the same time or deformed at the transformation temperature. Subsequent heat treatment can be either isothermal or the steel can be continuously cooled. The isothermal transformations result in most homogeneous structure and superior mechanical properties, but they are rather costly compared to just cooling in air. Air cooling, although cheaper, may give rise to formation of unwanted phases such as pearlite, upper bainite, or mixture of bainite and martensite. Obtaining a uniform homogeneous microstructure is difficult in continuous cooling processes. Hence, air cooled parts may not show the same strength levels as isothermally heat-treated parts. Dimensions of the part also become a problem in continuous cooling since thicker sections may retain their temperature at the interior for a longer time, giving rise to a property gradient across the part [68-76].

CHAPTER 3

EXPERIMENTAL PROCEDURE

The experiments and characterization methods of this study consists of elemental analysis, isothermal heat treatments, microstructural characterization by optical microscopy and SEM, quantitative phase analysis by XRD, and mechanical characterization by hardness measurements and tensile tests.

3.1   Material

The forging steel for isothermal heat treatments is supplied by ÇEMTAŞ A.Ş. The steel was received in forged condition in 4 pieces of 300 mm long bars with a diameter of 37 mm.

3.1.1   Chemical Composition

Optical Emission Spectrometry (OES) is used for the elemental analysis of the as received steel. The OES WAS Foundrymaster was used in the Foundry, Metal Processing and Automotive Materials Laboratory of METU Department of Metallurgical and Materials Engineering for elemental analysis and the results are given in Table 3.1.

Table 3.1 Chemical composition of the as received forging steel, the constituents are given in weight percent. Fe is balance.

%C	%Si	%Mn	%Cr+Mo	%P	%S	%V
0.22	1.30	1.46	1.45	0.01	0.066	0.01
(±0.01)	(±0.02)	(±0.03)	(±0.01)	(0.007)	(±0.004)	(±0.001)
%Ti	**%Nb**	**%N**	**%Ni**	**%Al**	**%Cu**	**%B**
0.0158	0.0360	0.0033	0.04	0.01	0.03	0.0027
(±0.0012)	(±0.0025)	(±0.001)	(±0.005)	(±0.01)	(±0.002)	(±0.001)

3.2   Heat Treatment Process

3.2.1   Equipment

The heat treatment equipment used in this study are the MSE Furnace M1200 open atmosphere muffle furnace and PROTHERM PCF 10/250/400 salt bath furnace. Muffle furnace is used in austenitization, and the salt bath is used for isothermal heat treatments. The salt used for the isothermal heat treatment is PETROFER AS135 Tempering Salt, which is a mixture of nitrate and nitrite salts and has a working range of 160ºC-550ºC. The temperature of the muffle furnace and salt bath is monitored by PROTHERM PC442T and Honeywell DC1010 thermocouples, respectively. Oil is used as the quenching medium. Figure 3.1 shows the equipment described above.

10 mm thick slices were cut from the 300 mm long bar and those slices were also cut into 4 pieces for the preliminary isothermal heat treatments. Larger slices of 20 mm were used for normalizing procedure and for obtaining martensitic structure by oil quenching. The specimens were sliced using METKON Metacut 251 Abrasive Cutter. Figure 3.2 illustrates how the slices were prepared and, Figure 3.3 shows the actual pieces and slices prior to heat treatments.

Figure 3.1. Heat treatment equipment used for experiments: MSE Furnace M1200 open atmosphere muffle furnace (left), PROTHERM Furnaces PCF 10/250/400 salt bath furnace (right)
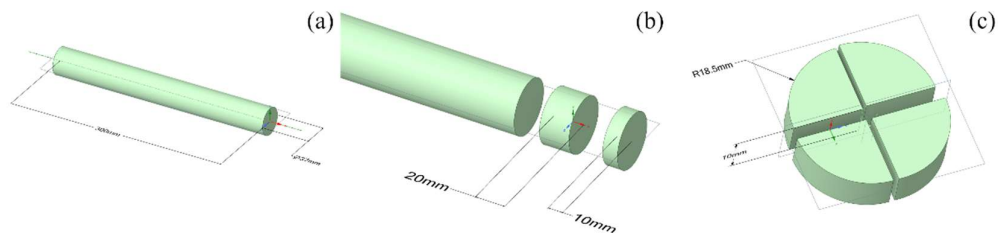
Figure 3.2. Illustration of the sectioning of the forged bar, drawn by the help of CAD software ANSYS® SpaceClaim®: (a) Original dimensions of the bar: Ø=37mm, L = 300mm, (b) Slices cut from the bar, (c) Sectioned slices to be heat-treated in different temperatures and/or durations
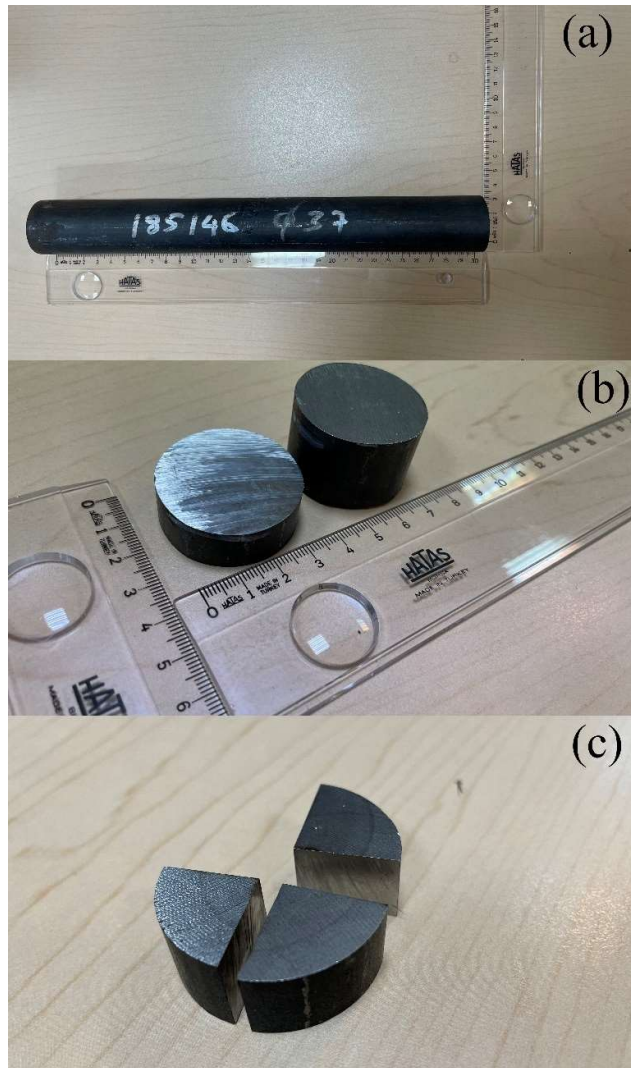
Figure 3.3. (a) As received bar shown with ruler as scale, (b) 10 cm and 20 cm slices shown with ruler as scale, (c) Sectioned slices to be heat-treated in different temperatures and/or durations

3.2.2 Parameters

The isothermal heat treatment parameters are determined from the calculated TTT curve of the steel. The TTT curve is calculated using JMatPro® 7.0 software. All specimens were austenitized at 1150°C for 45 minutes. The isothermal heat treatment temperatures were determined from the calculated TTT curve and the isothermal holding time was selected according to the 0.1% Bainite and 99.9% Bainite lines obtained from the TTT curve. But for some of the temperatures, holding times longer than 99.9% Bainite were applied to confirm that the calculated diagrams are in agreement with real experimental data. For lower temperatures, intermediate holding times were applied to study the bainitic-martensitic mixtures. Isothermal holding temperatures are selected as 360°C (just above M_s), 380°C, 400°C, and 420°C. After all isothermal heat treatments the specimens are quenched in oil. To observe martensitic structures, the steel is directly quenched into oil from the austenitization temperature. Normalizing is applied by cooling a sample in air after removing it from the furnace and simply letting the steel cool in air without any interruption.

3.3 Microstructural Characterization

Microstructural characterization was performed by preparing the specimen slices for metallographic examination under for optical microscopy and SEM. After isothermal heat treatment, all samples were sectioned using the Buehler Isomet 5000 Linear Precision Saw. The samples are cut from the middle so that the decarburized layer can be discarded. The sectioning is illustrated in Figure 3.4.
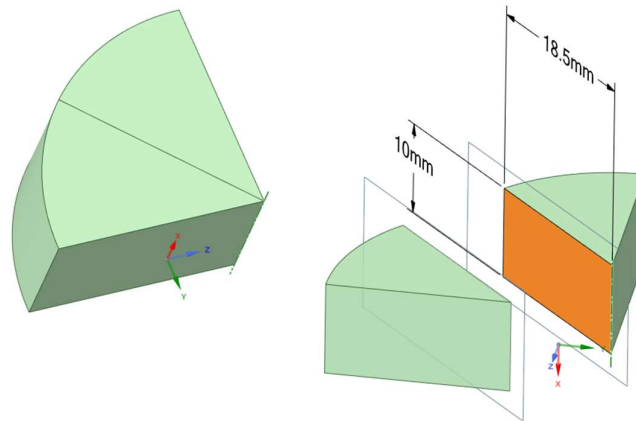
Figure 3.4. Sectioning of the heat-treated sample (left and surface to be prepared for microstructural examination (right, highlighted in orange)

After sectioning the specimen, the pieces are mounted into bakelite by mounting press Metkon Ecopress 100. Then, metallographic specimens are prepared by complying to standard grinding and polishing procedures [77]. Silicon carbide waterproof abrasive papers were used for the grinding, starting from 220 grit down to 2000 grit in the following order: 220, 320, 400, 500, 600, 800, 1000, 1200, 1500, 2000. Metkon Forcipol 2V Grinder – Polisher and Metkon Gripo 2V Grinder – Polisher machines were used for grinding. Then, polishing is applied to the samples with the help of Presi Mecapol P230 Polisher and Metkon Forcipol 2V Grinder – Polisher. Metkon FEDO-6J and FEDO-1S polishing cloths, Metkon Diapat-P water-based polycrystalline diamond suspension of 6 μm and 1 μm, and Metkon Diapat water-based diamond lubricant were used to polish the specimens.

2% Nital is used to etch and reveal the microstructure of specimens. Etching time for optical microscopy is around 8 seconds, and for SEM imaging, around 10 seconds. The etching time for martensitic specimens were longer, around 15 seconds.

Optical microscopy was performed by using Nikon Eclipse E200 and SEM imaging was performed by using FEI Nova NanoSEM 430 scanning electron microscope. Fractography for fractured tensile test specimens was also performed using the same SEM.

3.4 Quantitative Phase Analysis

X-Ray Diffraction was used for quantitative phase analysis. The integrated intensities of ferrite and retained austenite peaks in the XRD data can provide the respective amounts of each phase in volume percent. The specimens for XRD are prepared akin to the metallographic samples and complying with the ASTM E975-13 standard practice [78], but at the final step, repetitive polishing (with 1 μm diamond suspension) and etching is applied to remove the plastically deformed layers since some of the retained austenite might transform due to plastic deformation in prior grinding polishing and this may affect the quantitative analysis. Also, a smoother specimen surface provides XRD data with less background noise. The specimens were sectioned using Buehler Isomet 5000 Linear Precision Saw.

The XRD measurements are performed using Rigaku DMAX 2200 diffractometer with a fixed monochromator and Cu-Kα radiation of λ=1.5406 Å, with an operating voltage of 40 kV and an operating current of 30 mA. The specimens are scanned between 20º-140º (2θ) with a scan rate of 0.5º/min, in accordance with the ASTM E975-13 standard practice [78]. The data obtained from XRD measurement is then fed into the GSAS-II software to apply Rietveld Refinement so that phase fractions can be calculated from integrated intensities of the ferrite and austenite peaks [79].

The amount of blocky M/A amongst various specimens is compared using image analysis. The optical micrographs of the samples are analyzed using ImageJ software Thresholding feature, the area fraction of white islands of blocky M/A is calculated. Both low and high magnification micrographs are analyzed to compare microstructures so that a representative qualitative and quantitative analysis can be made.

3.5 Mechanical Characterization

3.5.1 Hardness Measurements

Hardness measurements were performed in accordance with the ASTM E92-17 standard [80]. The measurements are taken from the metallographic specimens mounted into bakelite, and they were performed with EMCO Test M4U-025 Universal Digital Hardness Testing Machine, using Vickers indenter under 30kgf load. Specimens were tested in as-polished condition since the standard dictates as such [80]. At least 5 indentations were performed for each specimen and arithmetic mean values with their standard deviation is calculated.

3.5.2 Tensile Tests

Tensile test specimens were machined from heat-treated bars, and tests were performed in compliance with the ASTM E8/E8M-21 standard, where the test speed was 0.54 mm/min until the yielding point and 4 mm/min after yielding [81]. 2 specimens were tested for isothermal transformation temperatures of interest and for air cooling and isothermal holding time was fixed at 24 hours for all samples. Figure 3.5 shows a photo of tensile test specimen and its technical drawing. The specimens were machined in a 3-axis Yang SL-20 CNC Linear Way lathe. Tensile tests were performed using BESMAK BMT-100E servo electromechanical universal testing machine.
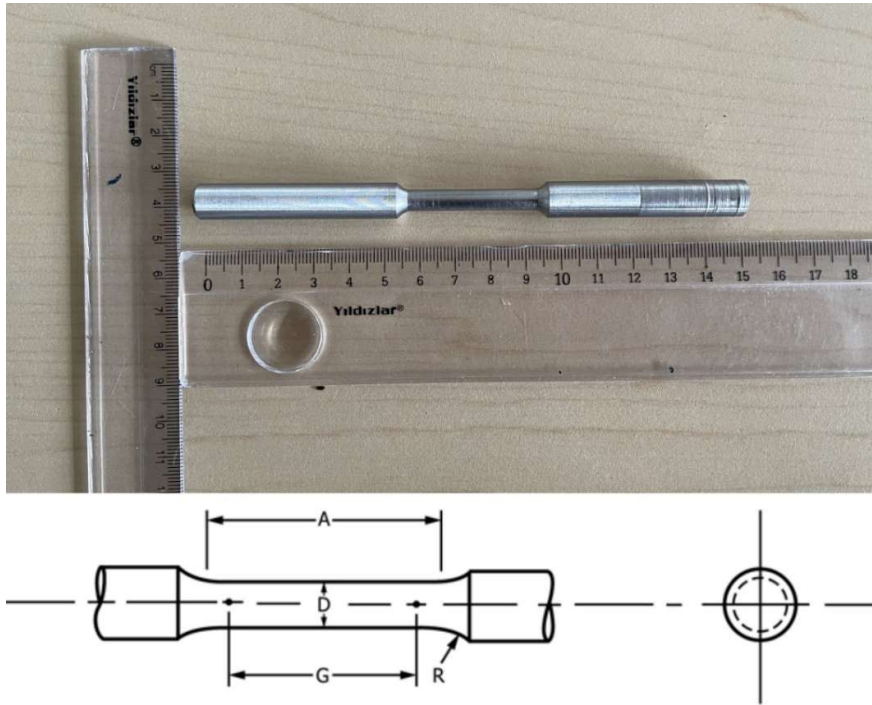
Figure 3.5. Photograph of the tensile test specimen (top) and the technical drawing (bottom) [80].
The dimensions are D = 6mm, A = 36mm, G = 30mm, R = 6mm

3.5.2.1 Fractography

The fractography analysis was conducted after the tensile tests. The tensile test fracture surfaces were cut from each sample using Buehler Isomet 5000 Linear Precision Saw. The fracture surfaces are cleaned in an ultrasonic bath, submerged in isopropyl alcohol.

CHAPTER 4

EXPERIMENTAL RESULTS

The isothermal transformation diagram is constructed using JMatPro® software and isothermal transformation temperatures and holding times are selected based on the calculated TTT diagram. The result of each experiment is characterized in terms of microstructure, volume of phases, and mechanical properties.

4.1   Isothermal Transfomation (TTT) Data

Isothermal transformation diagram of the steel is required to determine the isothermal transformation temperature and time, and to produce the desired bainitic, martensitic, and bainitic-martensitic structures. JMatPro® software is used to calculate the TTT diagram of the steel. The TTT diagram is given in Figure 4.1.

The data obtained from the calculated TTT curve suggests that the M_s temperature is 357°C and M_{90} is 242°C for this steel. Hence, the lowest isothermal transformation temperature is selected as 360°C since isothermal transformations which are just above the M_s temperature is proven to give a lower bainitic microstructure with superior mechanical properties [50]. To study the effect of transformation temperature to the microstructure morphology and mechanical properties, the transformation temperature is increased with an increment of 20°C, up to and including 420°C. The isothermal holding time for each temperature is determined from the data points and C-curves plotted on the diagram such that it corresponds to 0.1% Bainite and 99.9% Bainite. For 360°C, bainite starts to form after approximately 35 minutes and fully bainitic structure is predicted to be obtained, by extrapolation, after 24 hours. Table 4.1 summarizes the isothermal transformation temperature (ITT) and time data obtained from the calculated TTT diagram.
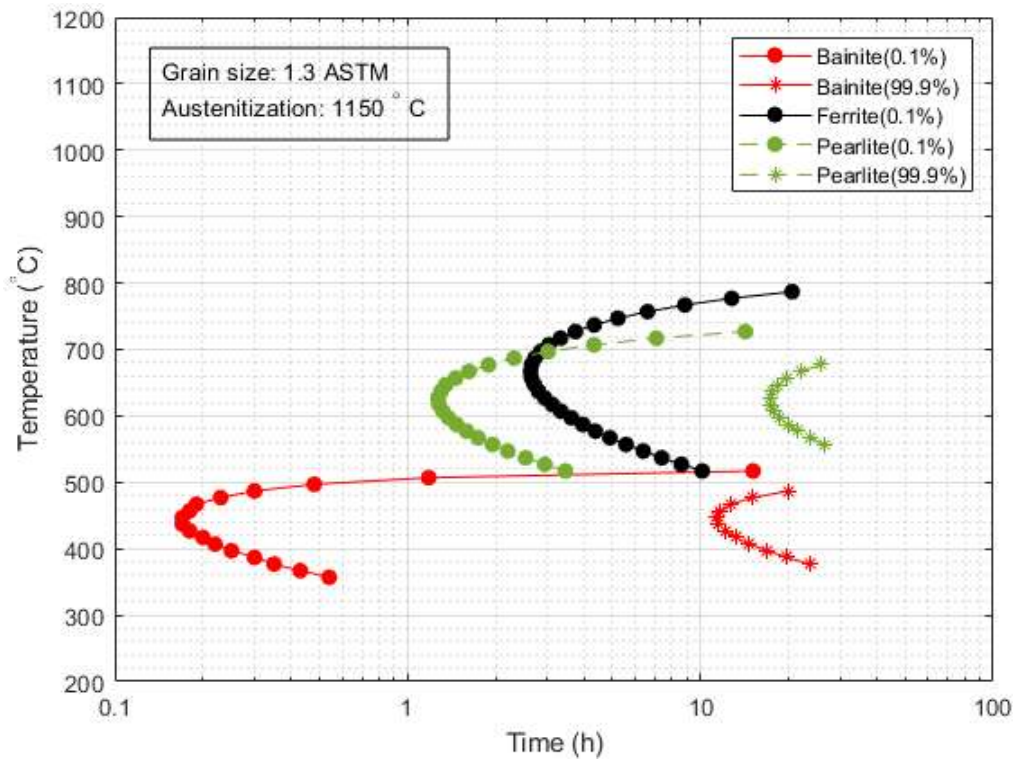
Figure 4.1. Calculated TTT diagram obtained from JMatPro® of the low carbon microalloyed steel.

Table 4.1 ITT selected for the study and their respective 0.1%B and 99.9%B times

Isothermal Transformation Temperature (ºC)	0.1% Bainite Time (hours)	99.9% Bainite Time (hours)
360	0.58	24
380	0.66	24
400	0.25	16
420	0.25	12

44

4.1.1 Heat Treatment Routes

The heat treatment routes are planned such that observations on bainitic and bainitic-martensitic microstructures are made in detail, and they are planned as described in the Experimental Procedure Section 3.2.2. Figure 4.2 (a) shows the heat treatment routes and the TTT diagram of the steel, the x-axis is given in terms of hours instead of seconds for visual clarity. Table 4.2 shows the list of isothermal holding temperatures and times and the label for each treatment.

For all heat treatment routes, austenitization starts at $1150^{\circ}C$ and lasts for 45 minutes. The austenitization temperature is selected such that the forging condition is simulated. The isothermal holding temperatures are selected so that the expected resulting microstructure is only lower bainite. For the bainitic-martensitic mixtures, a holding time of 12 hours is applied for $360^{\circ}C$, $380^{\circ}C$, and $400^{\circ}C$. For $360^{\circ}C$ a holding time of 30 hours, for $400^{\circ}C$ a holding time of 24 hours, and for $420^{\circ}C$ a holding time of 24 hours were applied, respectively, to verify whether the prediction of the calculated TTT diagram was accurate.

4.2 T_0 Curve

The T_0 curve for the forging steel was constructed using ThermoCalc ® 2018b TCFE9 database. The composition listed in Table 3.1 is fed into the software. The calculation results are given in Figure 4.2 (c).

(a)

(b)
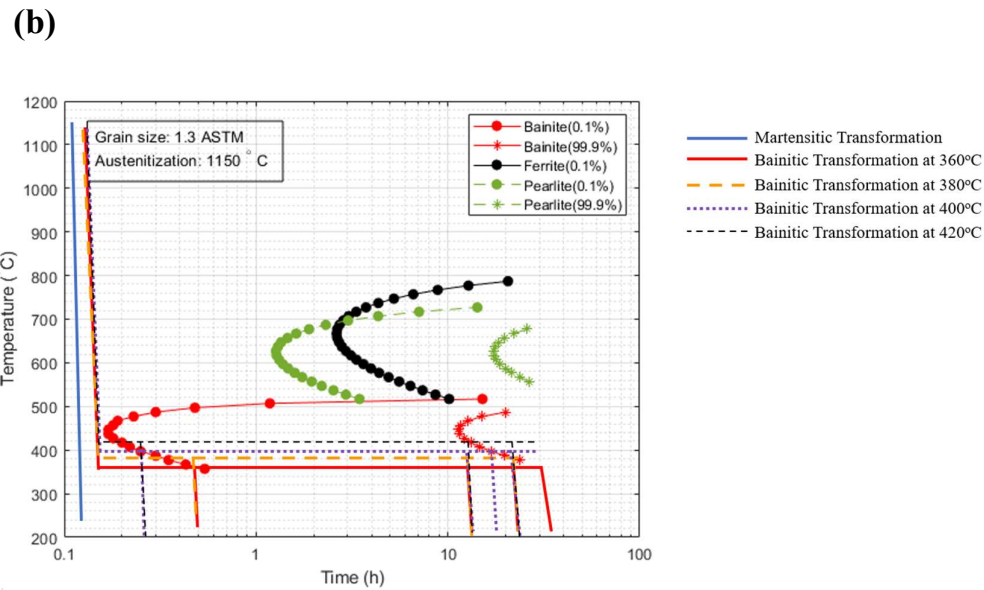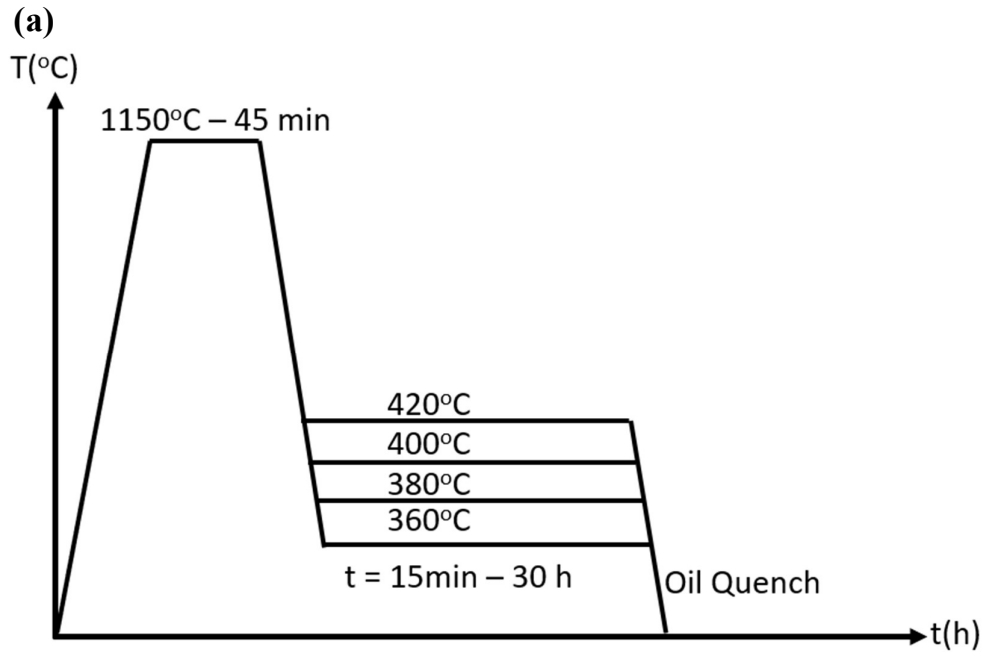
Figure 4.2. The heat treatment routes for bainitic transformations to be studied of the low carbon microalloyed steel and the T_0 curve. (a) Temperature vs time plot of the heat treatment schedules, not to scale. (b) Heat treatment routes superimposed on the TTT diagram. (c) T_0 curve of the forging steel. Y axis is Temperature in Kelvin, X axis is carbon concentration in weight fraction

2022.04.20.00.00.59
TCFE9: AL, B, C, CR, CU, FE, MN, MO, N, NB, P, S, SI, TI, V
T=690.468, W(SI)=1.3E-2, W(MN)=1.46E-2, W(CR)=1.25E-2, W(MO)=2.5E-3, W(P)=1E-4, W(S)=6.6E-4, W(V)=1E-4, W(TI)=1.58E-4, W(NB)=3.6E-4, W(N)=3.3E-5, W(AL)=1E-4, W(CU)=3E-4, W
(B)=2.7E-5, P=1E5, N=1.
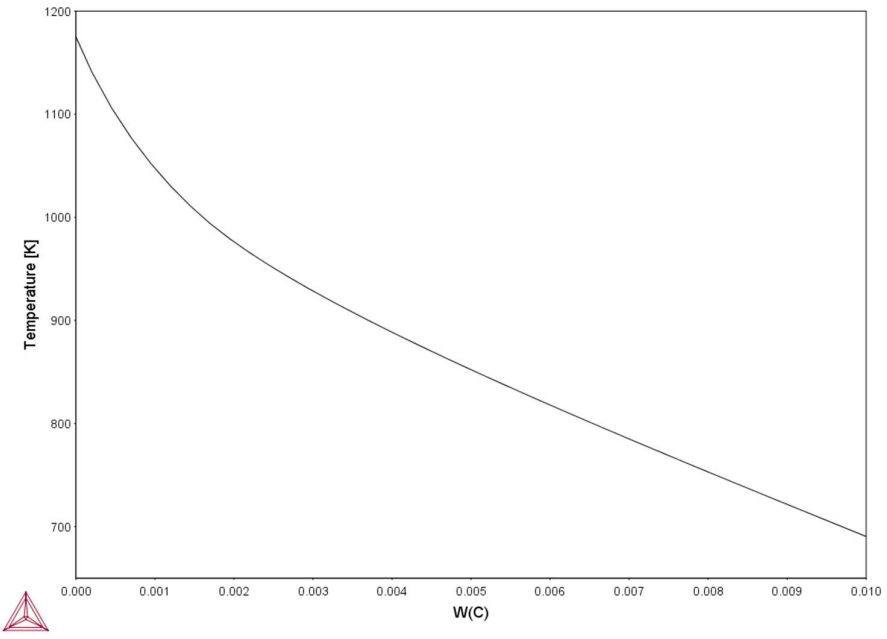
Figure 4.2. (continued)

Table 4.2 Isothermal heat treatment temperatures and times

	Isothermal Holding Temperature (ºC)	Isothermal Holding Time	Label
Austenitization at 1150ºC for 45 minutes	360	35 minutes	360C-35min
		12 hours	360C-12h
		24 hours	360C-24h
		30 hours	360C-30h
	380	40 minutes	380C-40min
		12 hours	380C-12h
		24 hours	380C-24h
	400	15 minutes	400C-15min
		12 hours	400C-12h
		16 hours	400C-16h
		24 hours	400C-24h
	420	15 minutes	420C-15min
		12 hours	420C-12h
		24 hours	420C-24h

4.3 Microstructural Characterization

4.3.1 Optical Microscopy Examination

4.3.1.1 As Received Microstructure

The as received microstructure of the steel is given in Figure 4.3 at low and high magnification under optical microscope. The microstructure consists of bainite and blocky martensite/austenite (white contrasted M/A regions are shown with an arrow). No carbide precipitation is observed under optical microscope but the inclusions due to alloying are clearly visible. The morphology of the inclusions indicates the rolling direction. The morphology of the bainitic structures appear to be in granular bainite and acicular ferrite and the internal structure of blocky M/A cannot be resolved clearly under optical microscope, so SEM is required for a better identification.

4.3.1.2 Martensitic Transformation Microstructure

The optical micrograph of oil quenched samples is given in Figure 4.4. The resulting microstructure is fully martensite with lath-type morphology. No carbide precipitation is observed under optical microscope. The orientation is observed to be random for the martensitic transformation. Inclusions resulting from alloying can be seen in both images.

4.3.1.3 Normalized Microstructure

The resulting microstructure was examined under optical microscope at low and high magnifications, which is given in Figure 4.5. The air-cooled steel has more blocky M/A white regions in terms of area fraction. The bainite is also clearly visible in both

images, however a detailed microstructural study needs SEM imaging. The inclusions can be observed clearly in both images.
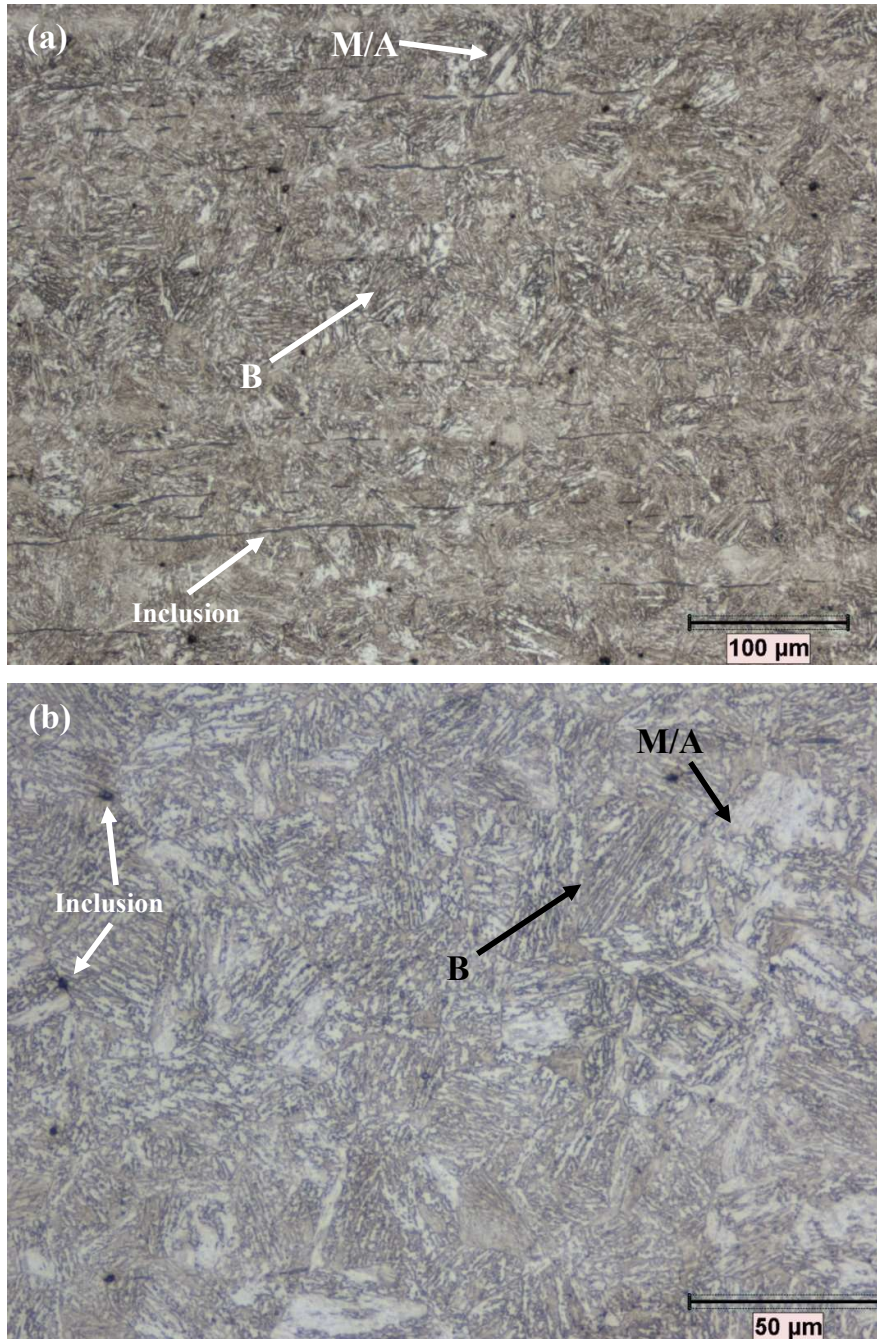
Figure 4.3. The as received microstructure of the microalloyed steel observed under optical microscope at (a) low and (b) high magnification. B: bainite, M/A: Martensite/Austenite
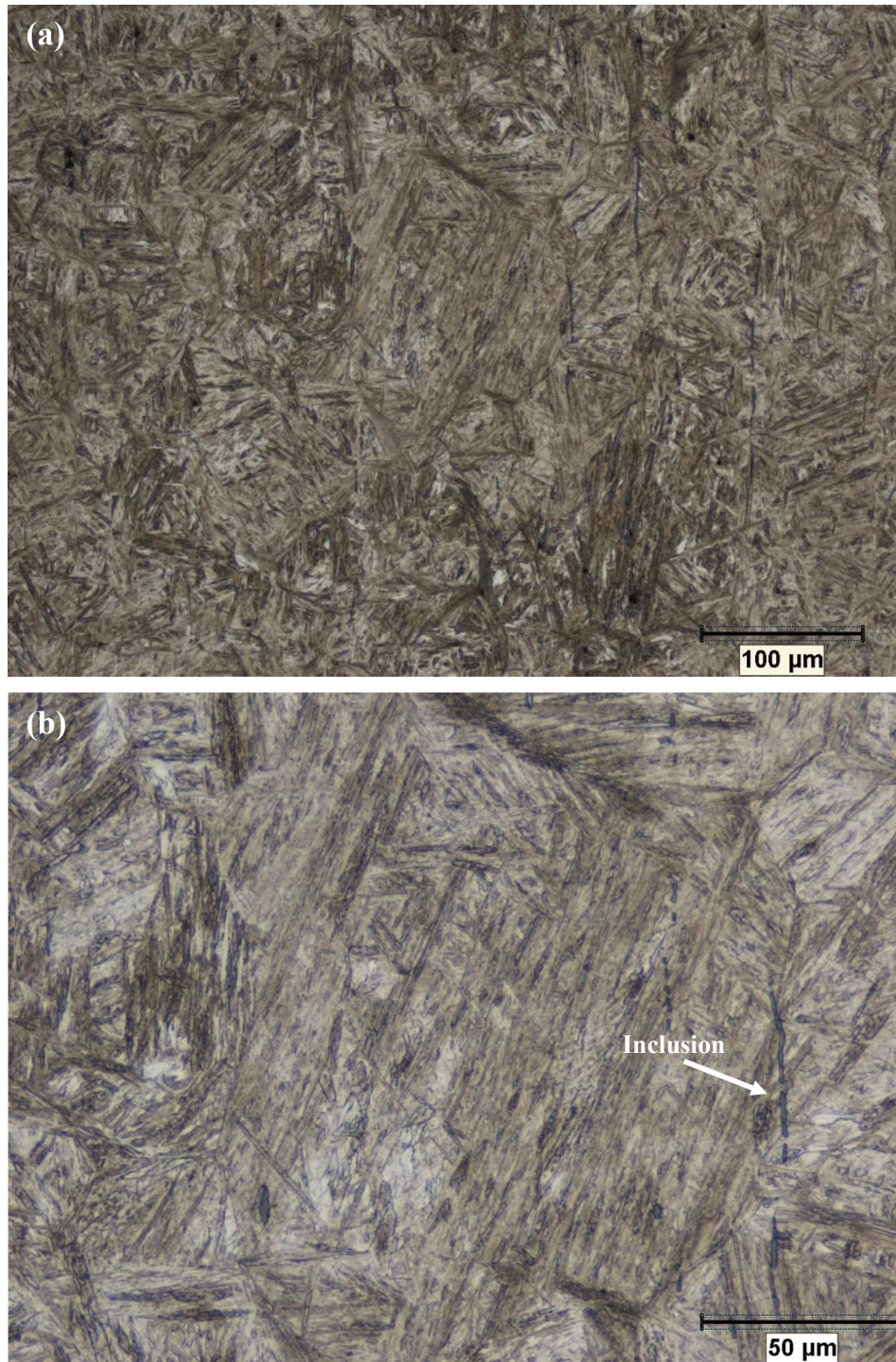
Figure 4.4. The martensite of the microalloyed steel observed under optical microscope at (a) low magnification and (b) high magnification, specimen was directly quenched in oil.
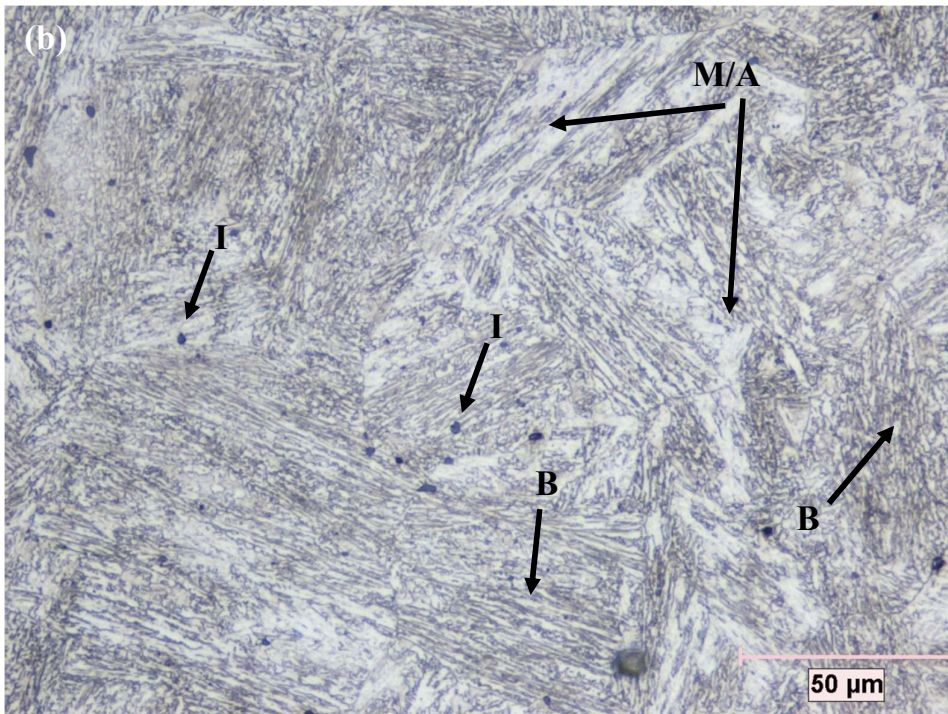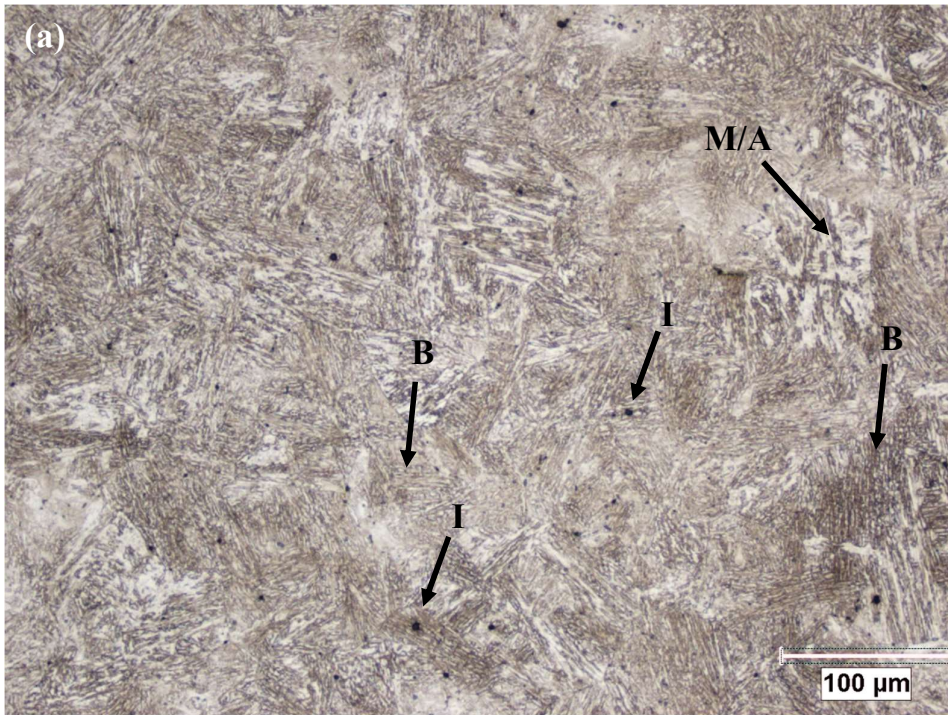
Figure 4.5. The normalized microstructure of the microalloyed steel observed under optical microscope at (a) low and (b) high magnification, specimen was cooled in air. B: bainite, M/A: martensite/austenite, I: inclusion

4.3.1.4 Isothermally Transformed Microstructures

Isothermal transformations were conducted at 360ºC, 380ºC, 400ºC, and 420ºC for various durations. In all optical micrographs of isothermally transformed specimens, bainitic phase (in the form of dark needles) and blocky M/A islands (as white regions) are observed. However, the resolution of optical micrography is not high enough to observe the structures formed inside M/A islands and to resolve the morphology of bainite. Inclusions are present in all samples as remnants of alloying and forging.

4.3.1.4.1 Isothermal Transformation at 360ºC

The isothermal bainitic transformation at 360ºC is predicted to start after holding for 35 minutes and finish after holding for 24 hours by TTT diagram in Figure 4.1. But the finish time was obtained by means of extrapolation so a longer holding time of 30 hours was applied to observe whether the prediction was correct. In addition, an intermediate time of 12 hours was selected to observe the bainitic-martensitic mixture at 360ºC.

Figure 4.6, Figure 4.7, Figure 4.8, and Figure 4.9 show the microstructures of the isothermally transformed samples at 360ºC under optical microscope at low and high magnifications for a holding time of 35 minutes, 12 hours, 24 hours, and 30 hours, respectively. In all micrographs, the needle-like bainitic phase and white islands of blocky M/A are clearly observed. Furthermore, as the holding time is increased, the amount of white M/A regions decreased.

The high magnification optical microscopy images of 360C-35min and 360C-12h show an interrupted, granular, bainitic morphology (Figure 4.6 and Figure 4.7) but optical microscopy might be insufficient for resolving the bainitic morphology, hence SEM examination is required for these specimens. At high magnification images, prior austenite grain boundaries are visible. (Figure 4.6(b), Figure 4.7(b), Figure 4.8(b), and Figure 4.9(b))

Figure 4.6. The microstructure of the microalloyed steel isothermally transformed at 360°C for 35 minutes observed under optical microscope at (a) low and (b) high magnification. B: bainite, GB: granular bainite, M/A: martensite/austenite, I: inclusion

Figure 4.7. The microstructure of the microalloyed steel isothermally transformed at 360°C for 12 hours observed under optical microscope at (a) low and (b) high magnification. B: bainite, GB: granular bainite, M/A: martensite/austenite, I: inclusion

Figure 4.8. The microstructure of the microalloyed steel isothermally transformed at 360°C for 24 hours observed under optical microscope at (a) low and (b) high magnification. B: bainite, M/A: martensite/austenite, I: inclusion
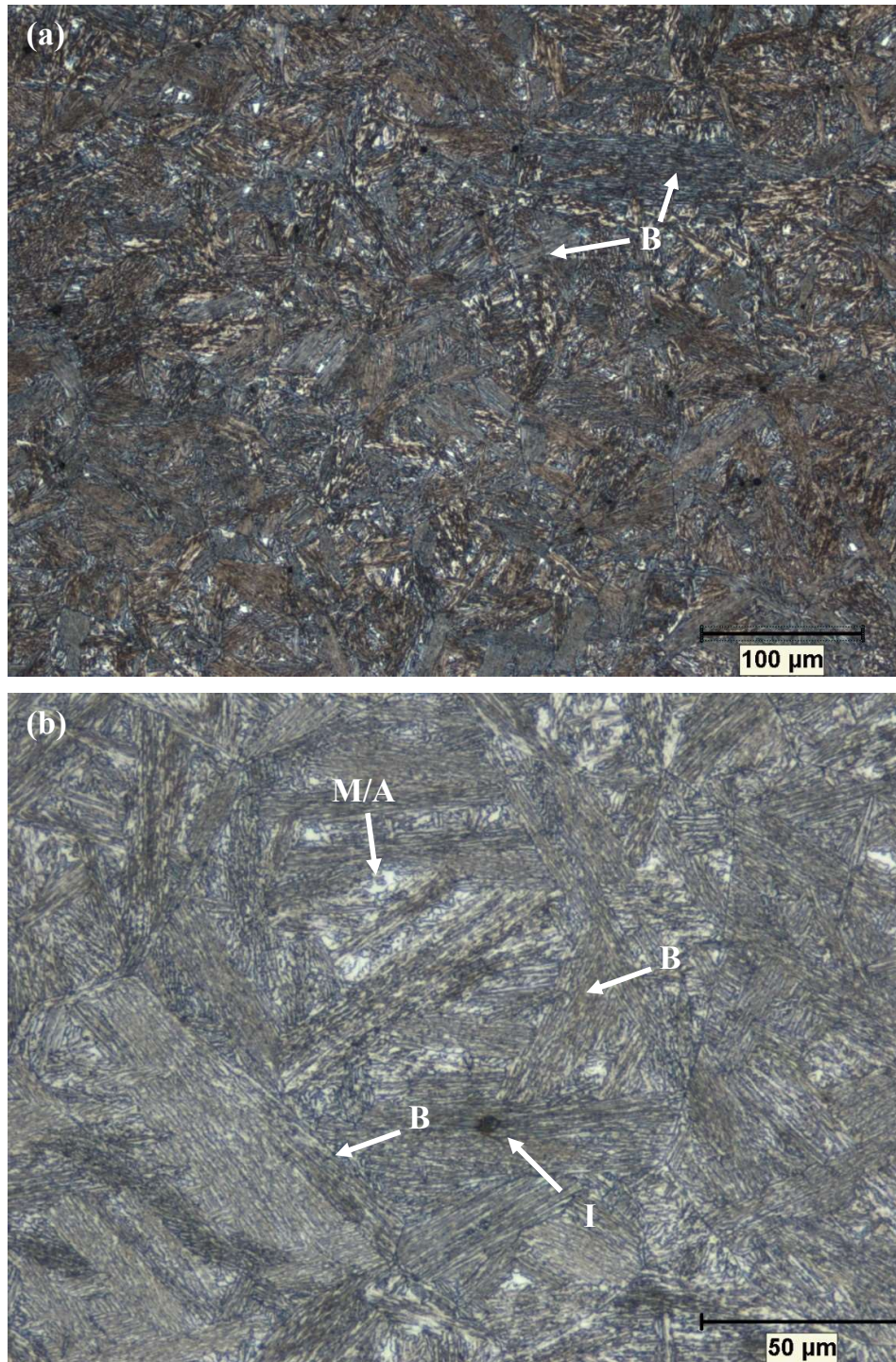
Figure 4.9. The microstructure of the microalloyed steel isothermally transformed at 360°C for 30 hours observed under optical microscope at (a) low and (b) high magnification. B: bainite, M/A: martensite/austenite, I: inclusion

4.3.1.4.2   Isothermal Transformation at 380°C

Isothermal transformation at 380°C is predicted to start after holding for 40 minutes and finish after holding for approximately 24 hours by TTT diagram in Figure 4.1. An intermediate holding time of 12 hours was also applied to observe bainitic-martensitic mixtures.

Figure 4.10, Figure 4.11, and Figure 4.12 show the optical micrographs at low and high magnifications of isothermally transformed samples held at 380°C for 40 minutes, 12 hours, and 24 hours, respectively. Micrographs of all samples show the needle-like bainitic microstructure along with granular bainite and white blocky M/A regions. As the holding time is increased, the amount of white M/A regions decreased.

Compared to the isothermal transformation performed at 360°C, the amount of white blocky M/A phase is observed to be approximately the same or somewhat higher.

SEM imaging is required for these specimens as well since the internal structure of the blocky M/A islands are not visible under optical microscope.

Prior austenite grain boundaries are visible in high magnification images, as in Figure 4.12(b).
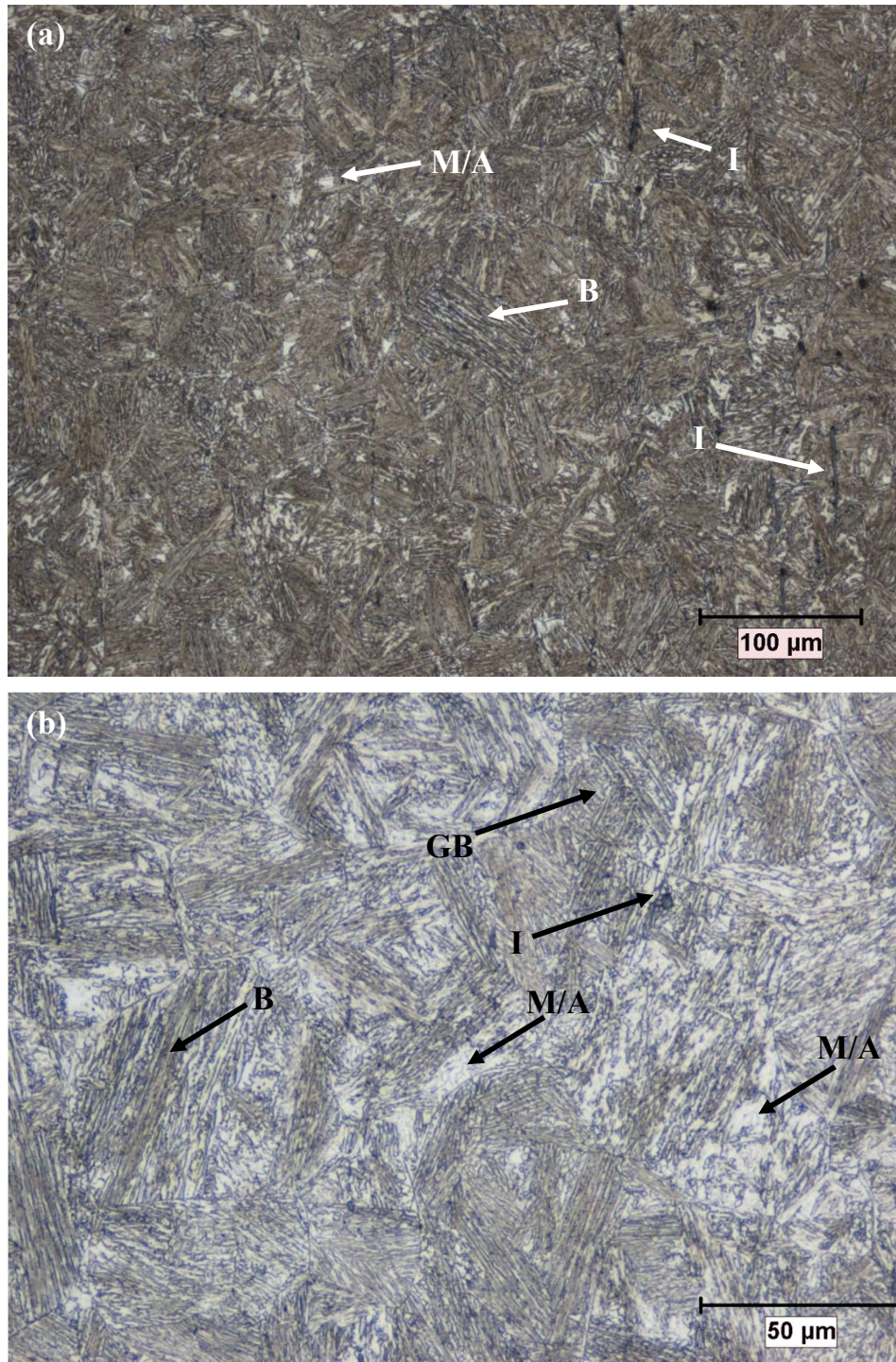
Figure 4.10. The microstructure of the microalloyed steel isothermally transformed at 380°C for 40 minutes observed under optical microscope at (a) low and (b) high magnification. B: bainite, GB: granular bainite, M/A: martensite/austenite, I: inclusion

Figure 4.11. The microstructure of the microalloyed steel isothermally transformed at 380°C for 12 hours observed under optical microscope at (a) low and (b) high magnification. B: bainite, M/A: martensite/austenite, I: inclusion

Figure 4.12. The microstructure of the microalloyed steel isothermally transformed at 380°C for 24 hours observed under optical microscope at (a) low and (b) high magnification. B: bainite, M/A: martensite/austenite, I: inclusion

4.3.1.4.3   Isothermal Transformation at 400ºC

Calculated TTT diagram in Figure 4.1 suggests that isothermal transformation at 400ºC will start after 15 minutes and finish after 16 hours of holding. A longer holding time of 24 hours was also applied to see whether the prediction was right. In addition, an intermediate holding time of 12 hours was chosen to study the bainitic-martensitic mixture at 400ºC.

Figure 4.13, Figure 4.14, Figure 4.15, and Figure 4.16 show the microstructures of isothermally transformed samples at 400ºC under optical microscope at low and high magnifications for 15 minutes, 12 hours, 16 hours, and 24 hours, respectively. Needle-like bainitic phase and large white islands of blocky M/A can be seen in all micrographs. Most of the bainitic microstructures are in needle-like form but some regions seem to be in granular form. Again, SEM study is required.

The transformation at 400ºC resulted in an increase of the blocky M/A regions compared to the transformations at 360ºC and 380ºC.

Prior austenite grain boundaries are visible at high magnification images, as in Figure 4.15(b).

Figure 4.13. The microstructure of the microalloyed steel isothermally transformed at 400°C for 15 minutes observed under optical microscope at (a) low and (b) high magnification. B: bainite, M/A: martensite/austenite. The bainite in needle morphology is marked in the micrograph as NB.

Figure 4.14. The microstructure of the microalloyed steel isothermally transformed at 400°C for 12 hours observed under optical microscope at (a) low and (b) high magnification. B: bainite, GB: granular bainite, M/A: martensite/austenite. Notice the increase in white blocky M/A islands.

Figure 4.15. The microstructure of the microalloyed steel isothermally transformed at 400°C for 16 hours observed under optical microscope at (a) low and (b) high magnification. B: bainite, GB: granular bainite, NB: needle bainite, M/A: martensite/austenite. Notice the increase in white blocky M/A islands.

Figure 4.16. The microstructure of the microalloyed steel isothermally transformed at 400ºC for 24 hours observed under optical microscope at (a) low and (b) high magnification. GB: granular bainite, NB: needle bainite, M/A: martensite/austenite. Notice the increase in white blocky M/A islands.

4.3.1.4.4 Isothermal Transformation at 420ºC

For the isothermal transformation at 420ºC, the calculated TTT diagram gives the bainite start time as 15 minutes and finish time as 12 hours. As was the case with the previous isothermal experiments, a longer holding time of 24 hours was also conducted.

Figure 4.17, Figure 4.18, and Figure 4.19 show the microstructures of the samples isothermally heat-treated at 420ºC for durations of 15 minutes, 12 hours, and 24 hours, respectively, under optical microscope at low and high magnifications. Needle-like and granular-like bainitic structures and white blocky M/A islands are present in all images. SEM imaging is necessary to resolve the bainite morphology.

The transformation at 420ºC has the largest white M/A islands, when compared with micrographs of other samples, held at 360ºC, 380ºC, and 400ºC.

Figure 4.17. The microstructure of the microalloyed steel isothermally transformed at 420ºC for 15 minutes observed under optical microscope at (a) low and (b) high magnification. B: bainite, M/A: martensite/austenite. Notice the increase in white blocky M/A islands.

Figure 4.18. The microstructure of the microalloyed steel isothermally transformed at 420°C for 12 hours observed under optical microscope at (a) low and (b) high magnification. B: bainite, M/A: martensite/austenite, I: inclusion. Notice the increase in white blocky M/A islands.
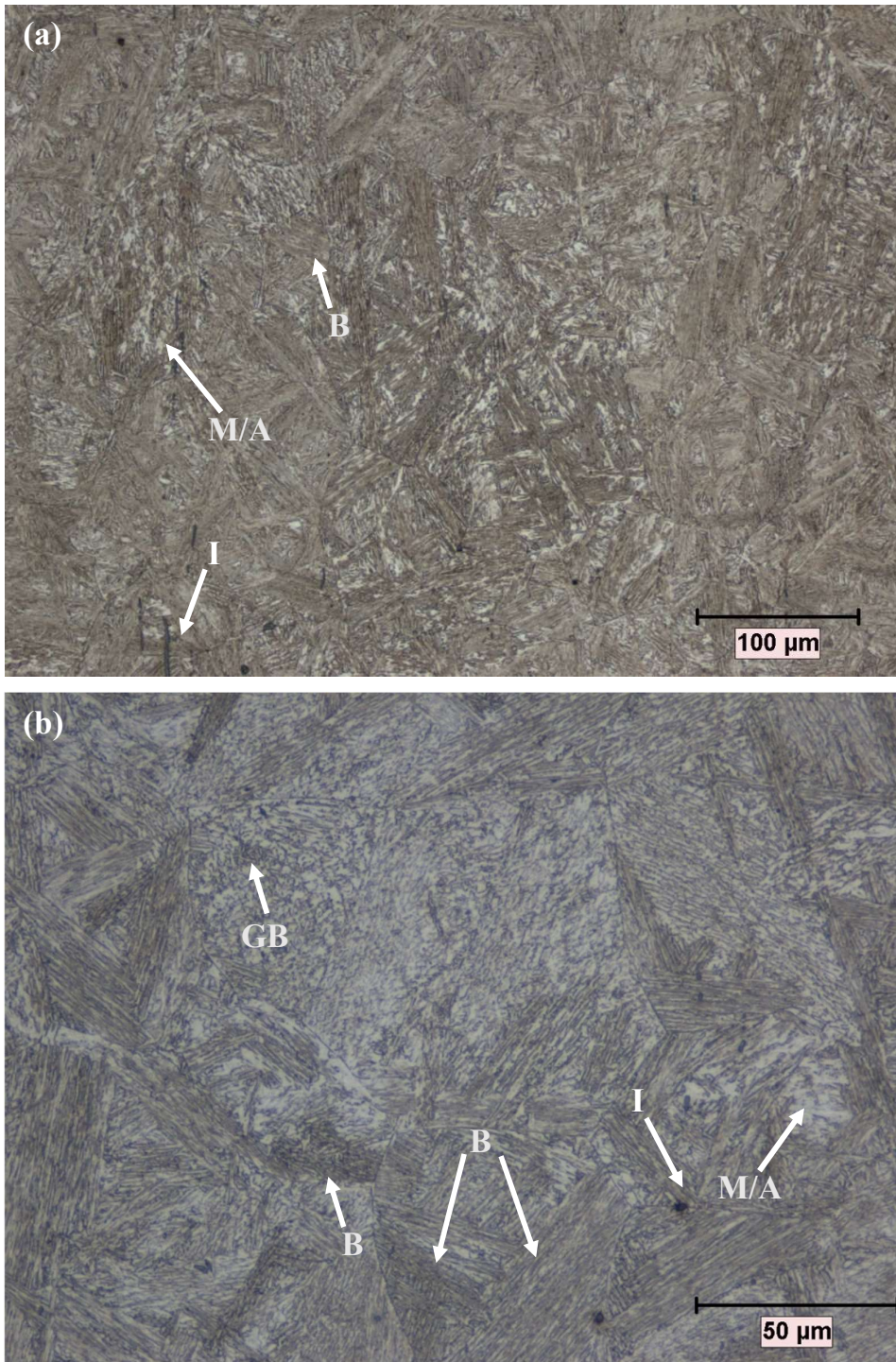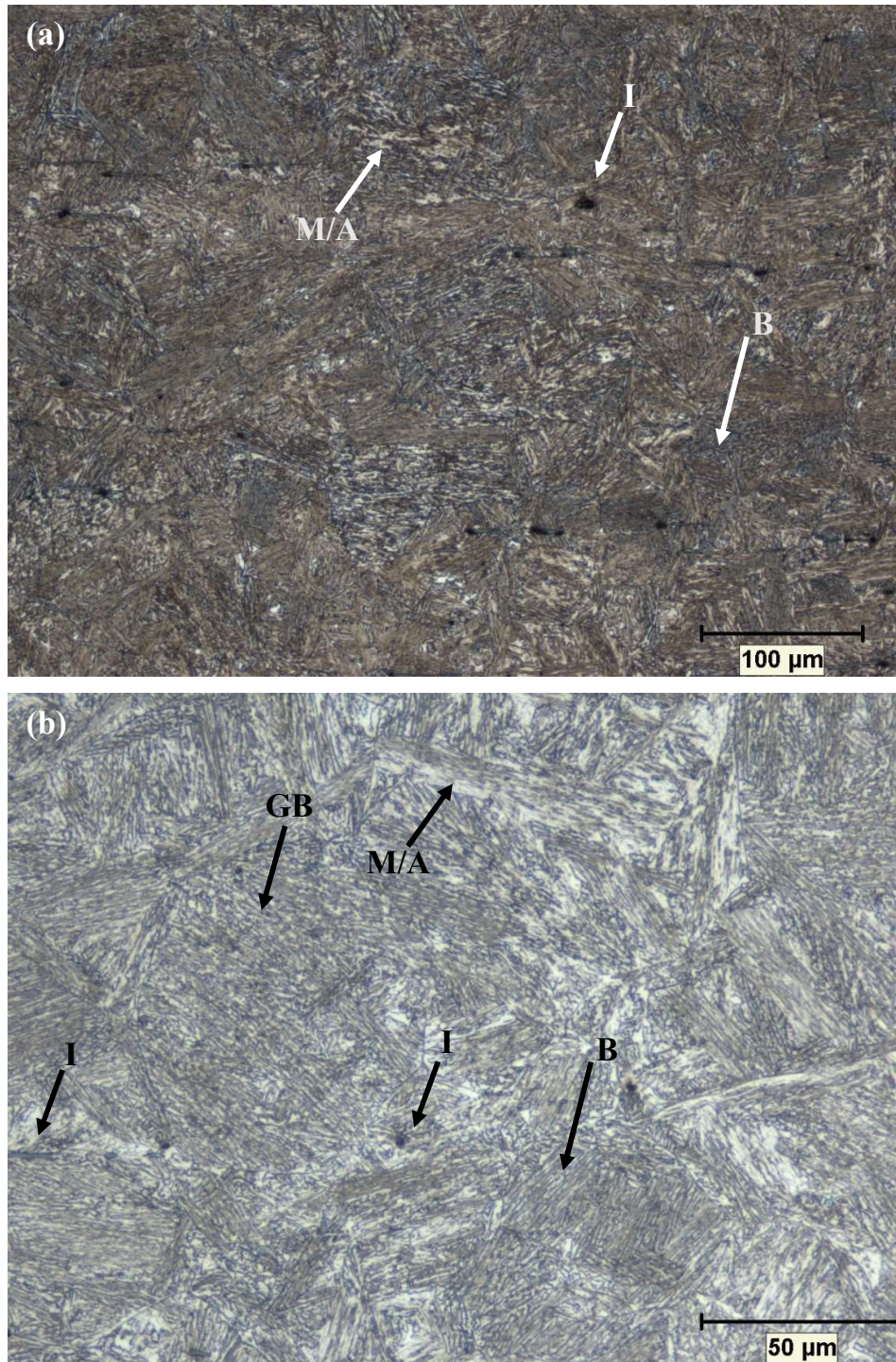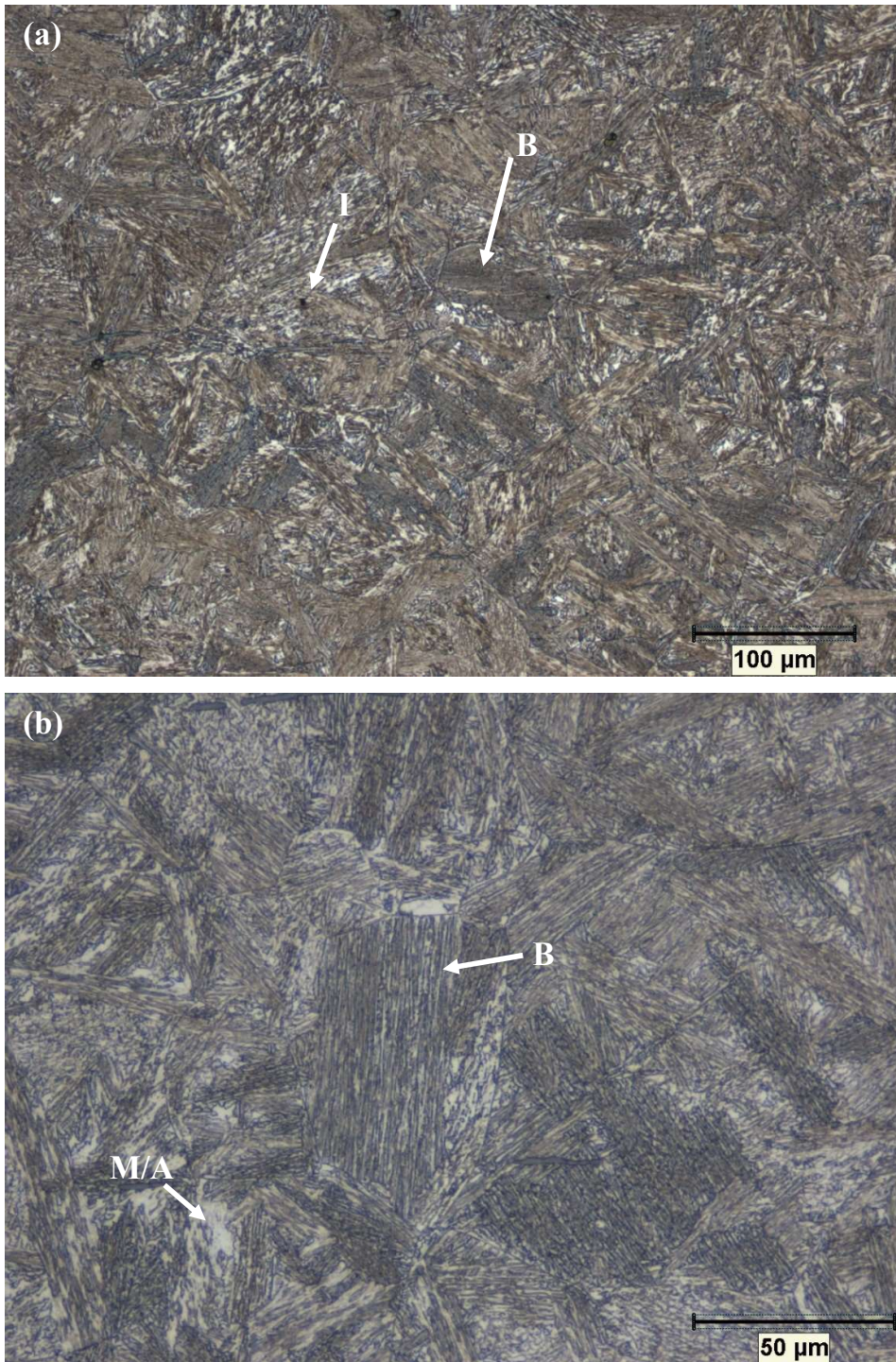
Figure 4.19. The microstructure of the microalloyed steel isothermally transformed at 420°C for 24 hours observed under optical microscope at (a) low and (b) high magnification. B: bainite, M/A: martensite/austenite, I: inclusion. Notice the increase in white blocky M/A islands.

4.3.2   Scanning Electron Microscopy Examination

The resolution of optical microscopes is not sufficient to observe all the microstructural features, such as the bainite morphology, the internal structure of M/A islands, and the presence of carbides and their morphology. Under SEM, the bainite is observed to be in needle-like lower bainite morphology, as expected. Flat blocky M/A islands are observed clearly in all images, but with varying amounts. The internal structure of M/A islands is not clear even under SEM but in several regions, some features are visible, which indicates a transformation has taken place within these islands. Prior austenite grain boundaries are distinctly visible at low magnification images. In none of the images, carbide precipitation is observed.

4.3.2.1   As Received Microstructure

The SEM images of as received steel are given in Figure 4.20. The microstructure consists of bainite and blocky M/A which are indicated on the images. The morphology of bainite is needle-like and the bainitic sheaves are visible at low magnifications. At high magnifications, there are features that can be considered as an indicator of martensitic transformation inside the blocky flat M/A islands. No carbide precipitation is present in any of the images.

4.3.2.2   Martensitic Transformation Microstructure

The SEM images samples that are directly quenched in oil after austenitization are given in Figure 4.21. The microstructure is fully martensitic, and the microstructure is clearly different from the normalized and isothermally treated samples. Martensite of this steel is in lath morphology. No carbide precipitation is present in any of the images.

4.3.2.3   Normalized Microstructure

SEM images of air-cooled sample are given in Figure 4.22. The microstructure consists of bainite and blocky flat M/A islands, as indicated on the images. At low magnifications, bainite sheaves are clearly observed. At high magnifications, the insides of the blocky M/A islands have a distinct morphology which is present in the as received and isothermally treated samples. The bainite formed by normalizing appears to be in needle-like lower bainite morphology. No carbide precipitation is observed in this sample.
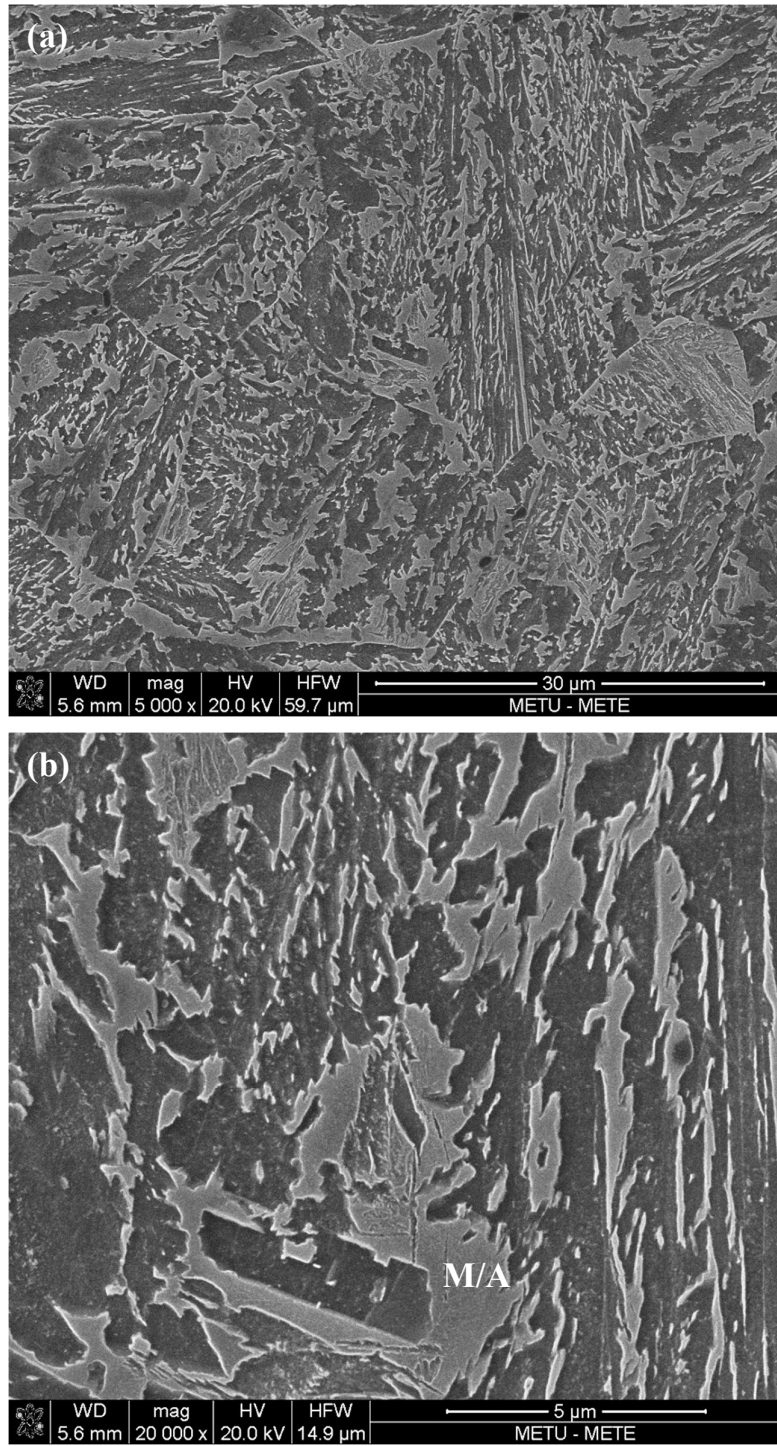
Figure 4.20. The as received microstructure of the microalloyed steel observed under SEM at (a) low magnification and (b) high magnification
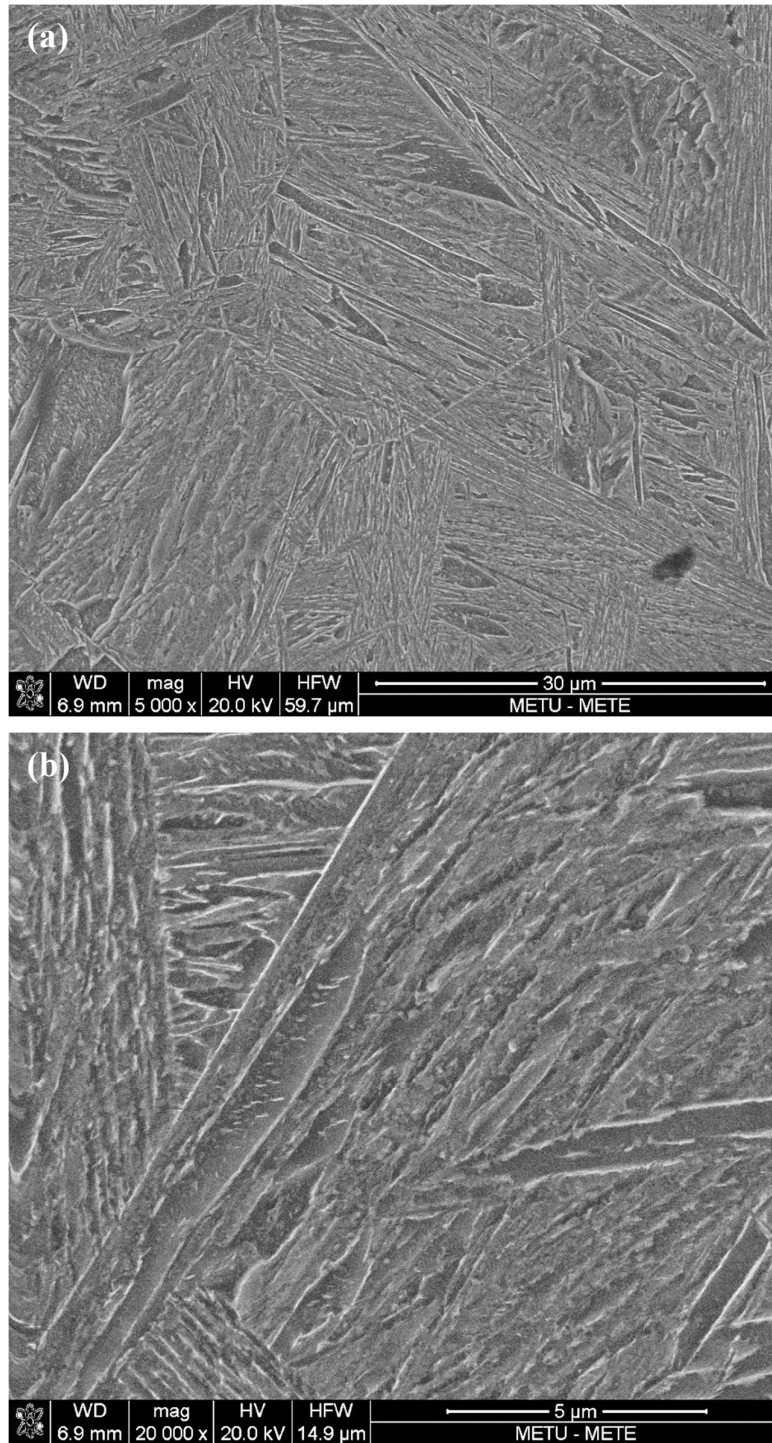
Figure 4.21. The martensite of the microalloyed steel observed under SEM at (a) low magnification and (b) high magnification. Specimen was directly quenched in oil.
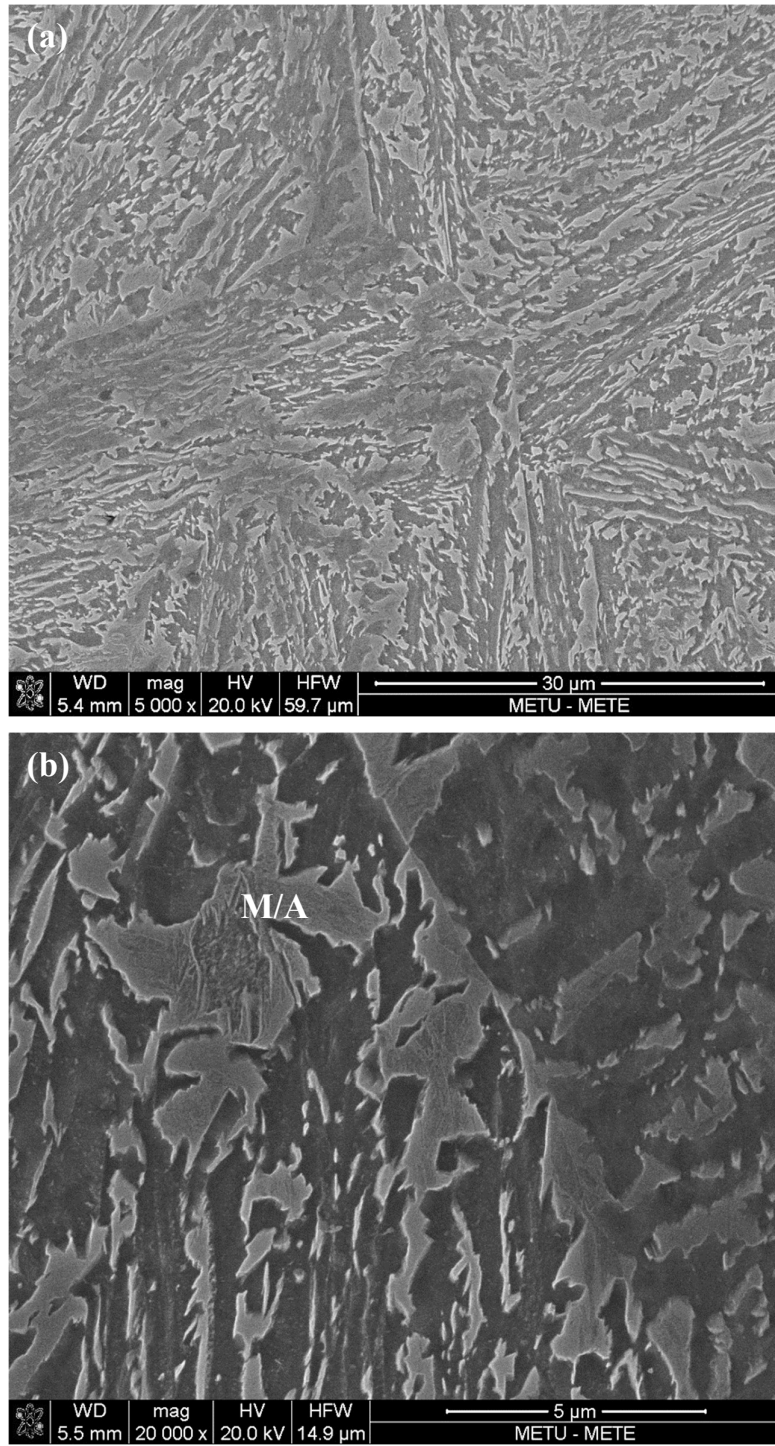
Figure 4.22. The normalized microstructure of the microalloyed steel observed under SEM at (a) low magnification and (b) high magnification.

4.3.2.4   Isothermally Transformed Microstructures

Isothermal transformations were applied at 360ºC, 380ºC, 400ºC, and 420ºC for various holding times. In all SEM images, bainitic sheaves and blocky M/A islands are present. The amount of M/A phase changes with the transformation temperature and holding time. The ITT also influenced the bainite sheave thickness.

4.3.2.4.1   Isothermal Transformation at 360ºC

Figure 4.23, Figure 4.24, Figure 4.25, and Figure 4.26 show the microstructures of the isothermally transformed samples at 360ºC under SEM at low and high magnifications for a holding time of 35 minutes, 12 hours, 24 hours, and 30 hours, respectively. In all SEM images, bainitic ferrite needles of lower bainite is present throughout the microstructure and blocky flat M/A islands are also observed, and as the holding time is increased, the amount of flat M/A regions decrease. No carbide precipitation is observed in any of the samples.

The bainite morphology of specimens 360C-35min and 360C-12h were thought to be granular but the SEM images clearly show a needle-like morphology.
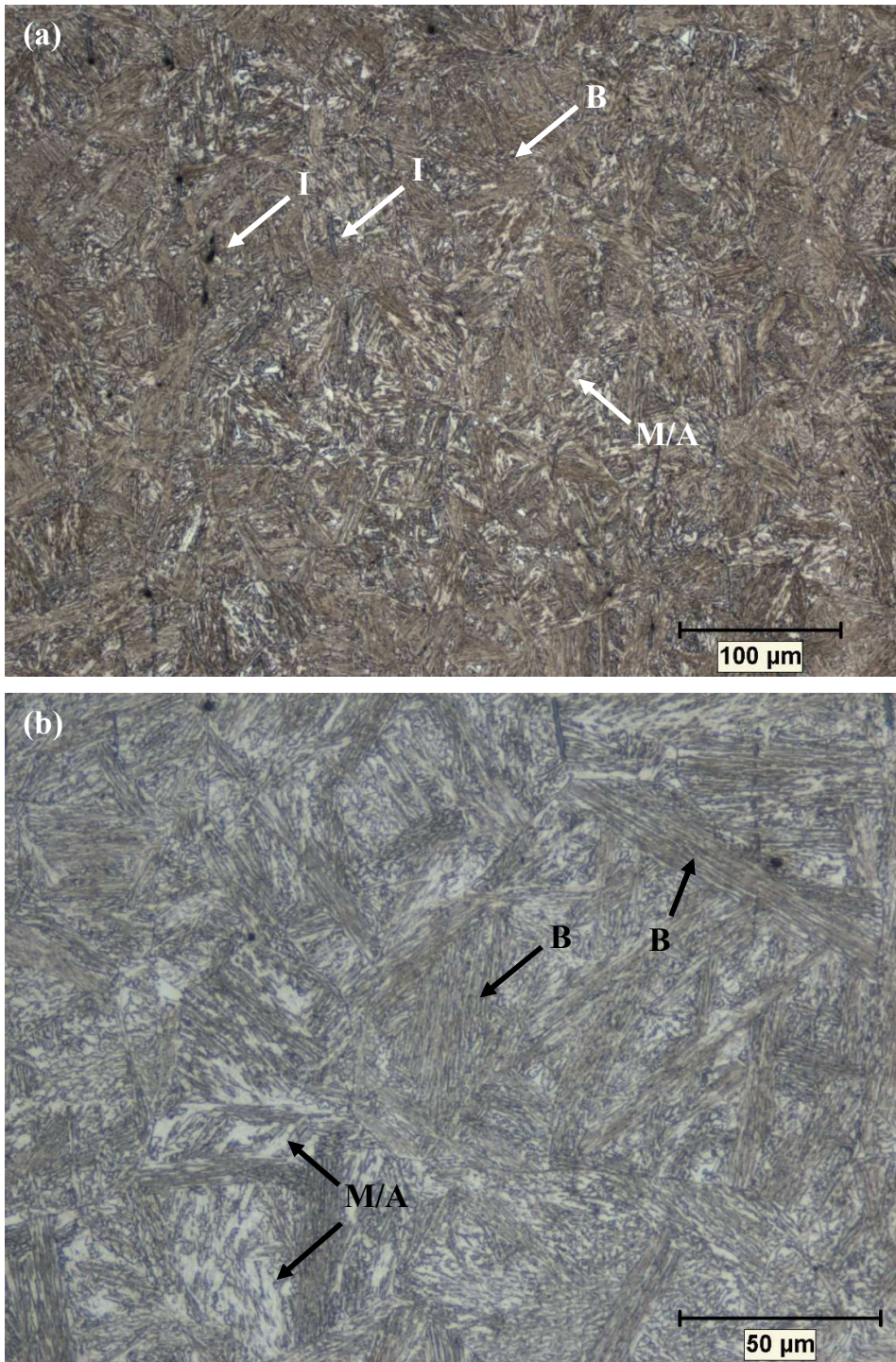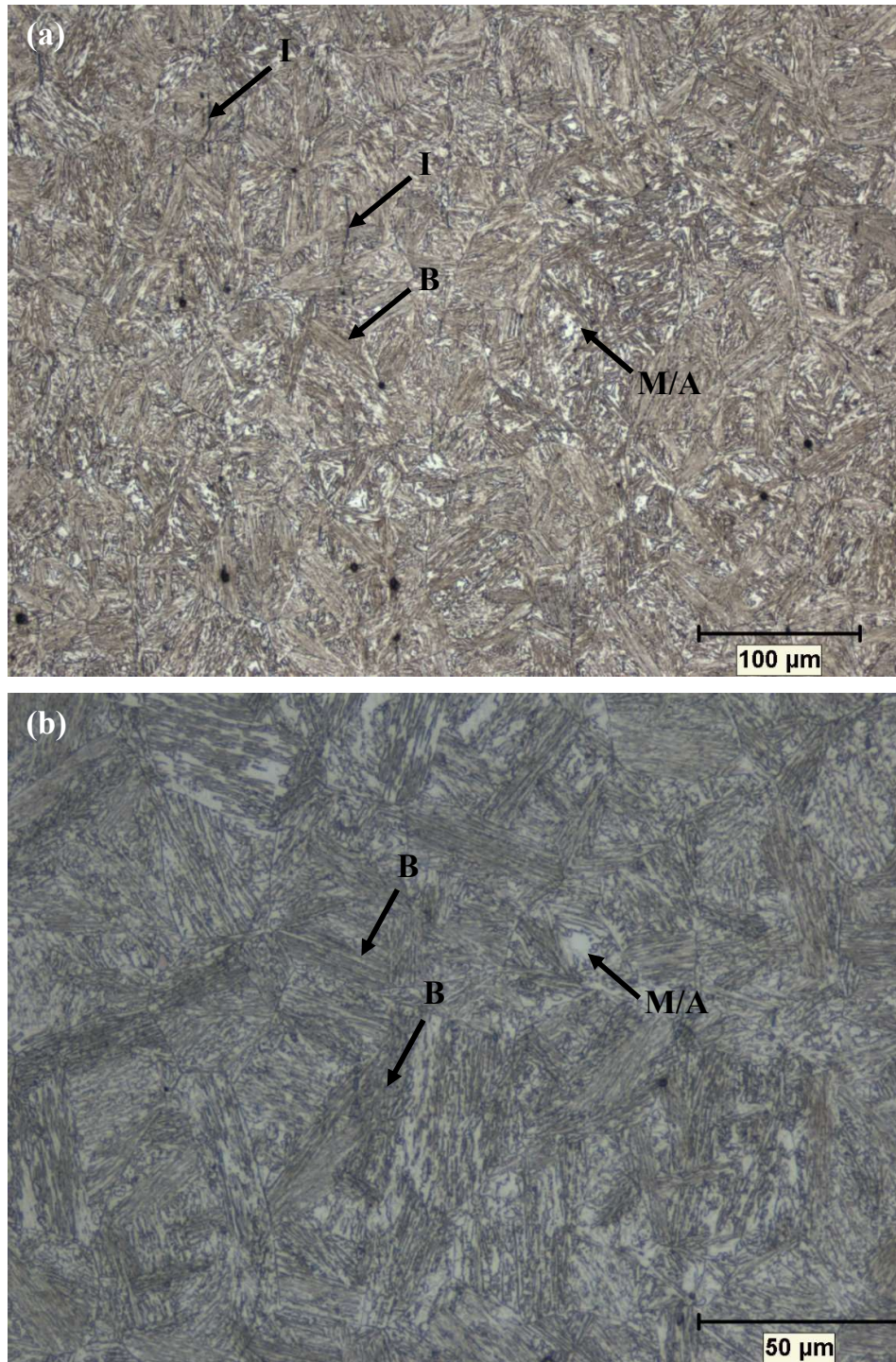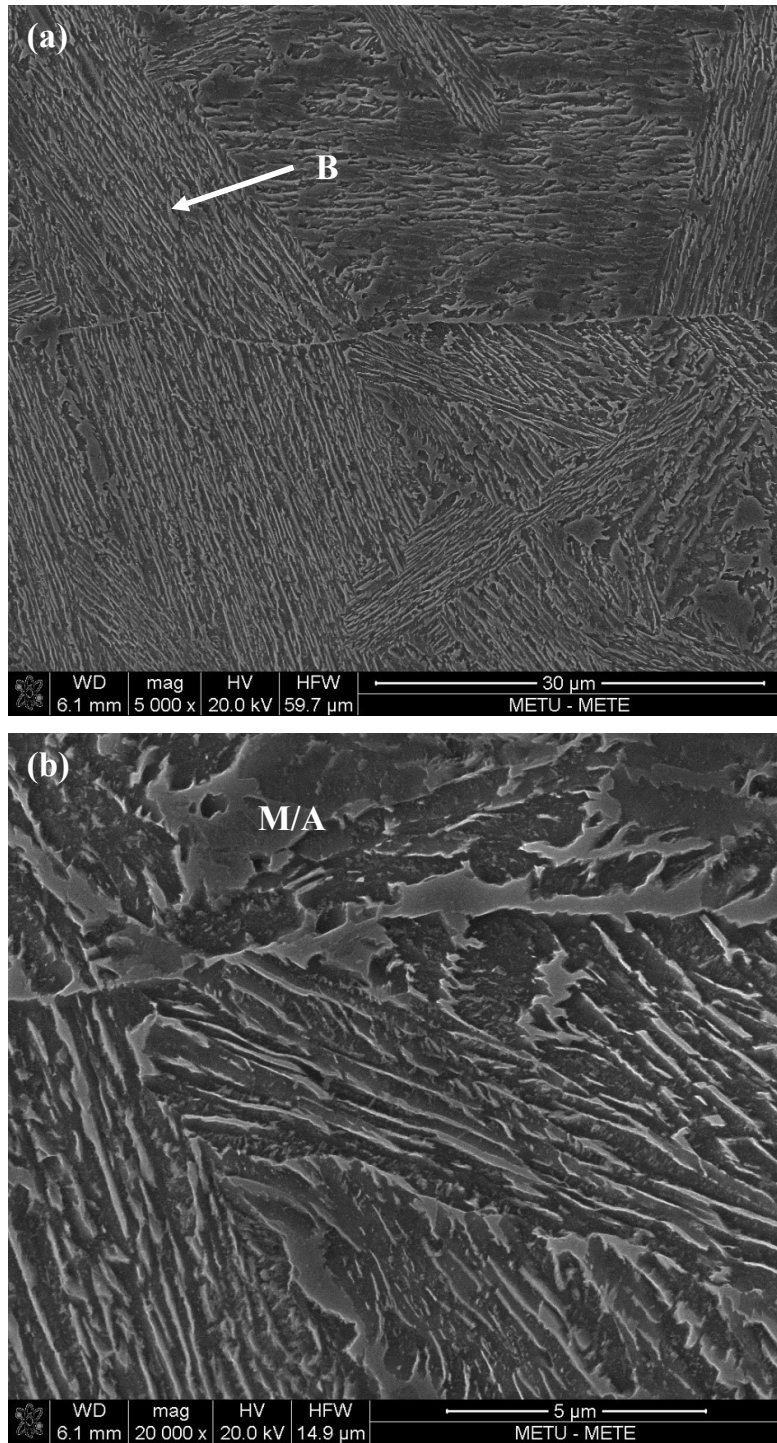
Figure 4.23. The microstructure of the microalloyed steel isothermally transformed at 360°C for 35 minutes observed under SEM at (a) low magnification and (b) high magnification.
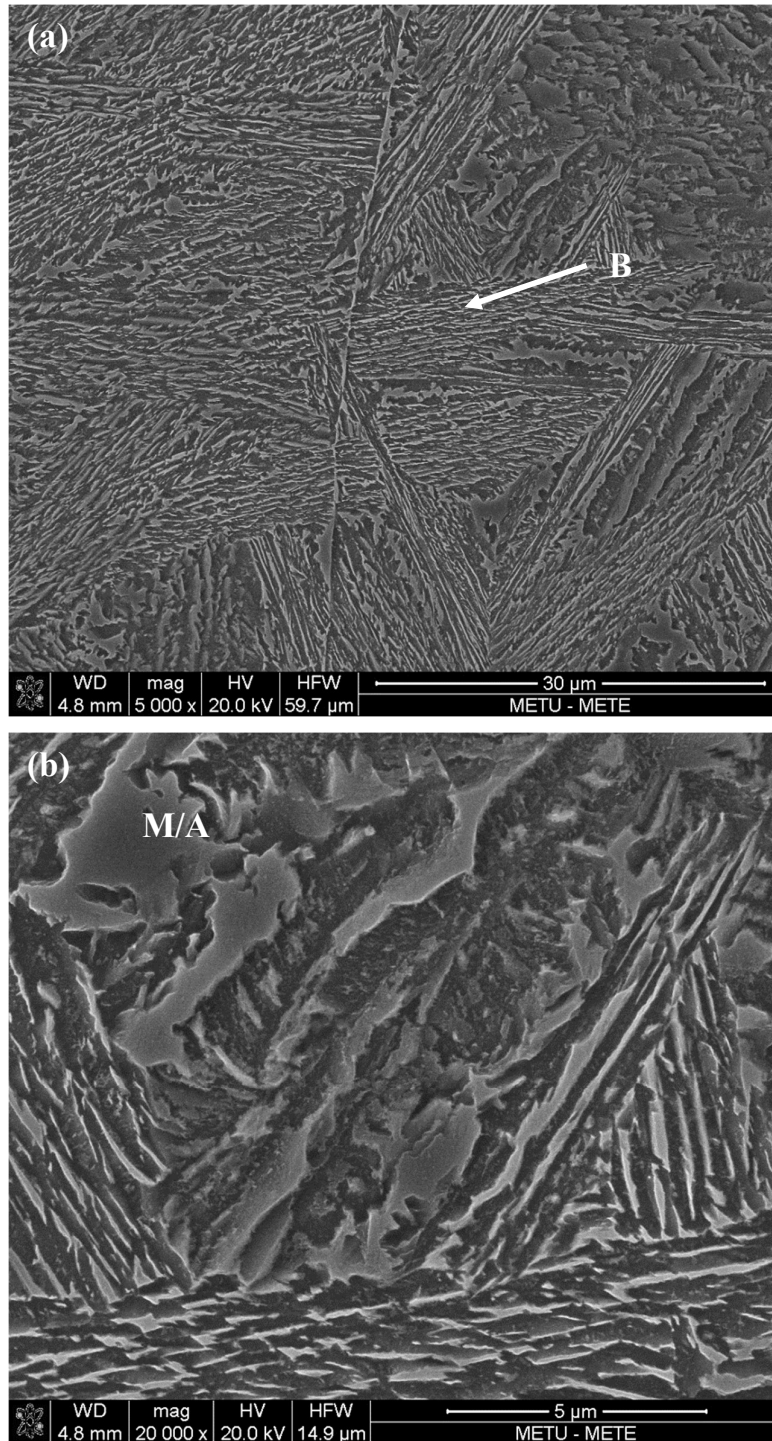
Figure 4.24. The microstructure of the microalloyed steel isothermally transformed at 360°C for 12 hours observed under SEM at (a) low magnification and (b) high magnification.
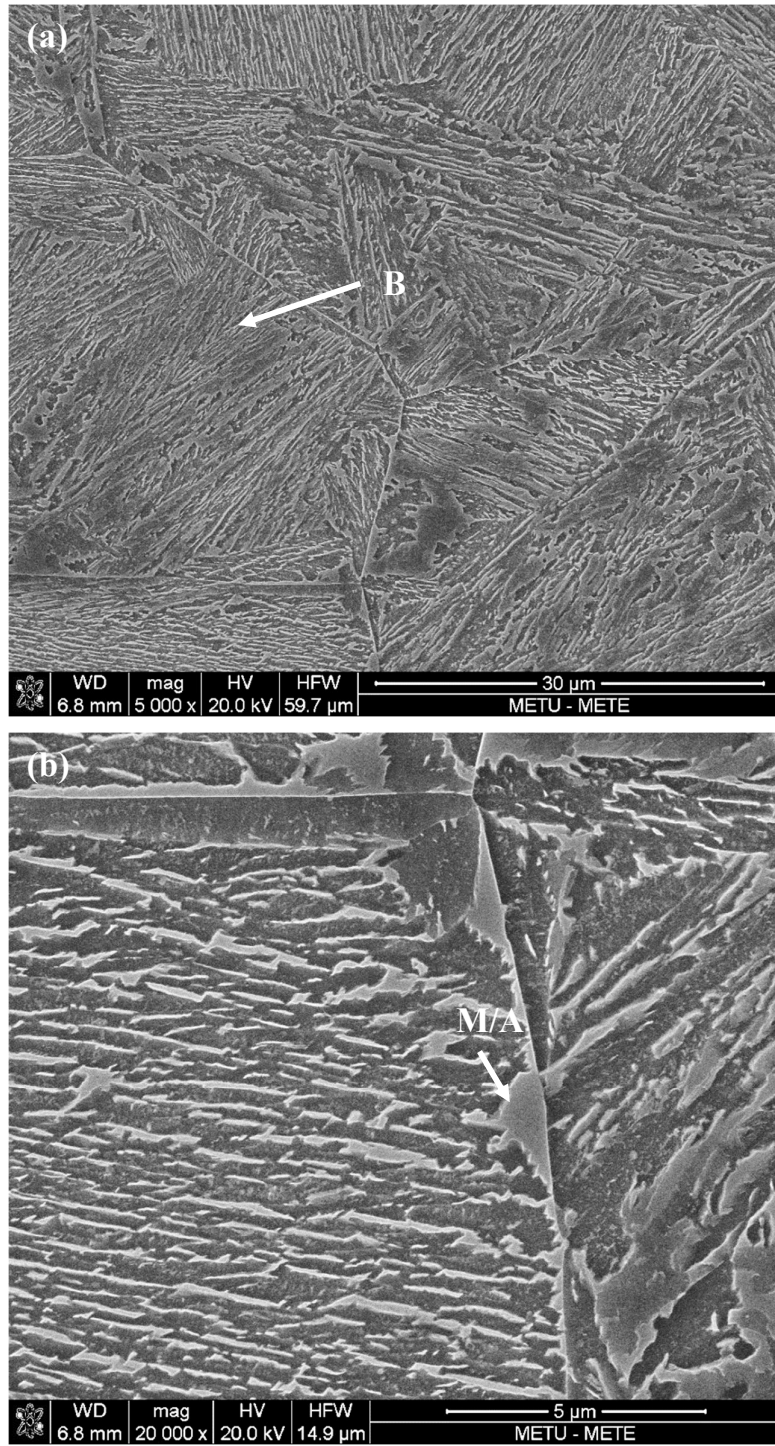
Figure 4.25. The microstructure of the microalloyed steel isothermally transformed at 360°C for 24 hours observed under SEM at (a) low magnification and (b) high magnification.
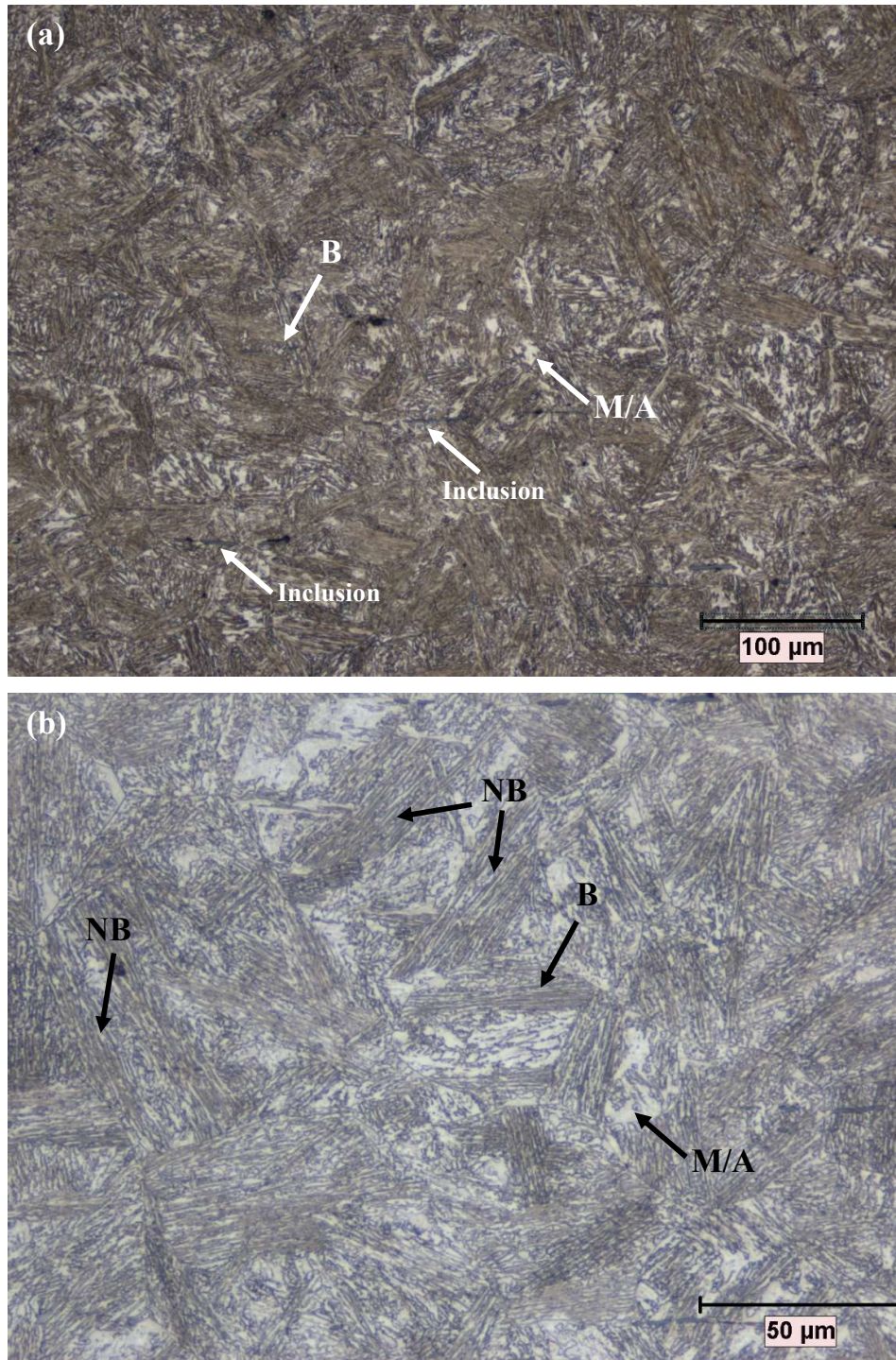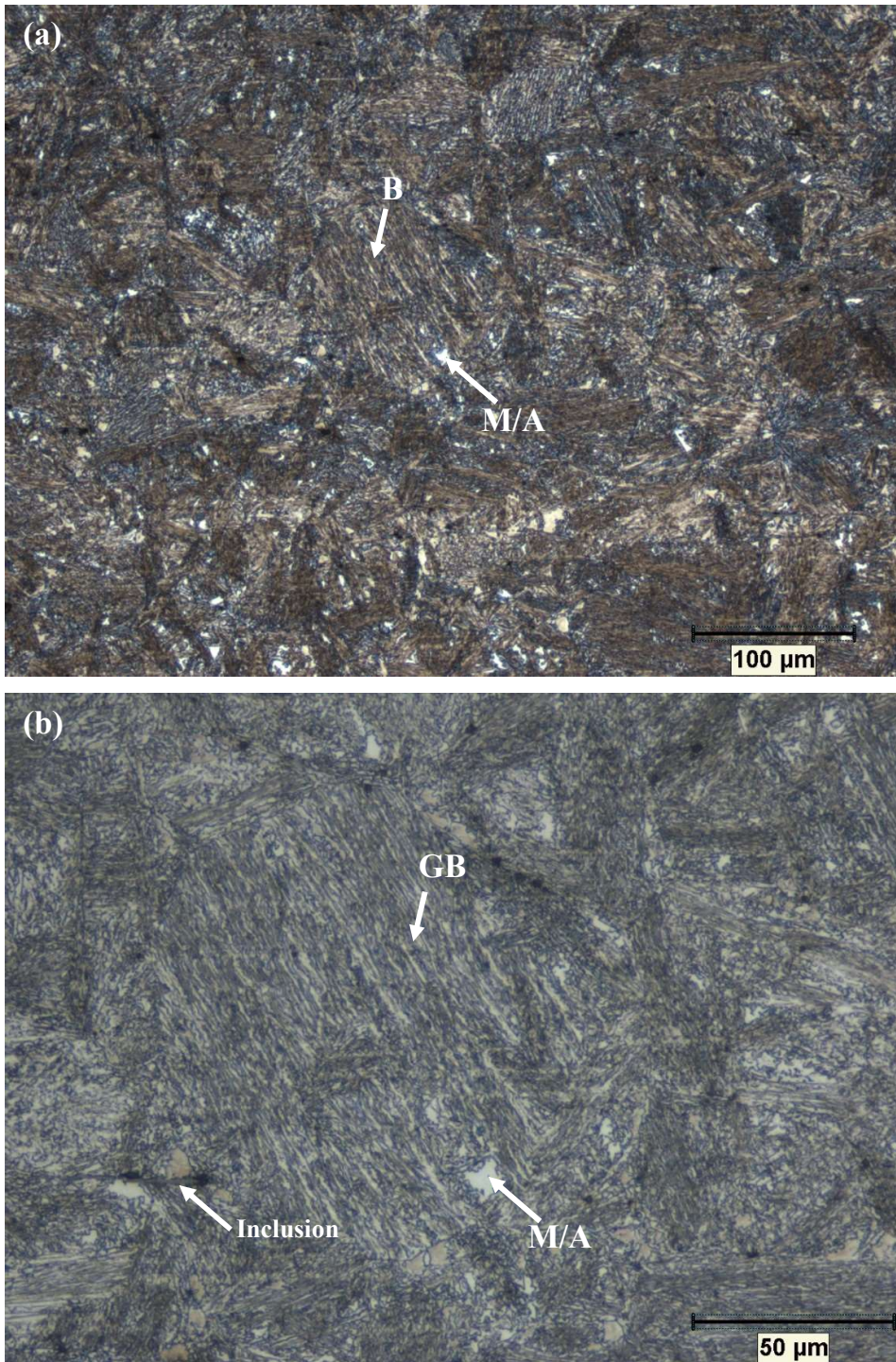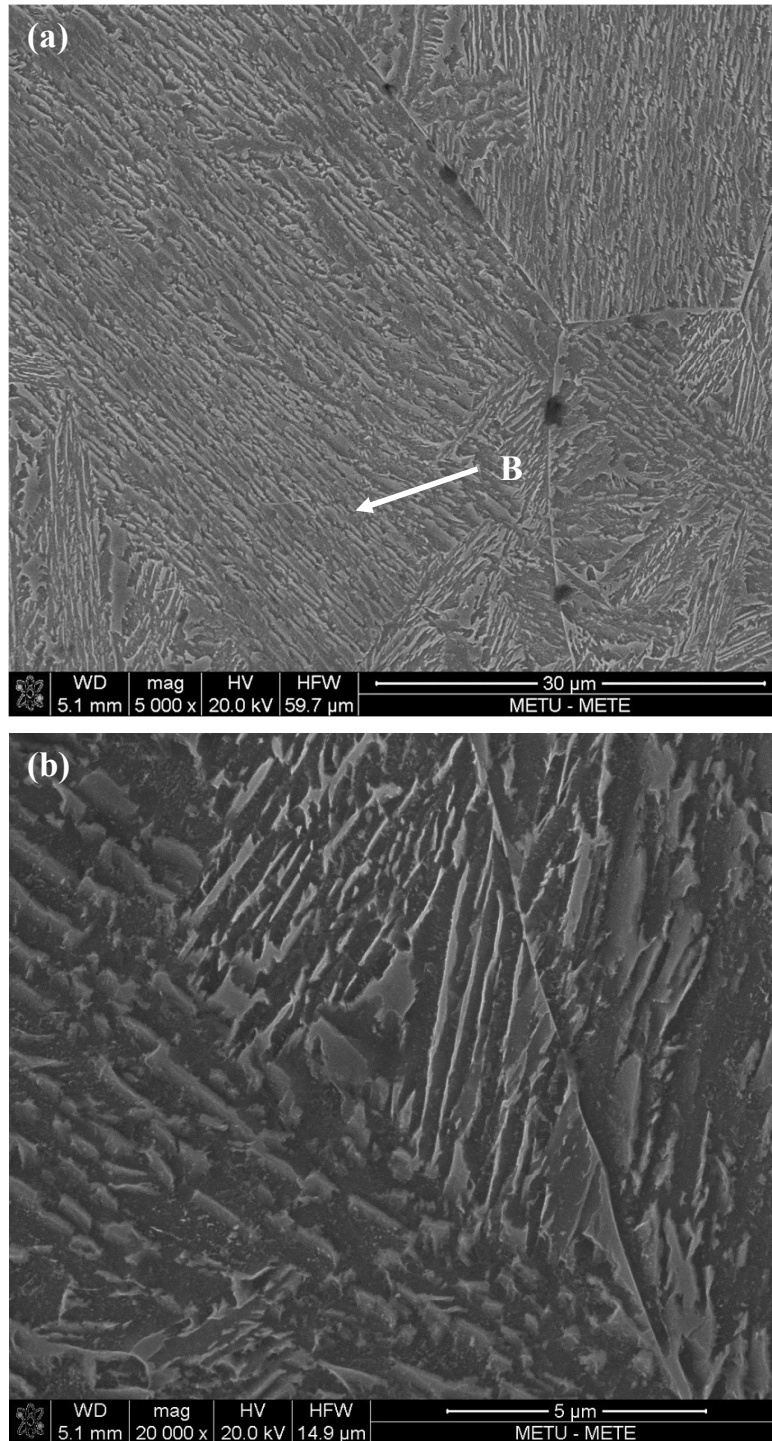
Figure 4.26. The microstructure of the microalloyed steel isothermally transformed at 360ºC for 30 hours observed under SEM at (a) low magnification and (b) high magnification.

4.3.2.4.2 Isothermal Transformation at 380ºC

Figure 4.27, Figure 4.28, and Figure 4.29 show the SEM images at low and high magnifications of isothermally transformed samples held at 380ºC for 40 minutes, 12 hours, and 24 hours, respectively. All samples have needle-like lower bainitic microstructure along with blocky M/A regions. As the holding time is increased, the amount of M/A regions decrease but M/A islands are present in all images. No carbide precipitation is observed in any of the images.

Compared to the isothermal transformation performed at 360ºC, there is no significant difference in terms of bainite morphology. However, the size of blocky M/A appears to be larger.

In high magnification images, Figure 4.27(b) and Figure 4.29(b), the blocky flat M/A islands show different surface features which suggests martensitic transformation has taken place in these islands.
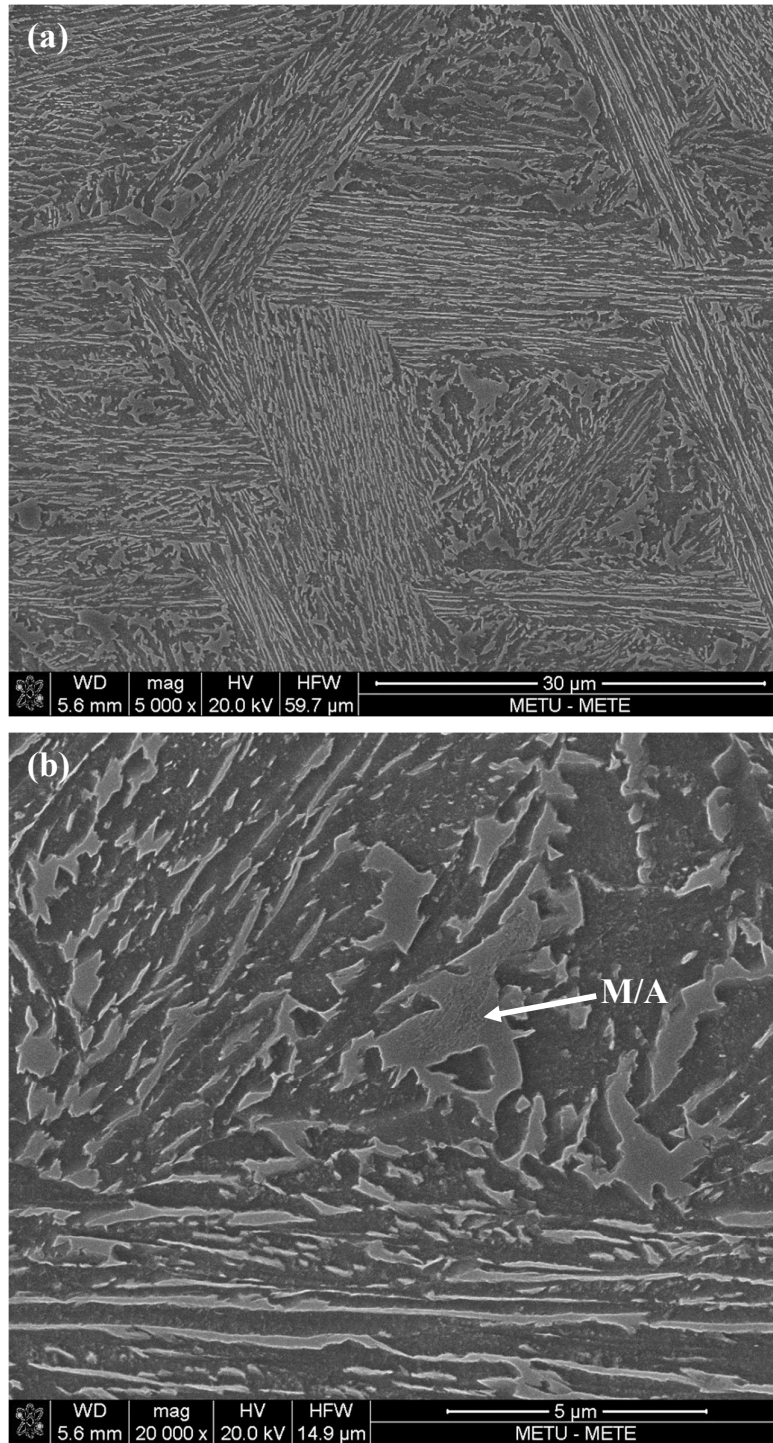
Figure 4.27. The microstructure of the microalloyed steel isothermally transformed at 380°C for 40 minutes observed under SEM at (a) low magnification and (b) high magnification.
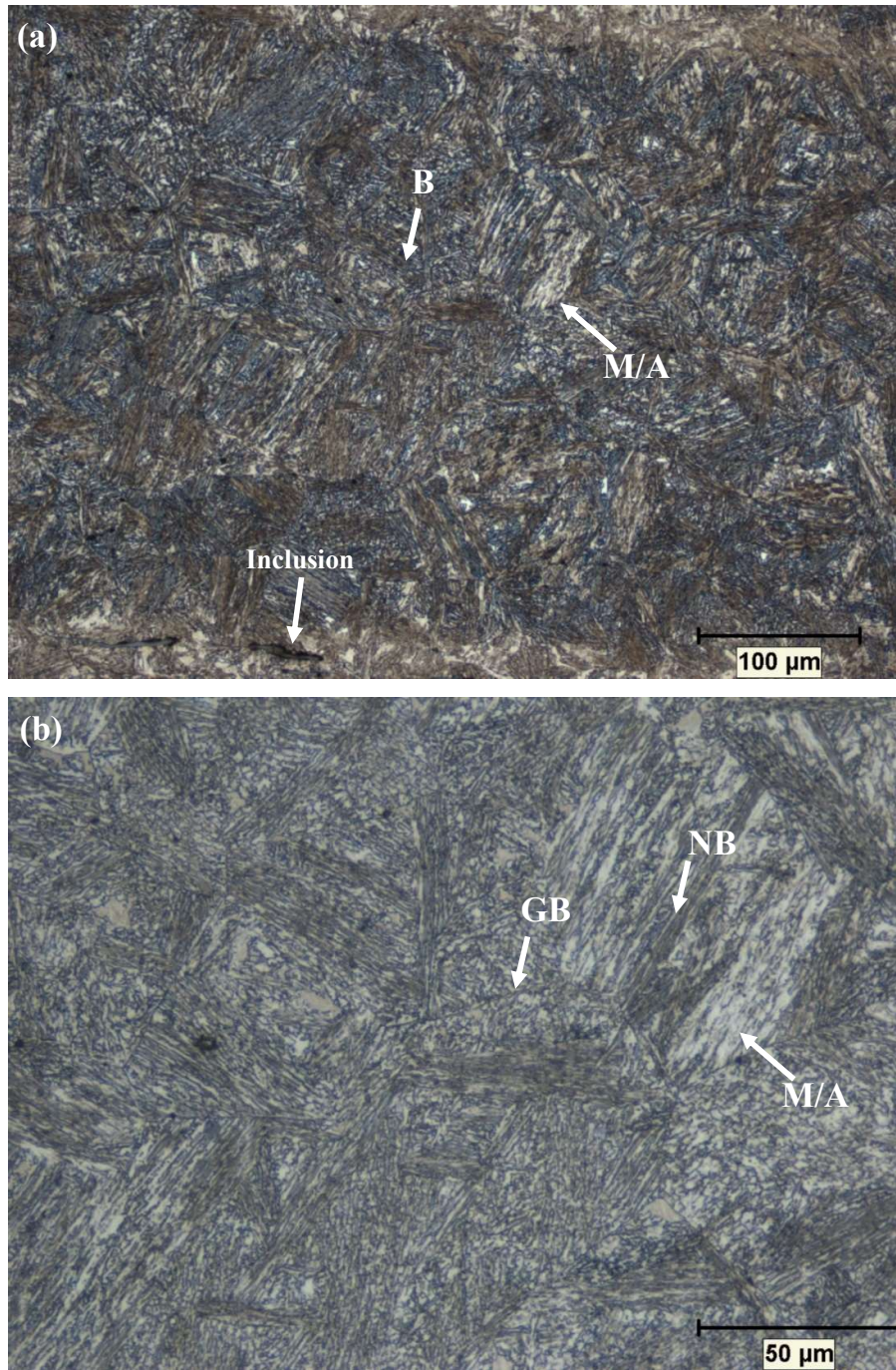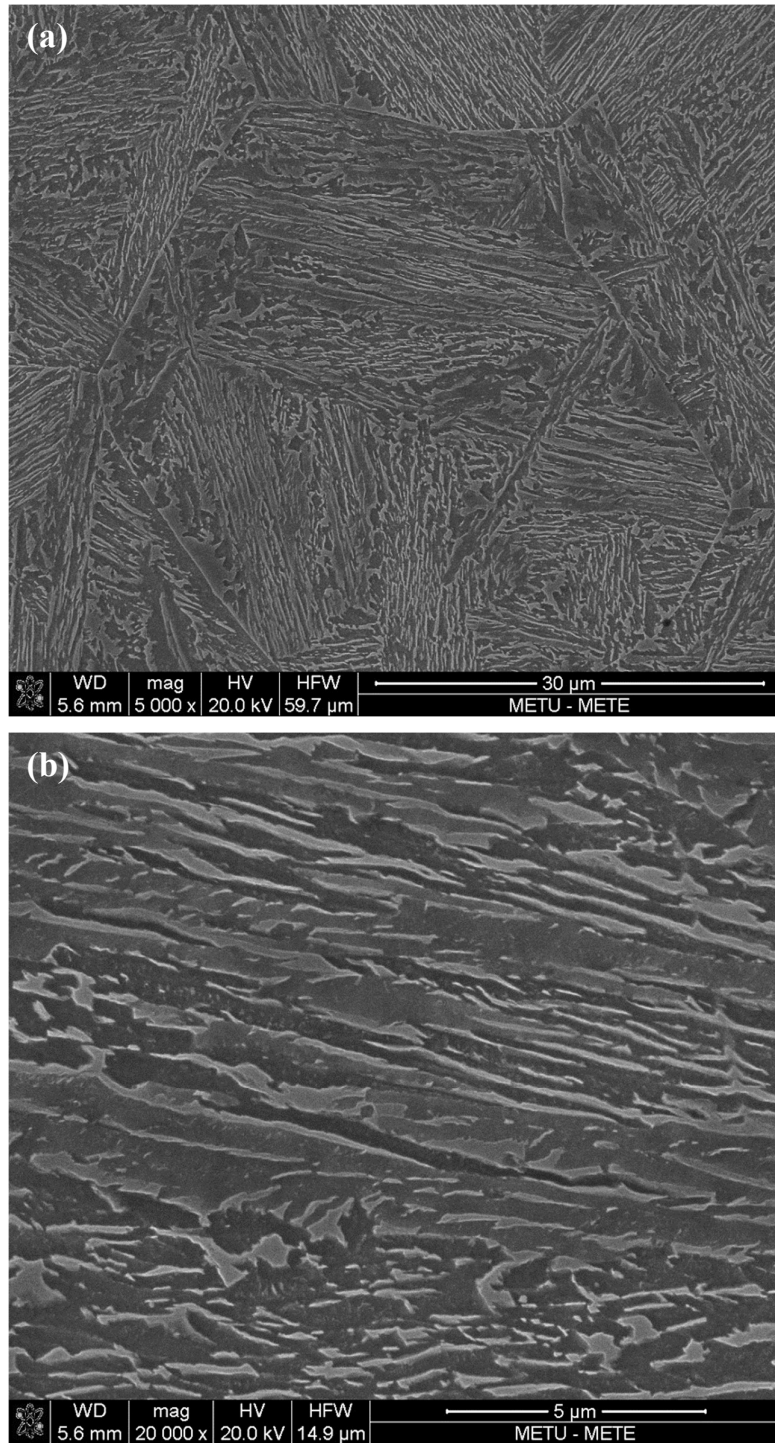
Figure 4.28. The microstructure of the microalloyed steel isothermally transformed at 380°C for 12 hours observed under SEM at (a) low magnification and (b) high magnification.
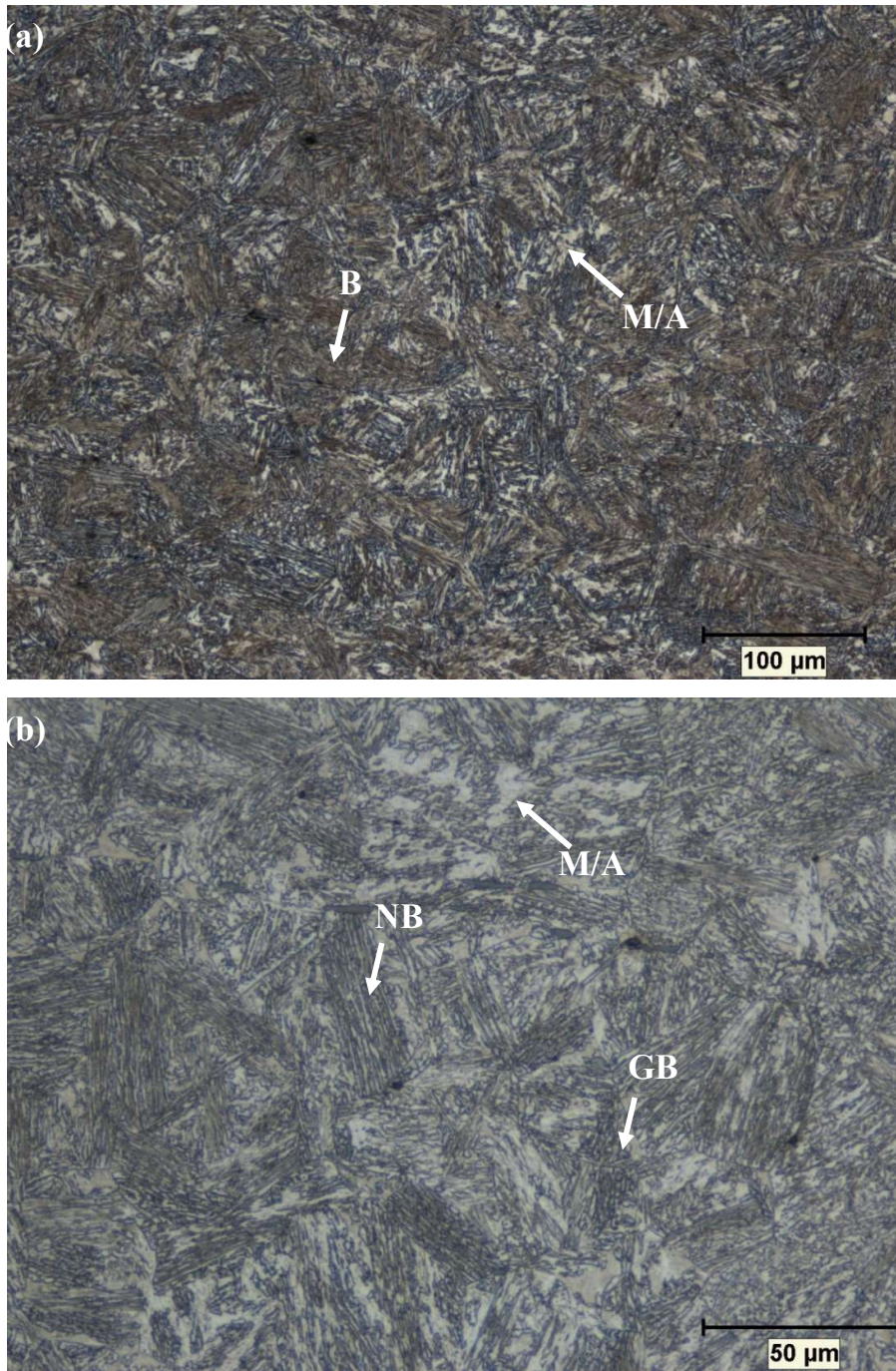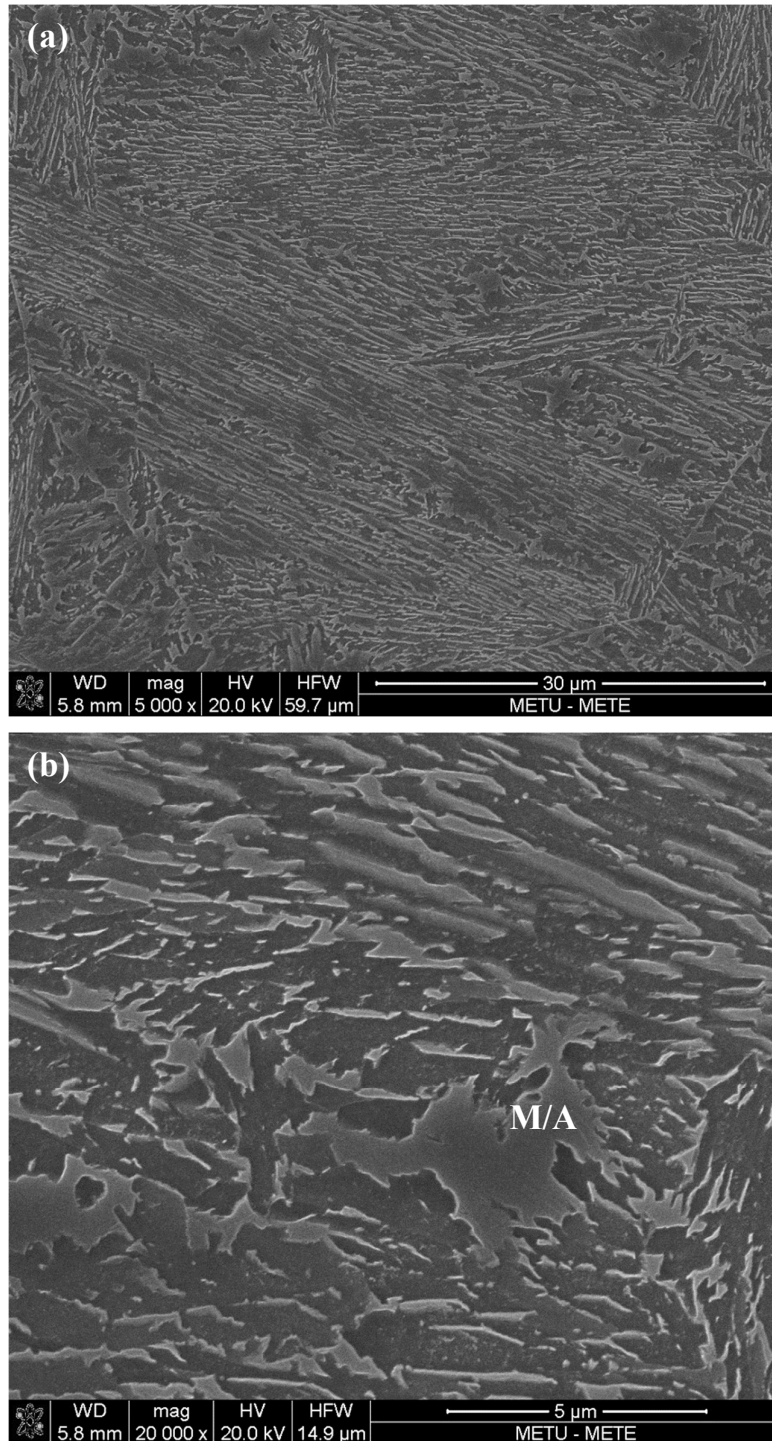
Figure 4.29. The microstructure of the microalloyed steel isothermally transformed at 380°C for 24 hours observed under SEM at (a) low magnification and (b) high magnification.

4.3.2.4.3 Isothermal Transformation at 400ºC

Figure 4.30, Figure 4.31, Figure 4.32, and Figure 4.33 show the SEM images of isothermally transformed samples at 400ºC at low and high magnifications for 15 minutes, 12 hours, 16 hours, and 24 hours, respectively. Bainite and large islands of blocky M/A can be seen in all images. The bainite morphology for 400ºC is quite different from the transformations at 360ºC and 380ºC: the bainitic ferrite at 400ºC is not as thin as the ones at 360ºC and 380ºC and it appears to be discontinuous to some degree, but still in needle-like form. The blocky M/A phase occupies a larger fraction, compared to microstructures of 360ºC and 380ºC samples. No carbide precipitation is observed in any of the images.

At high magnification, such as Figure 4.30(b), and Figure 4.33(b), the blocky flat M/A islands show different surface features which suggests that martensitic transformation has taken place in these islands.
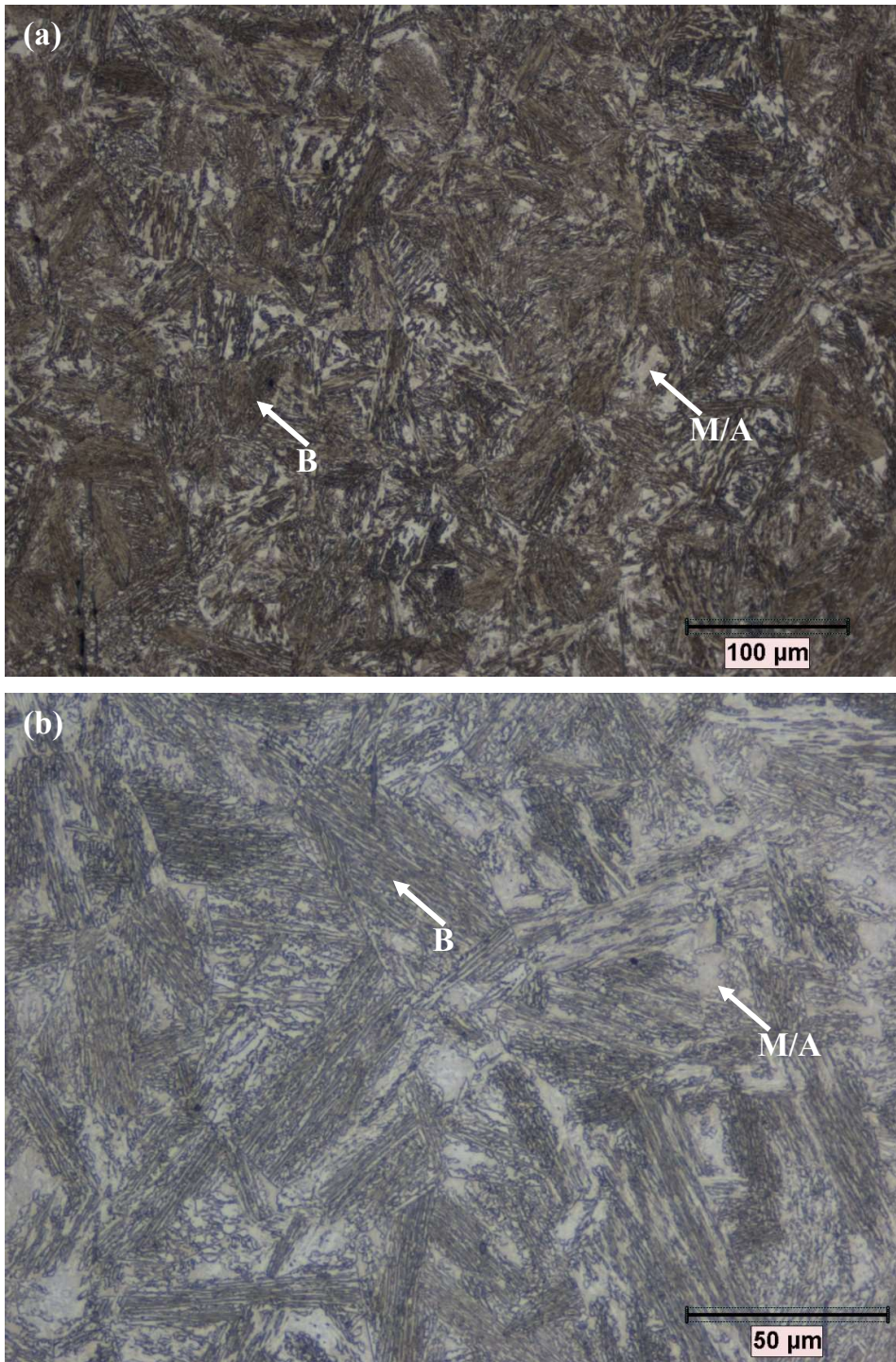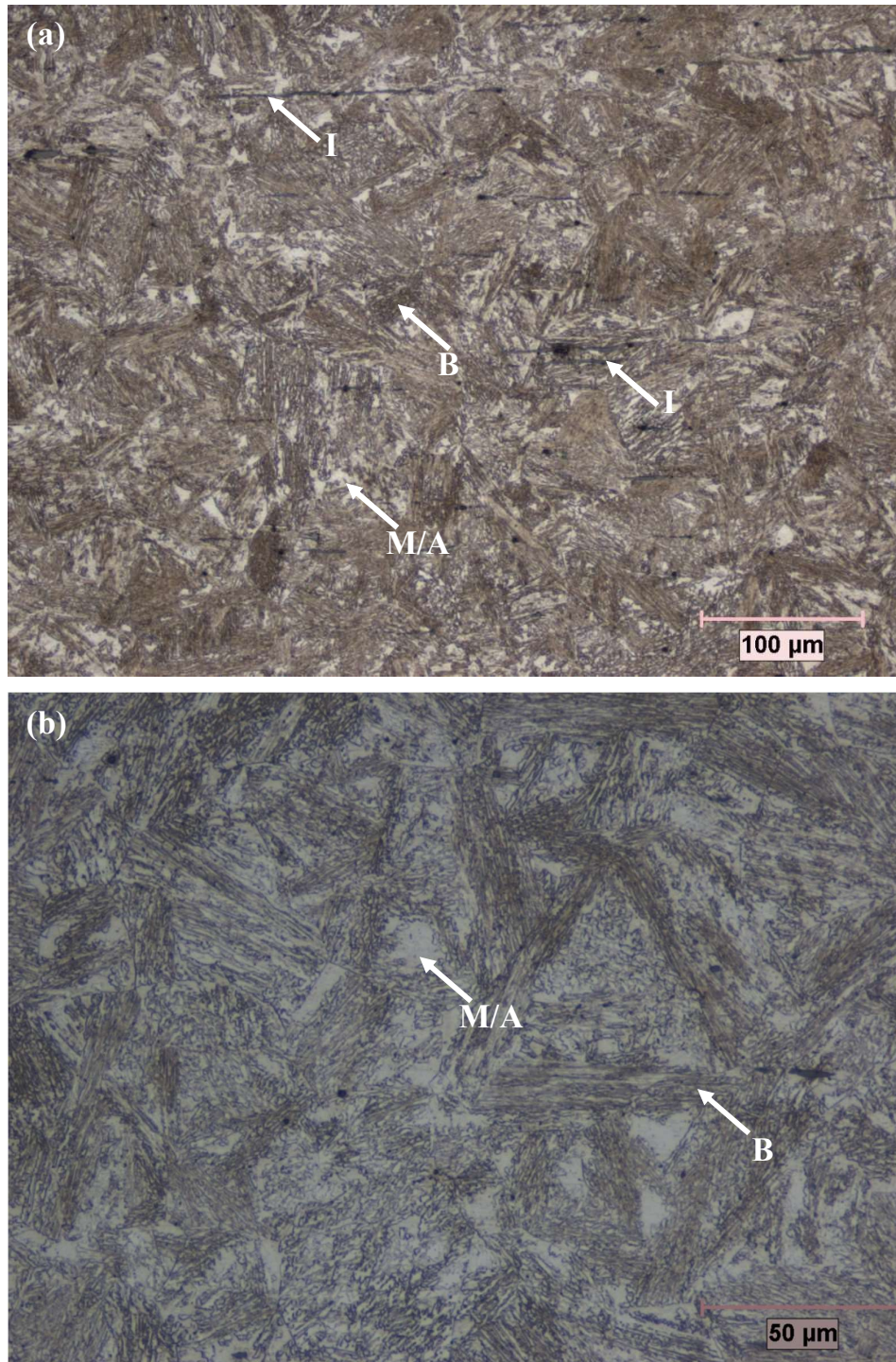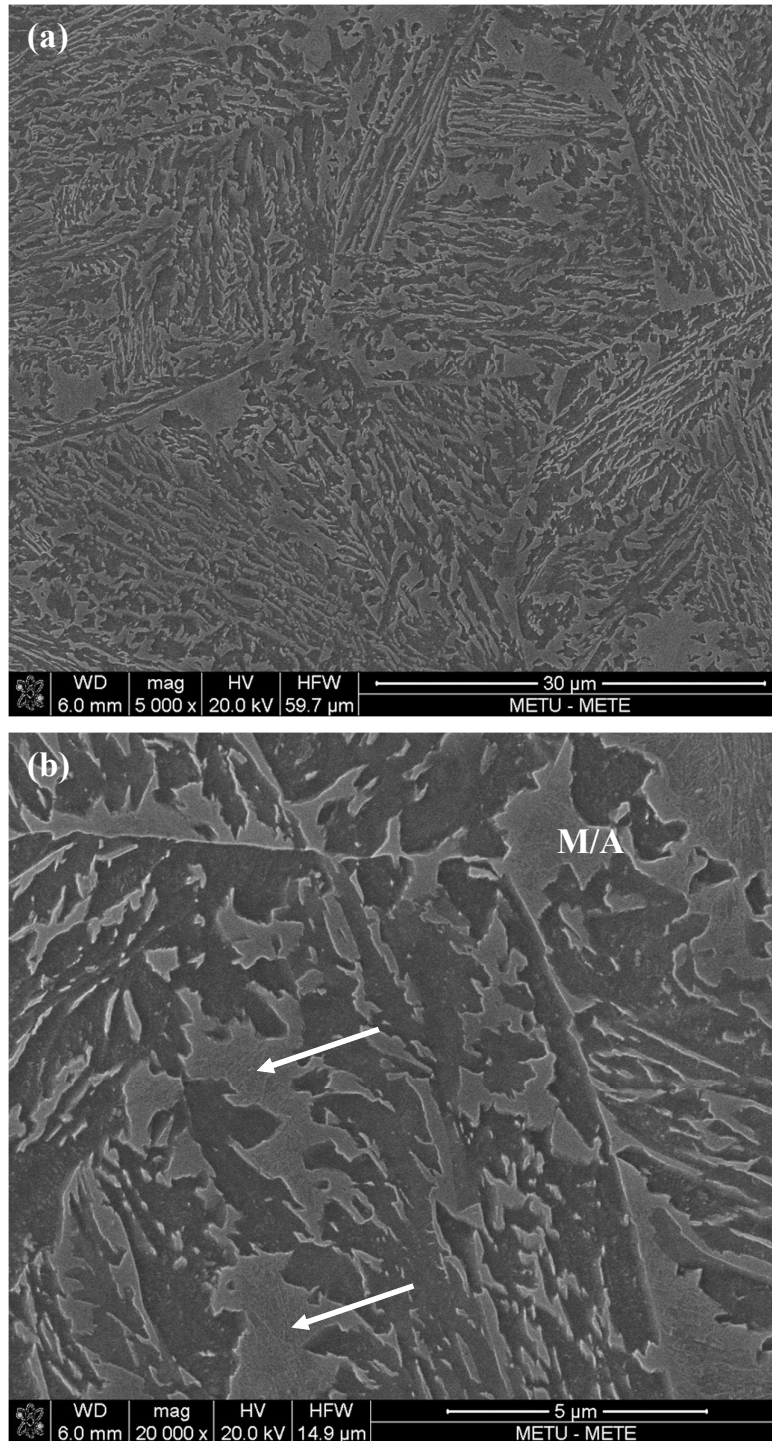
Figure 4.30. The microstructure of the microalloyed steel isothermally transformed at 400°C for 15 minutes observed under SEM at (a) low magnification and (b) high magnification. The islands that have transformed to martensite are shown on the micrograph.
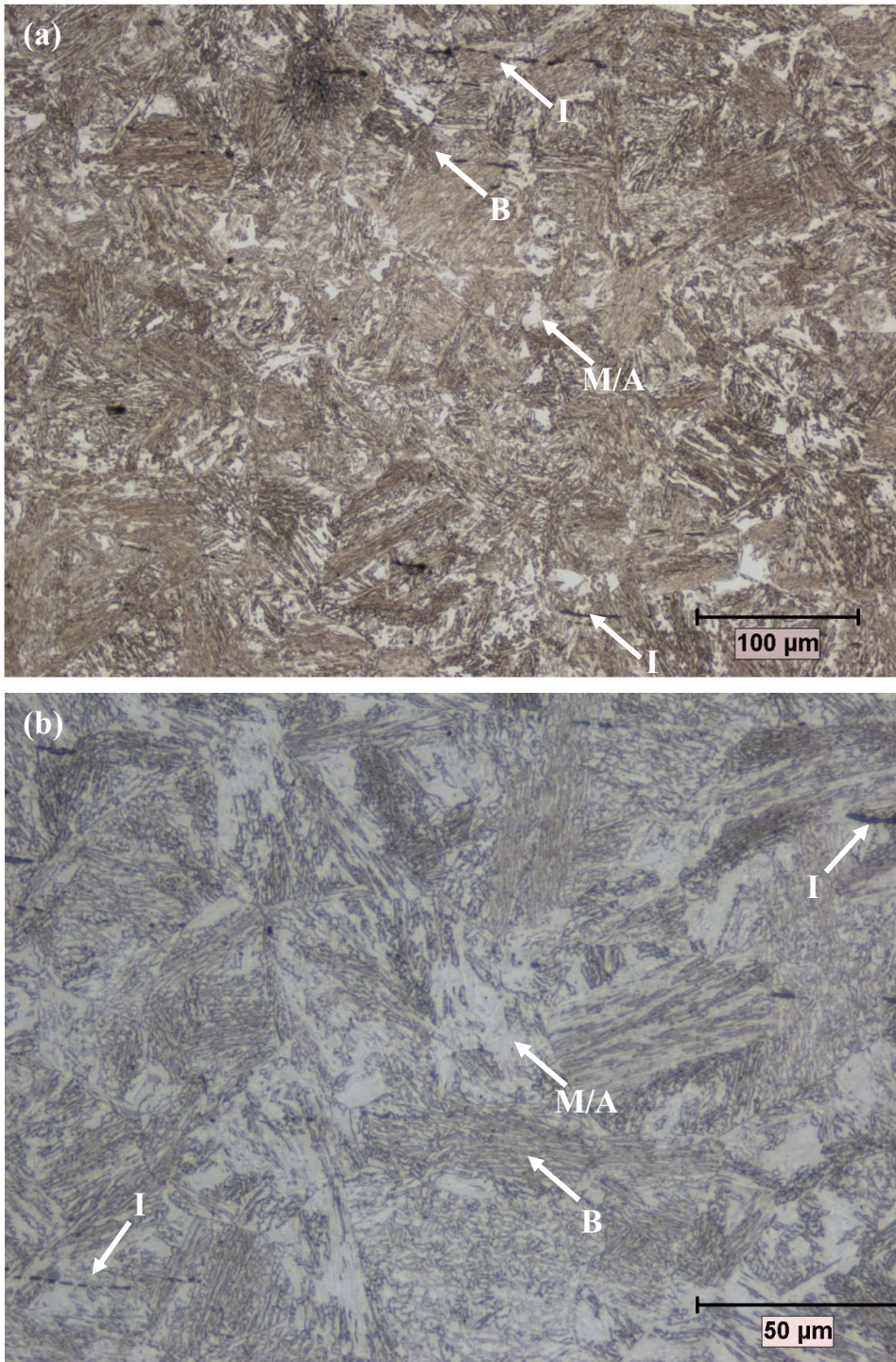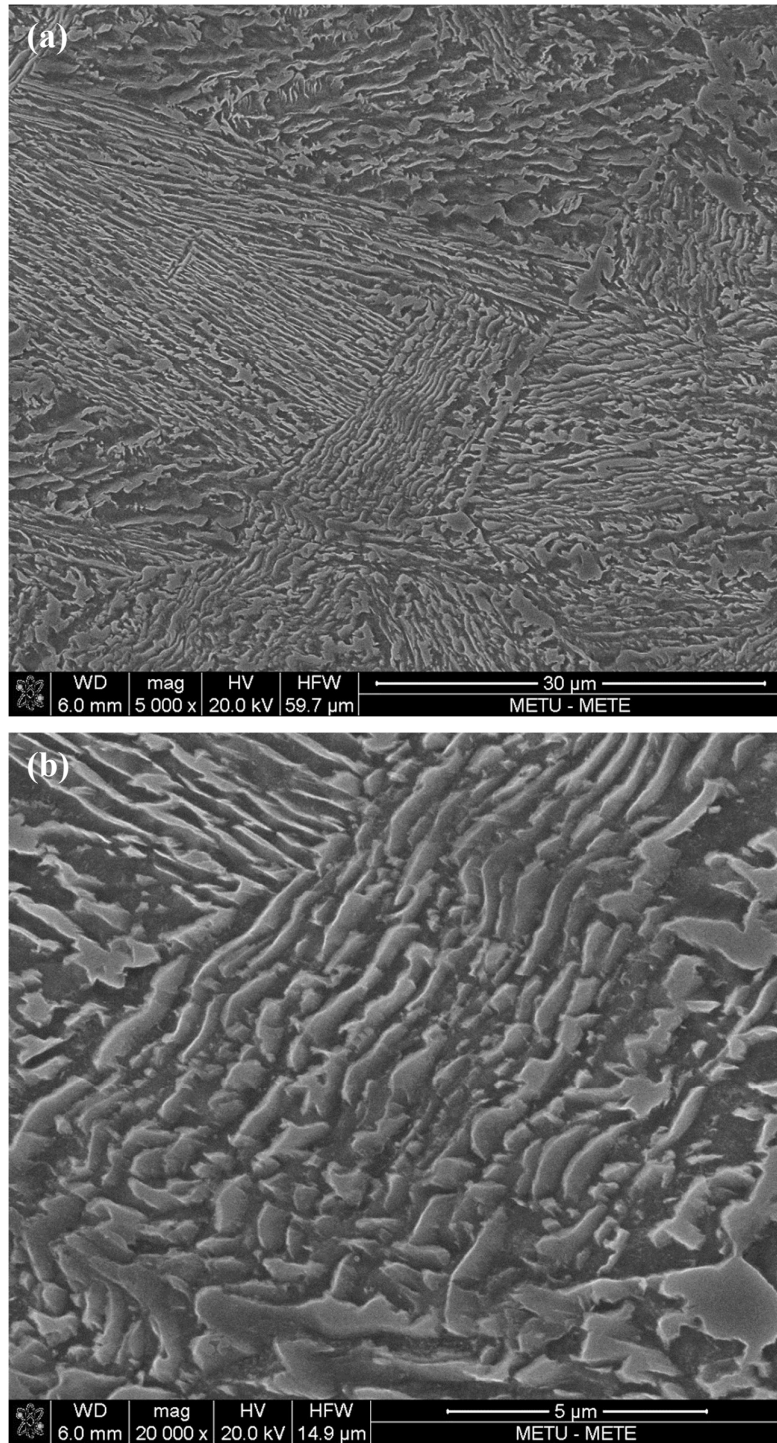
Figure 4.31. The microstructure of the microalloyed steel isothermally transformed at 400°C for 12 hours observed under SEM at (a) low magnification and (b) high magnification.
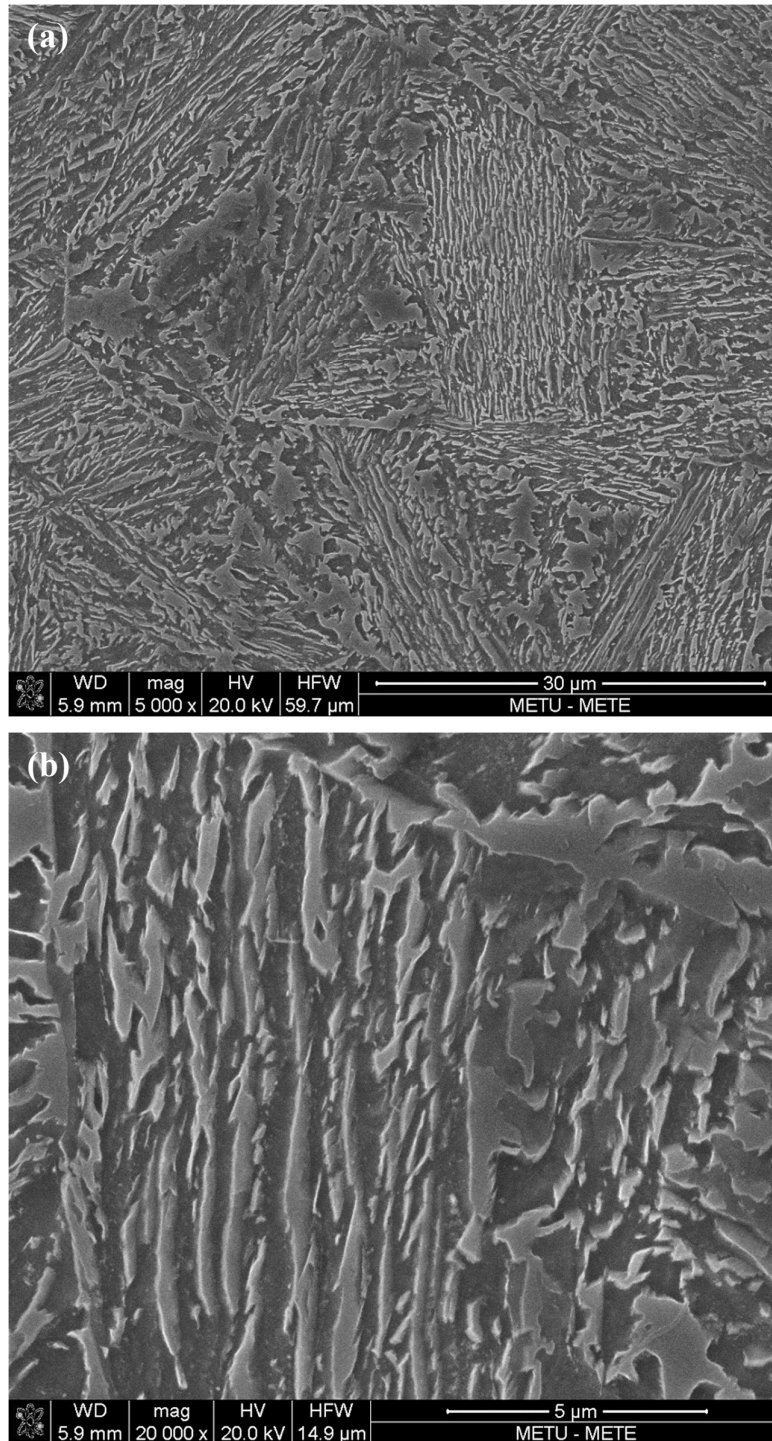
Figure 4.32. The microstructure of the microalloyed steel isothermally transformed at 400ºC for 16 hours observed under SEM at (a) low magnification and (b) high magnification.
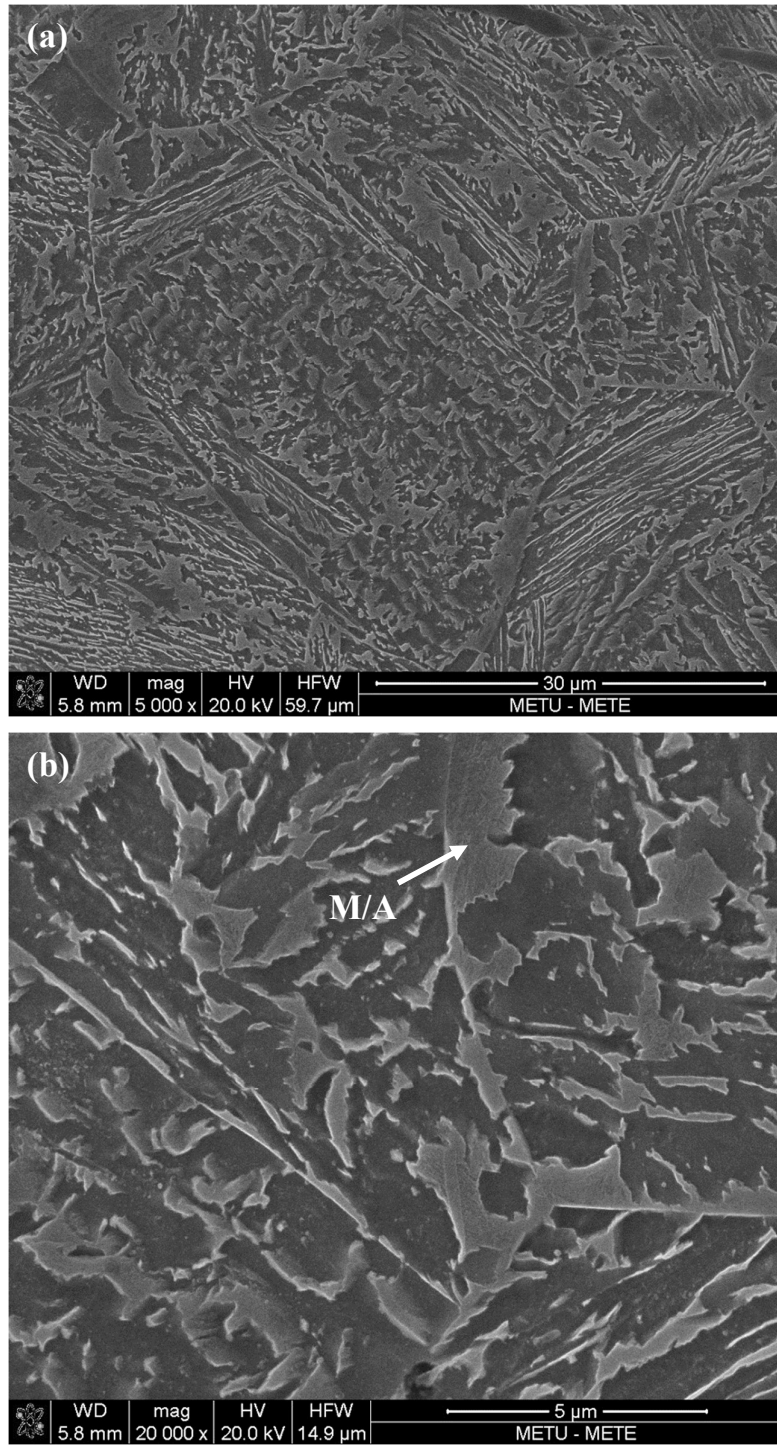
Figure 4.33. The microstructure of the microalloyed steel isothermally transformed at 400°C for 24 hours observed under SEM at (a) low magnification and (b) high magnification.

4.3.2.4.4　Isothermal Transformation at 420ºC

Figure 4.34, Figure 4.35, Figure 4.36 show the SEM images of the samples isothermally heat-treated at 420°C for durations of 15 minutes, 12 hours, and 24 hours, respectively, at low and high magnifications. The bainite morphology is needle-like but similar to transformation at 400°C, it shows thicker bainite sheaves and bainitic ferrite is discontinuous. Blocky M/A islands are present in all images and samples that are heat-treated at 420°C have the largest M/A islands. The surface features that may suggest a martensitic transformation in M/A islands are present in Figure 4.35(b), and Figure 4.36(b).
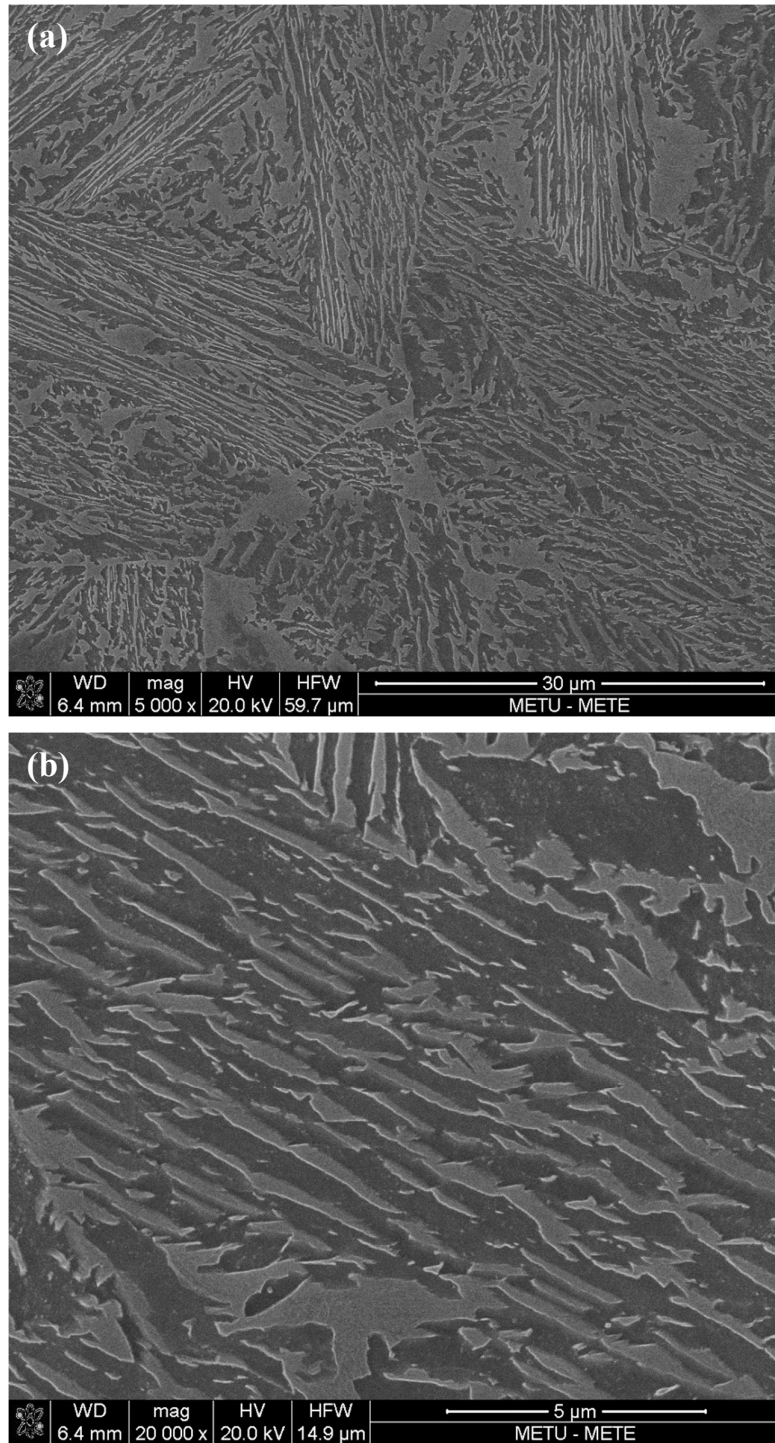
Figure 4.34. The microstructure of the microalloyed steel isothermally transformed at 420ºC for 15 minutes observed under SEM at (a) low magnification and (b) high magnification.
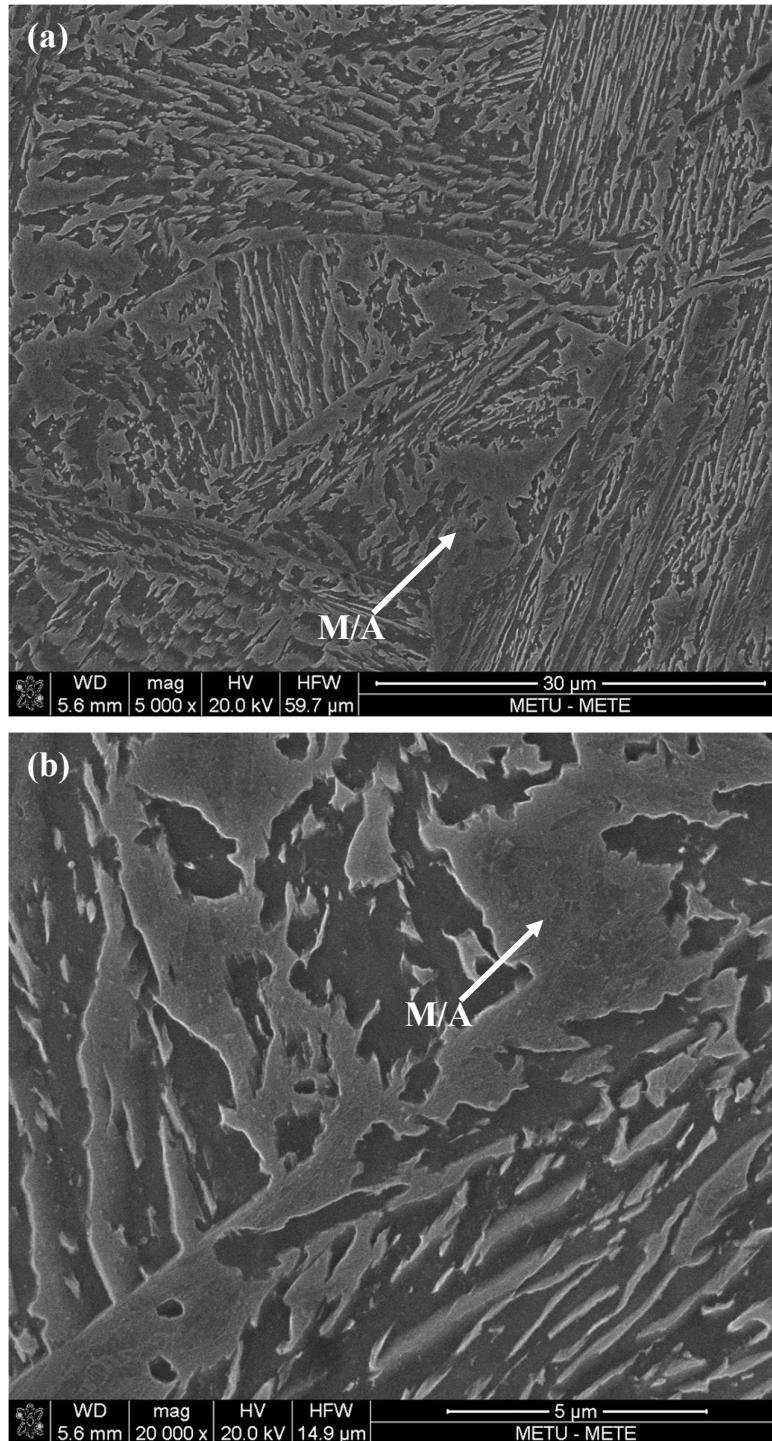
Figure 4.35. The microstructure of the microalloyed steel isothermally transformed at 420°C for 12 hours observed under SEM at (a) low magnification and (b) high magnification. The islands that have transformed to martensite are shown on the micrograph.
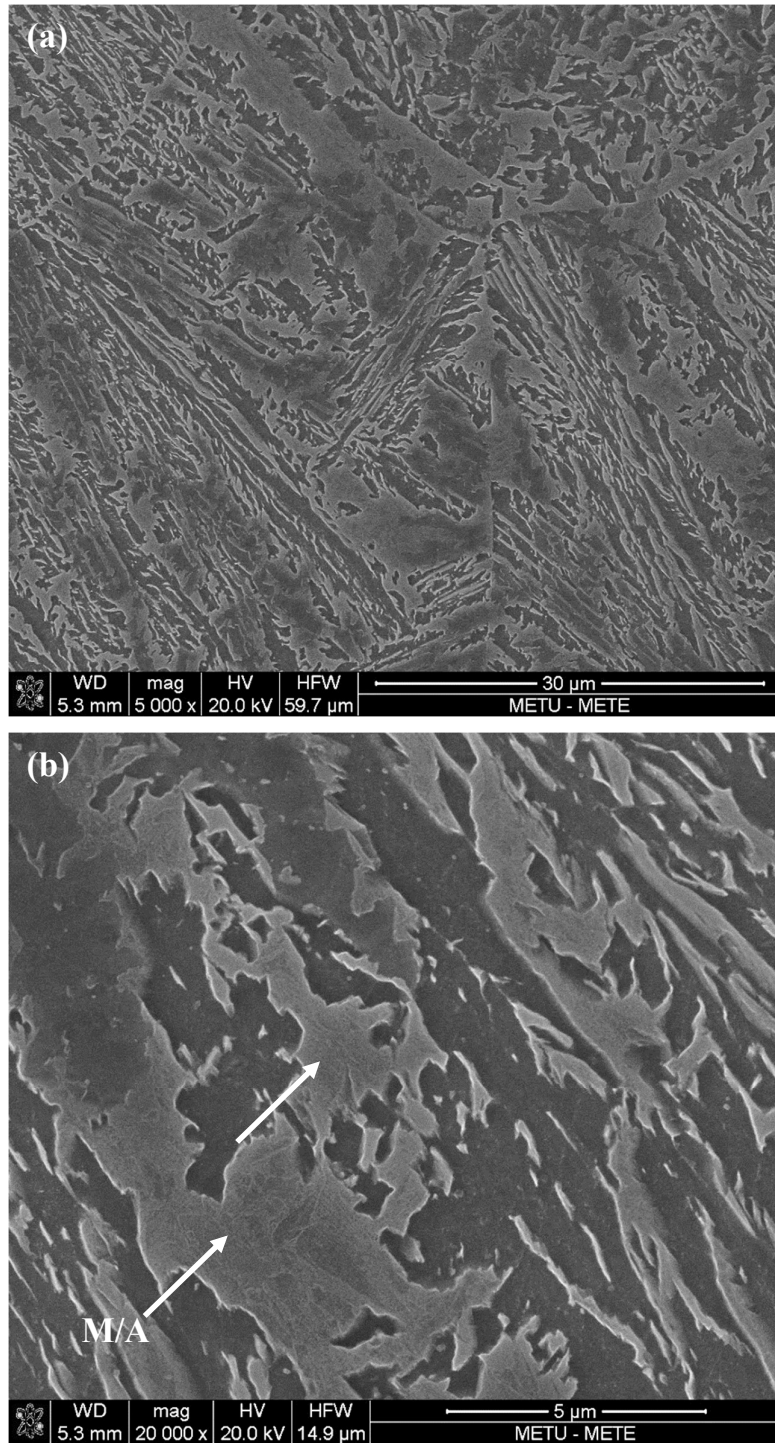
Figure 4.36. The microstructure of the microalloyed steel isothermally transformed at 420°C for 24 hours observed under SEM at (a) low magnification and (b) high magnification. The islands that have transformed to martensite are shown on the micrograph.

4.4   Quantitative Phase Analysis

4.4.1   Retained Austenite Measurements

Quantitative phase analysis, by means of X-Ray Diffraction, is required to measure the retained austenite content of the samples after isothermal heat treatments. The XRD data of ferrite and austenite are given in Table 4.3 [82]. Figure 4.37, Figure 4.38, Figure 4.39, Figure 4.40, and Figure 4.41 exhibit the XRD patterns of the isothermally treated, normalized, and oil quenched samples. The XRD patterns are labeled according to the plane and peak angle information given in Table 4.3. There is no significant shift in peak angles, but the peak intensities vary from sample to sample. XRD patterns of martensite and ferrite coincide with each other, so ferrite refers to both phases in the analysis. The results of XRD and quantitative phase analysis are given in Table 4.4 and plotted as a bar chart in Figure 4.42.

Table 4.3 XRD data of ferrite and austenite, plane indices and peak angles [82].

Ferrite		Austenite	
Plane Indices	Peak Angle, 2θ (deg)	Plane Indices	Peak Angle, 2θ (deg)
(110)	44.67	(111)	43.26
(200)	65.02	(200)	50.38
(211)	82.33	(220)	74.00
(220)	98.94	(311)	89.78
(310)	116.38	(222)	94.98
(222)	137.13	(400)	116.68

Table 4.4 Amount of retained austenite in each sample as volume percent

Sample	Retained Austenite Content (%Vol)
360C-35min	4.7
360C-12h	5.8
360C-24h	5.5
360C-30h	4.9
380C-40min	6.6
380C-12h	4.9
380C-24h	5.4
400C-15min	5.8
400C-12h	5.5
400C-16h	4.6
400C-24h	4.1
420C-15min	6.0
420C-12h	4.1
420C-24h	4.3
As Received	7.0
Oil Quenched	2.9
Normalized	5.8

Figure 4.37, Figure 4.38, Figure 4.39 and, Figure 4.40 show that the effect of isothermal holding time on the amount of retained austenite is not very significant. For the 400C-24h sample in Figure 4.39, the austenite peak intensities are quite weak. In Figure 4.41, as received and normalized samples show the most intense austenite peaks and oil quenched sample does not show any austenite peaks beyond the γ(200) peak.
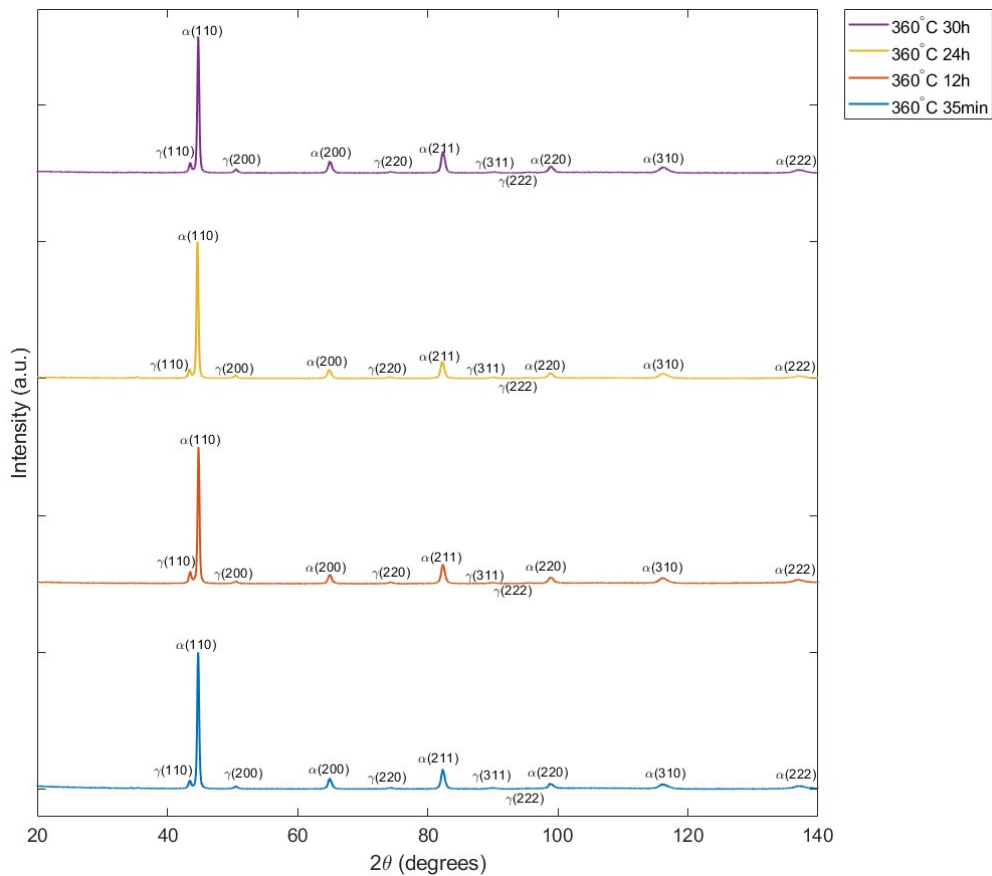
Figure 4.37. XRD patterns of samples isothermally heat-treated at 360ºC, α: Ferrite, γ: Austenite
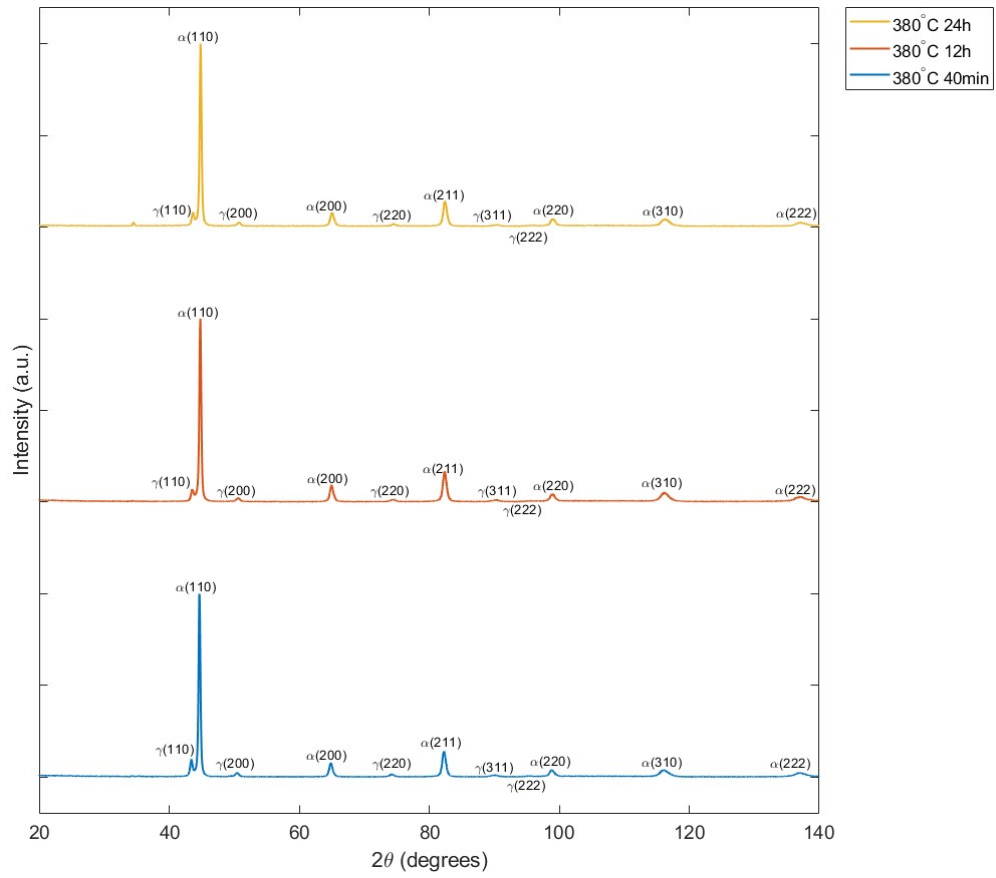
Figure 4.38. XRD patterns of samples isothermally heat-treated at 380ºC, α: Ferrite, γ: Austenite
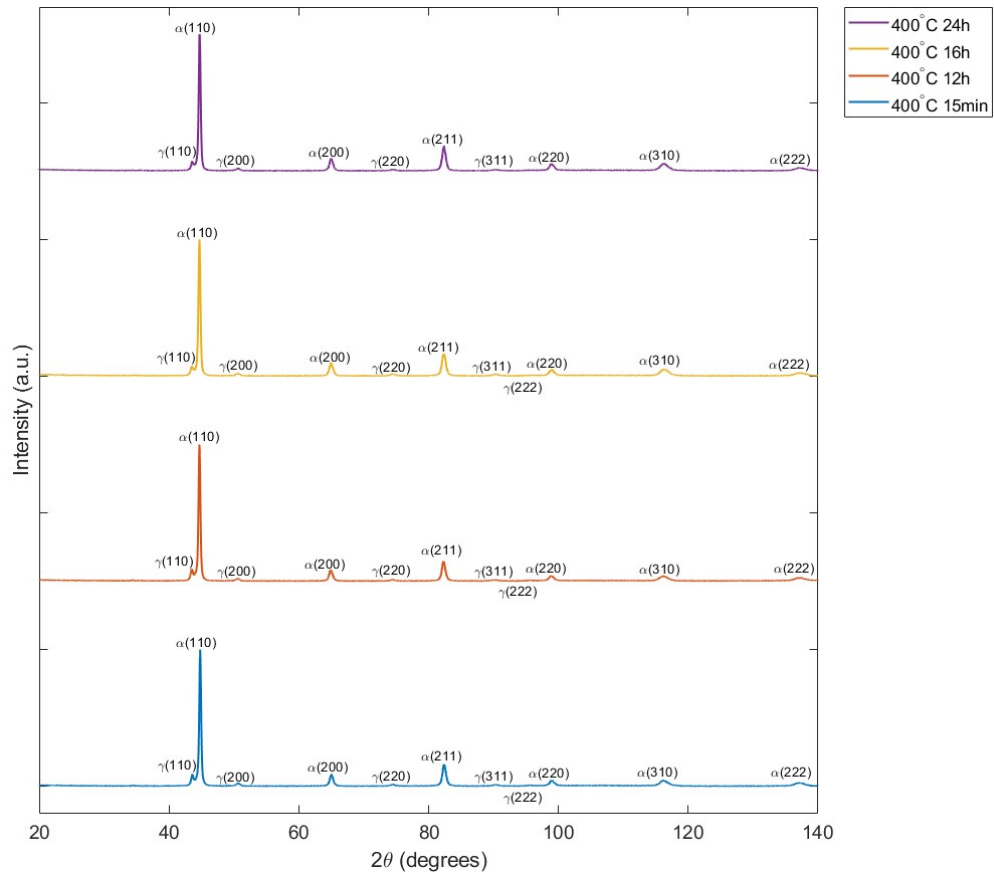
Figure 4.39. XRD patterns of samples isothermally heat-treated at 400ºC, α: Ferrite, γ: Austenite
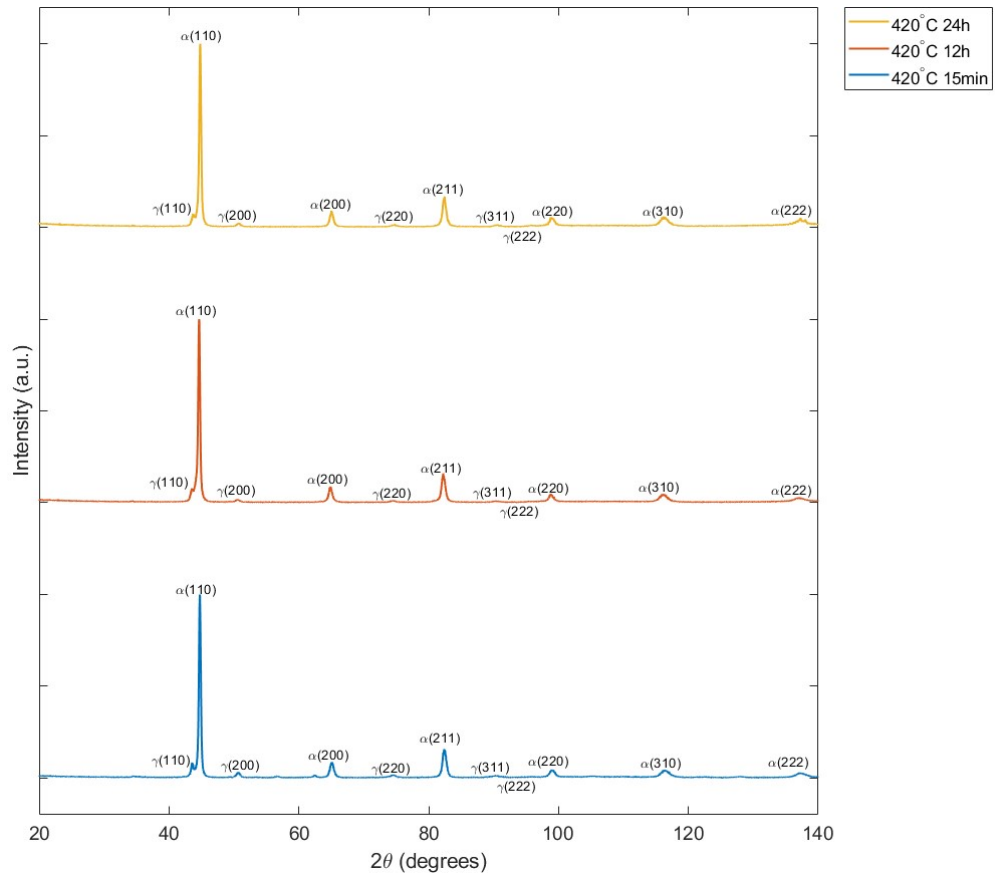
Figure 4.40. XRD patterns of samples isothermally heat-treated at 420ºC, α: Ferrite, γ: Austenite
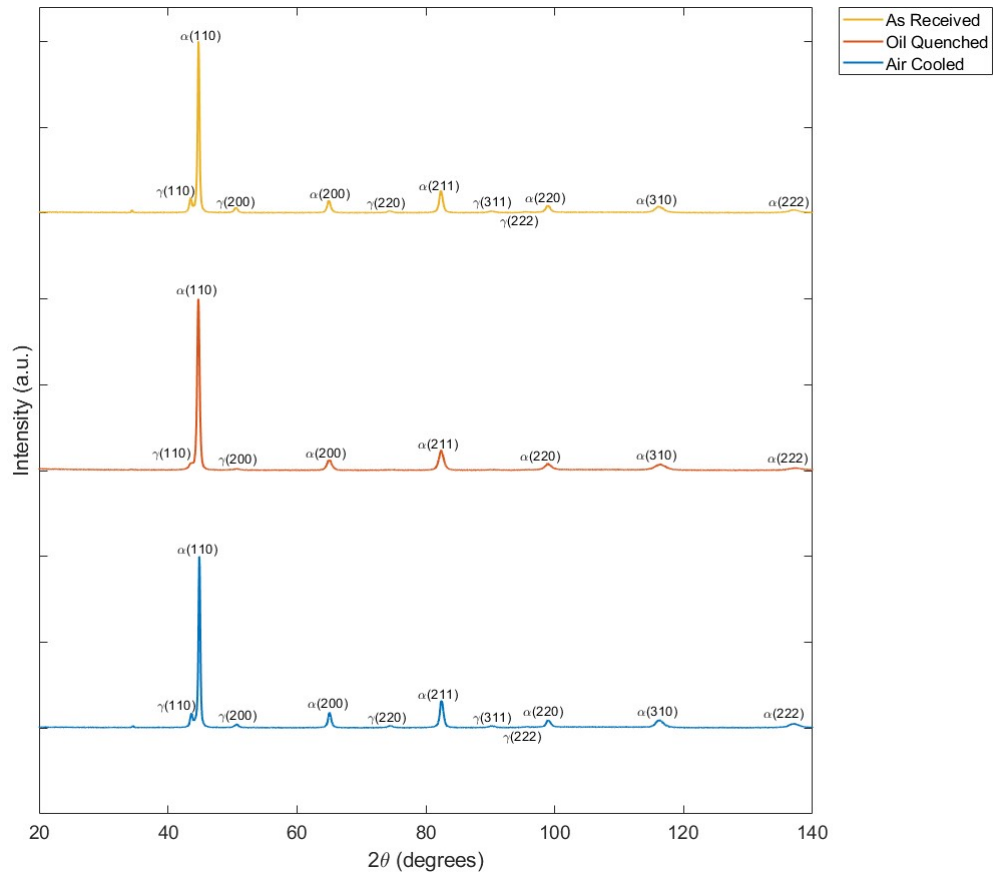
Figure 4.41. XRD patterns of samples normalized, directly quenched in oil and in as received condition, α: Ferrite, γ: Austenite
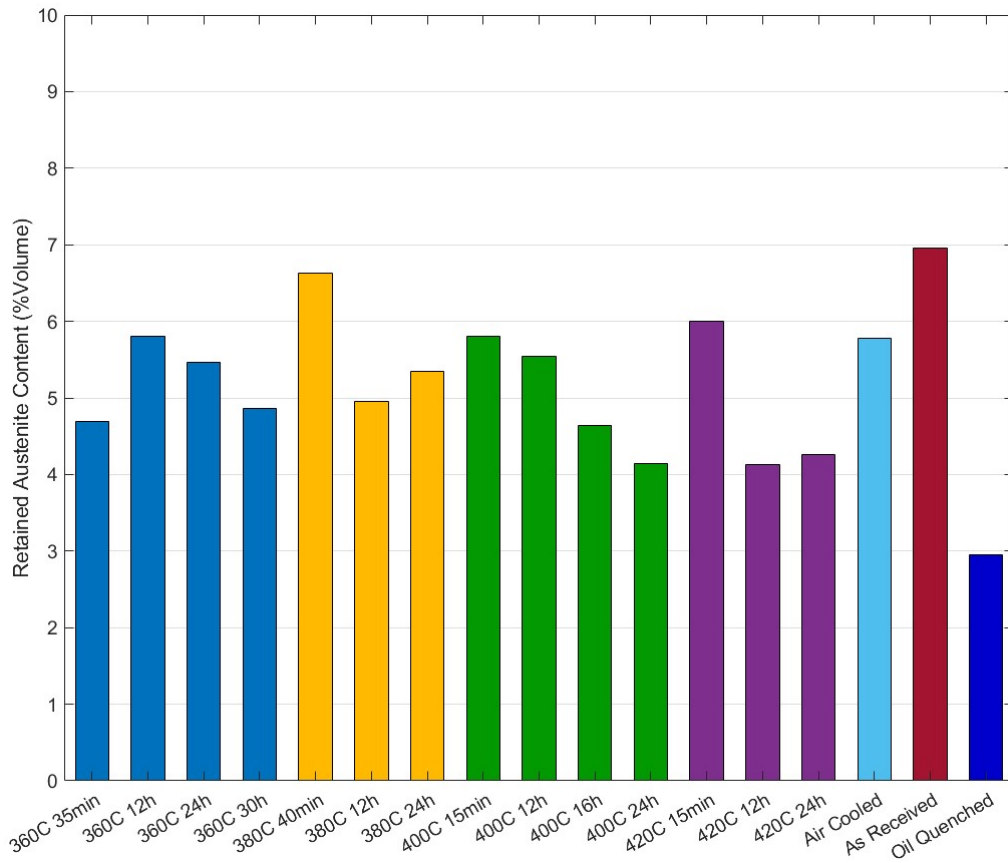
Figure 4.42. Retained austenite content of all samples plotted as a bar chart

Figure 4.42 shows that there is no significant change in retained austenite, the amounts calculated from XRD data are approximately the same, and the values are around the detection limit of XRD equipment. The retained austenite amounts given here possibly belong to the austenite present between bainite sheaves, not the blocky M/A. The oil quenched sample shows the smallest amount of austenite, and the as received and normalized samples show the largest. The transformation temperature does not have a significant effect on retained austenite content, but the heat treatment route does; directly quenching the steel produced the minimum amount of retained austenite and air cooling produced the largest.

4.4.2 Image Analysis for M/A

The optical micrographs at 200x and 500x magnification are analyzed with ImageJ software. The area fraction of white M/A islands on all micrographs are calculated and the results are tabulated in Table 4.5 and Table 4.6. An example of the image analysis is given in Figure 4.43. The analysis is applied to both magnifications since the magnification levels affect the resolution and higher resolution images give a more detailed analysis.

Table 4.5 Area Fraction results for all samples, 200x optical micrographs

Sample ID	Image	Area Percent of White M/A Regions
360C-35min	200x	15.3 (±5.5)
360C-12h	200x	5.0 (±0.2)
360C-24h	200x	5.9 (±1.7)
360C-30h	200x	4.4 (±1.3)
380C-40min	200x	9.5 (±0.8)
380C-12h	200x	9.0 (±1.4)
380C-24h	200x	2.7 (±0.4)
400C-15min	200x	16.7 (±0.8)
400C-12h	200x	7.2 (±1.8)
400C-16h	200x	10.5 (±3.9)
400C-24h	200x	4.4 (±4.8)
420C-15min	200x	28.7 (±2.7)
420C-12h	200x	21.9 (±1.0)
420C-24h	200x	19.8 (±1.0)
Normalized	200x	17.2 (±0.6)
As Received	200x	14.8 (±0.4)

Table 4.6 Area Fraction results for all samples, 500x optical micrographs

Sample ID	Image	Area Percent of White M/A Regions
360C-35min	500x	22.9 (±1.2)
360C-12h	500x	15.2 (±3.9)
360C-24h	500x	16.5 (±2.0)
360C-30h	500x	7.8 (±1.4)
380C-40min	500x	20.2 (±1.7)
380C-12h	500x	23.9 (±2.2)
380C-24h	500x	18.4 (±3.4)
400C-15min	500x	36.1 (±2.5)
400C-12h	500x	21.1 (±1.9)
400C-16h	500x	20.8 (±6.7)
400C-24h	500x	27.4 (±2.3)
420C-15min	500x	34.8 (±2.6)
420C-12h	500x	32.9 (±3.7)
420C-24h	500x	30.8 (±0.3)
Normalized	500x	33.1 (±3.6)
As Received	500x	23.5 (±0.6)

The results in Table 4.5 and Table 4.6 confirm the observations made qualitatively in the microstructural characterization of isothermally transformed samples in a quantitative manner. The area fraction studies show that martensite/austenite islands indeed increase with increasing isothermal transformation temperature and decrease with increasing holding time.
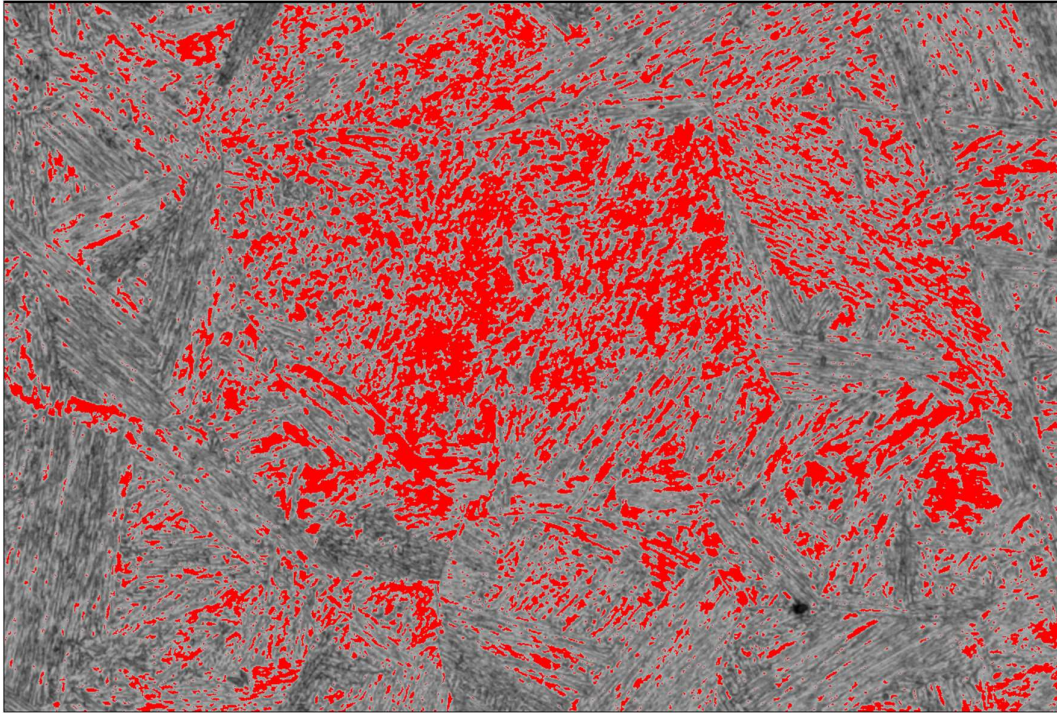
Figure 4.43. 500x magnification optical micrograph of 360C-35min analyzed for M/A area fraction. The image is converted into a 16-bit black-and-white image and thresholding is applied to color in the white M/A regions to red.
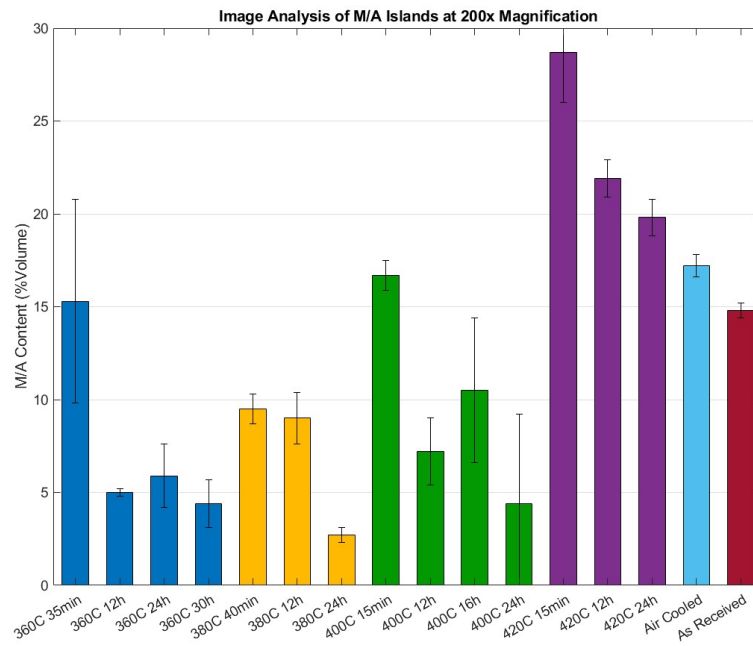
Figure 4.44. M/A Image Analysis results for all samples at 200x magnification plotted as a bar chart
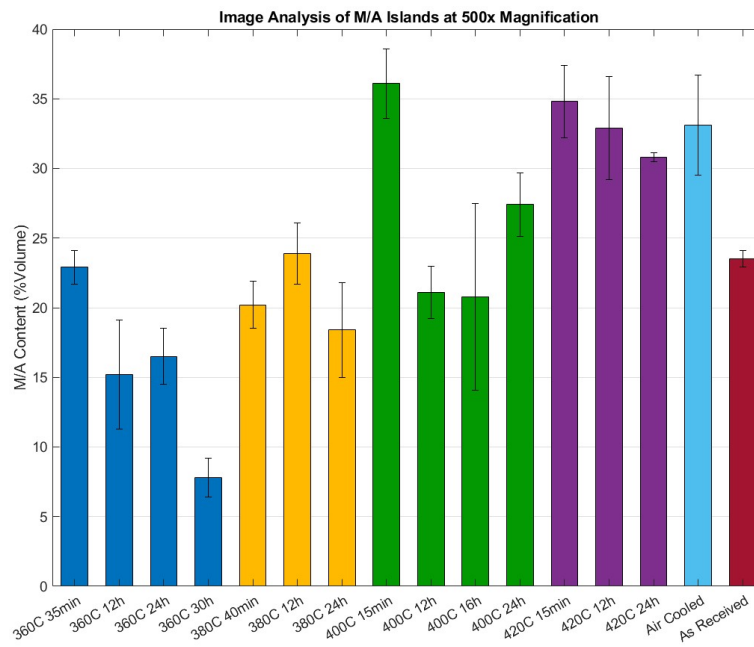
Figure 4.45. M/A Image Analysis results for all samples at 500x magnification plotted as a bar chart

4.5   Mechanical Characterization

4.5.1   Hardness Measurements

Hardness measurements of each specimen, and their final microstructure, are listed in Table 4.7 and visually presented as a bar plot in Figure 4.46.

Table 4.7 Sample ID, resulting microstructure and hardness values (mean and standard deviation) for each sample

Sample	Microstructure	Hardness (HV30)
360C-35min	LB+M/A	406 ($\pm$7)
360C-12h	LB+M/A	403 ($\pm$3)
360C-24h	LB+M/A	391 ($\pm$7)
360C-30h	LB+M/A	420 ($\pm$2)
380C-40min	LB+M/A	404 ($\pm$1)
380C-12h	LB+M/A	390 ($\pm$5)
380C-24h	LB+M/A	389 ($\pm$9)
400C-15min	LB+M/A	383 ($\pm$5)
400C-12h	LB+M/A	395 ($\pm$2)
400C-16h	LB+M/A	378 ($\pm$4)
400C-24h	LB+M/A	390 ($\pm$4)
420C-15min	LB+M/A	396 ($\pm$6)
420C-12h	LB+M/A	413 ($\pm$3)
420C-24h	LB+M/A	421 ($\pm$1)
As Received	LB+M/A	395 ($\pm$2)
Oil Quenched	M	526 ($\pm$4)
Normalized	LB+M/A	389 ($\pm$4)
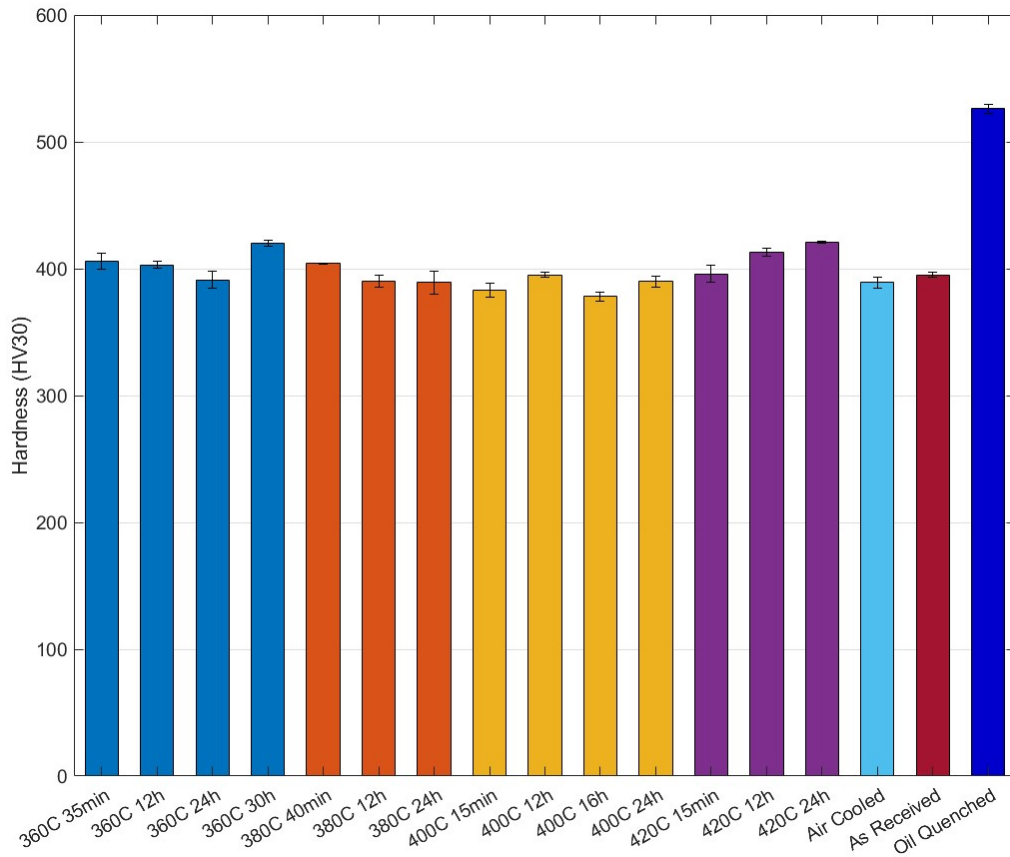
Figure 4.46. Hardness measurements of all specimens, plotted as a bar chart

Oil quenching produced the hardest specimens since martensite is the hardest phase among all the phases characterized, it has average hardness value of 526 HV. Normalizing produces the softest specimen, with an average hardness of 389 HV. Isothermally heat-treated specimens have similar hardness values, but there is a slight increase as the transformation temperature is increased. Isothermal heat treatments produce hardness values in the range of 380-420 HV. The holding time appears to increase the hardness values across some of the transformation temperatures, such as 360℃ and 420℃.

4.5.2   Tensile Test Results

Tensile test results are given in Table 4.8 and stress-strain diagrams obtained from the test are given in Figure 4.47. The results show that as the transformation temperature is increased, higher tensile strength values are obtained, at the expense of plastic deformation capability (as indicated by percent elongation and reduction in area). The results in Table 4.6 are the values of the 2 samples tested for each ITT. The highest observed UTS belongs to 420C-24h at 1427 MPa, whereas the maximum observed yield strength belongs to 360C-24h as 1145 MPa. The largest elongation and area reduction was observed for 360C-24h specimen with values of 17.6% and 53.4%, respectively.

Table 4.8 Tensile test results

Sample	Hardness (HV30)	YS (MPa)	UTS (MPa)	%EL	%RA
360C-24h	391 (±7)	1100-1145	1255-1264	16.7-17.6	49.2-53.4
400C-24h	390 (±4)	757-788	1364-1375	11.4-13.1	34.1-34.3
420C-24h	421 (±1)	862-1109	1397-1414	11.4-13.1	28.8-28.9
Normalized	389 (±4)	1093	1264	13.2	44.8
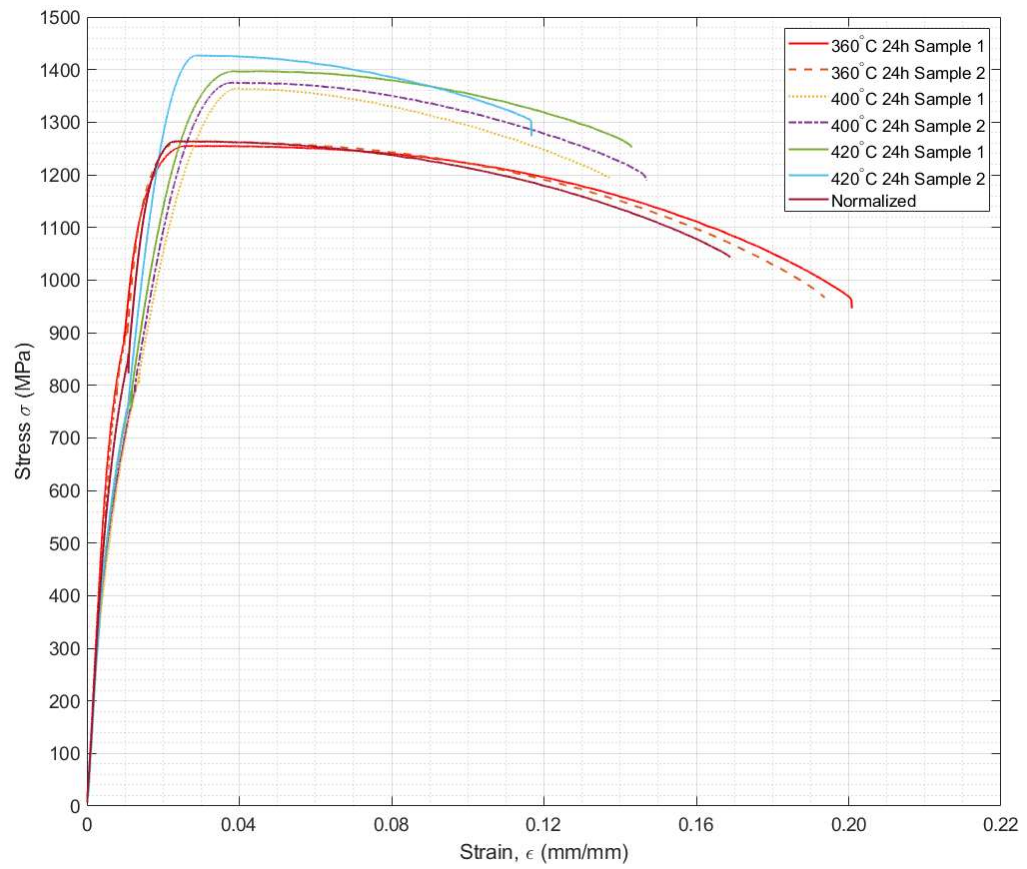
Figure 4.47. Stress-strain diagram of each sample

4.5.2.1   Fractography

The fractography studies were conducted using the tensile test fracture surfaces obtained from the test. Figure 4.48 gives the fracture surface of the normalized sample, Figure 4.49, Figure 4.50, and Figure 4.51 show the fracture surfaces of isothermally transformed samples at temperatures 360ºC, 400ºC, and 420ºC, respectively. The normalized fracture surface in Figure 4.48 and 360ºC sample in Figure 4.49 show the typical behavior of ductile fracture surfaces, with dimples and second phase particles. However, the fracture surfaces in Figure 4.50, and Figure 4.51 show a mixture of ductile and brittle fracture surface features such as dimples, second phase particles, and cleavages.
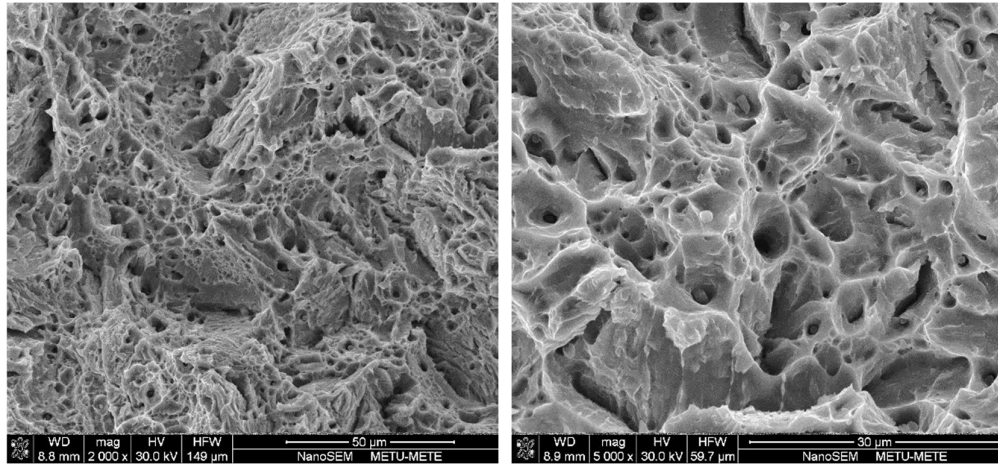
Figure 4.48. Fracture surface of normalized tensile test specimen
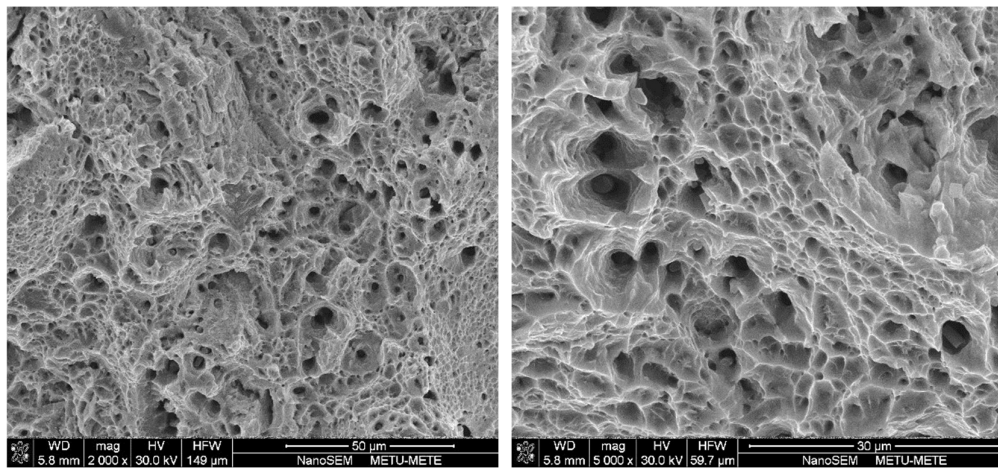
Figure 4.49. Fracture surface of 360C-24h tensile test specimen
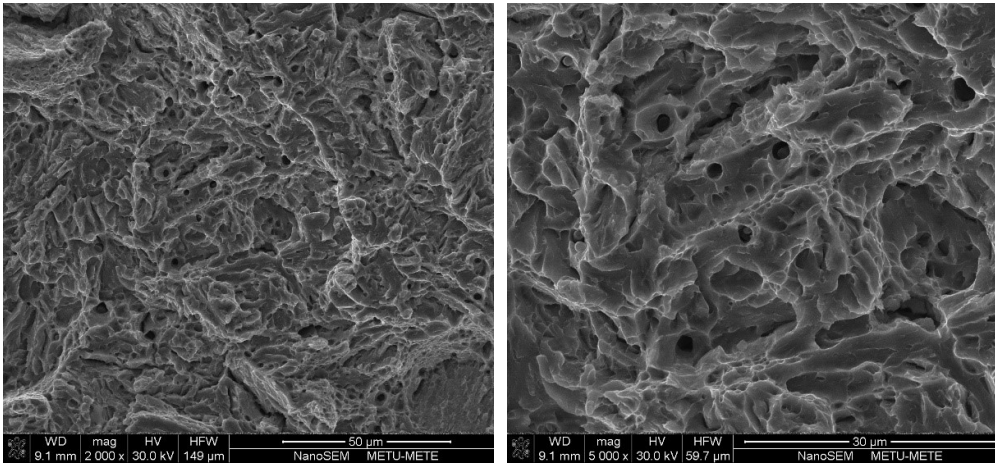
Figure 4.50. Fracture surface of 400C-24h tensile test specimen
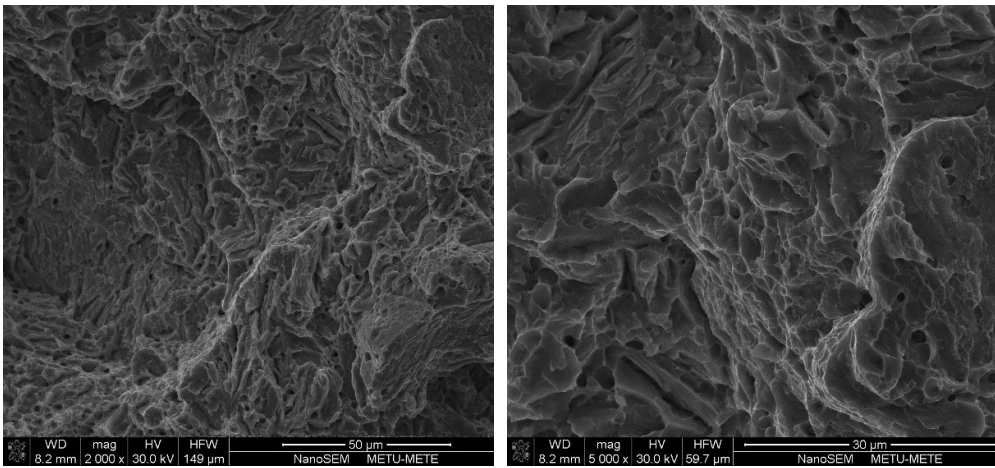
Figure 4.51. Fracture surface of 420C-24h tensile test specimen

CHAPTER 5

DISCUSSION

In this study, isothermal heat treatments and continuous cooling were applied to a bainitic forging steel to obtain bainitic and bainitic-martensitic mixtures. Microstructural characterization, quantitative phase analysis, and mechanical tests were applied to determine an optimum processing route so that a microstructure is obtained which results in the best mechanical properties.

5.1   Microstructural Characterization

The optical microscopy and SEM imaging shows that all specimens, aside from oil quenched, show bainitic microstructures with islands of blocky M/A. No carbide or cementite precipitation is observed. Large, elongated inclusions are present, arising from the previous process history and chemical composition.

5.1.1   As Received, Air Cooled, and Martensitic Microstructures

Metallographic examinations of as received and normalized microstructures reveal that the air-cooling results in formation of granular bainite with islands of blocky M/A which can be observed in Figure 4.3 and Figure 4.5. The SEM imaging of the same specimens reveal that large islands or chunks of blocky M/A are present in the microstructure. High magnification SEM images reveal the internal structure of blocky M/A islands and there are indications that these islands are transformed into martensite upon oil quenching to room temperature, as seen in Figure 4.20(b) and Figure 4.22(b). The granular bainite formation in air-cooled samples is expected since granular bainite microstructure is usually a product of continuous cooling procedures.

113

The specimen directly quenched in oil produced fully martensitic structure in lath morphology as it is observed in Figure 4.4 and Figure 4.21.

In these specimens, the remnants of hot deformation are present as elongated S-type inclusions. The lower magnification image in Figure 4.3 clearly shows these inclusions. The point like inclusions in Figure 4.5 are also clearly visible. The presence of these inclusions is due to high Mn and S content of the steel.

In none of the images that belong to as received, oil quenched, and air-cooled specimens, carbide precipitation is observed. This is due to high Si content of the steel. Silicon is a carbide suppressor in bainitic steels, and its effect is clearly present in these microstructures. The carbide suppression causes carbon partitioning between bainitic ferrite and surrounding austenite and that in turn stabilizes the austenite. The retained austenite is generally seen as a thin film between the bainite sheaves. The islands of blocky M/A can transform to martensite or stabilize as retained austenite and for this reason they are named as M/A.

5.1.2   Isothermally Transformed Microstructures

The isothermal transformations were done at temperatures 360°C, 380°C, 400°C, and 420°C for various durations and they exhibited in mostly bainitic microstructures. As the transformation temperature is increased, amount of blocky M/A also increased. Incomplete transformation phenomenon is observed, and the transformation stopped much before the durations predicted by JMatPro software. In none of the isothermally transformed samples, carbide precipitation is observed.

The microstructures formed at 360°C appears to be lower bainite together with islands of M/A under optical microscope. 360C-35min sample has the highest amount of M/A islands, as seen in Figure 4.6 and Figure 4.23. The 360C-12h, 360C-24h, and 360C-30h samples were similar in terms of morphology, with bainitic ferrite growing into the austenite grains, as seen in Figure 4.23, Figure 4.24, Figure 4.25, and Figure 4.26. The austenite grain boundaries are visible in SEM images,

Figure 4.23, Figure 4.24, Figure 4.25, and Figure 4.26. The optical microscopy images in Figure 4.6, Figure 4.7, Figure 4.8, and Figure 4.9 contain both lower bainite and granular bainite regions with small white islands of blocky M/A. The SEM images also show mostly lower bainitic microstructure, with small regions of blocky M/A along prior austenite grain boundaries. Among all the specimens, transformations at 360°C produced the smallest M/A islands, possibly due to low transformation temperature. The bainitic ferrite sheave thickness appears to be the smallest for 360°C, again, possibly due to low transformation temperature. As the transformation duration is increased, the amount of blocky M/A decreased.

The microstructural features of isothermally heat-treated specimen at 380 °C is similar to that of 360 °C specimens. For 380C-40min specimen, the high magnification optical microscope image in Figure 4.10 appears to have larger white M/A islands with lower and granular bainitic microstructure. The presence of larger M/A islands are indicative of incomplete bainite transformation. For 380C-12h and 380C-24h specimens, in Figure 4.11 and Figure 4.12, the amount of M/A islands appears to be similar, and there are no significant microstructural differences between the images. The high magnification SEM images of 380C-40min and 380C-24h contain large flat regions of M/A islands in Figure 4.27 and Figure 4.29, respectively. The low magnification images of 380C-40min, 380C-12h, and 380C-24h in Figure 4.27, Figure 4.28, Figure 4.29 show the same bainite morphology with austenite grain boundaries visible in each image. Compared to 360°C, there is no significant difference in bainite morphology, as expected, since both transformation temperatures are low enough to produce lower bainite. As the transformation duration is increased, the amount of blocky M/A decreased.

The optical microscopy images of samples heat-treated at 400 °C, given in Figure 4.13, Figure 4.14, Figure 4.15, and Figure 4.16, also show similar features to previous samples. However, the high magnification images in show that amount of white M/A islands are are larger compared to 360 °C and 380 °C, especially in Figure 4.14 and Figure 4.16. The low magnification images also have more white M/A islands at different spots, but the images are darker, which is indicative of a change

in microstructure and morphology. The samples, when compared amongst themselves, all show white M/A islands, meaning the transformation did not reach to completion. The white M/A phase is more pronounced in 400C-15min specimen, but 400C-12h, 400C-16h and 400C-24h are similar to each other. The high magnification images in Figure 4.14, Figure 4.15, and Figure 4.16 show lower and granular bainite with M/A islands. Since they are similar to each other in terms of microstructural features, it is possible that the transformation stops before completion, i.e., T_0 curve is reached. The SEM images reveal that for 400C-15min sample, the amount of flat M/A regions are larger, compared to previous specimens heat-treated at 360 ^{o}C and 380 ^{o}C. The bainite morphology is closer to granular bainite with sporadic distribution of lower bainite. SEM images of 400C-12h, 400C-16h and 400C-24h reveal that flat blocky M/A islands are larger in comparison to 360C and 380C samples and the bainite morphology is different. The lower bainite is not as pronounced in these samples, granular bainite is present instead. The wavy images in Figure 4.31 for 400C-12h could be due to overetching, or a transition from granular to lower bainite was happening. The transformation duration for 400°C does not appear to have a significant effect on the amount of blocky M/A present in the structure, based on the observations from optical microscope and SEM examinations. The largest M/A islands are present on 400C-15min SEM images in Figure 4.30. The SEM images show that on the M/A islands, there are morphological indicators that the blocky M/A in the structure transformed to mostly martensite. The retained austenite results also indicate that bainite transformation is complete across the specimens and austenite in the structure is most probably present only between the sheaves of bainite. The blocky M/A in the structure transformed into martensite and since the martensite and bainitic ferrite peaks overlap in XRD data, there is no way of separating or objectively determining whether the blocky M/A completely transformed into martensite. TEM studies are required for confirmation.

Optical microscopy images of samples heat-treated at 420°C reveal that they have the highest fraction of white M/A islands. The bainite morphology appears to be granular and/or acicular under optical microscope and under SEM, a combination of

116

granular and lower bainite is present in the microstructure. The SEM images in Figure 4.34, Figure 4.35, and Figure 4.36 reveal that 420°C samples have the largest M/A islands in the structure. As the transformation temperature is increased, for a constant carbon concentration, the T_0 curve will be reached earlier during transformation, which leads to a lower fraction of bainitic ferrite and higher fraction of untransformed austenite. Upon quenching, the austenite transforms into martensite and some austenite will be retained since the austenite is rich enough due to carbon partitioning. In addition, it is apparent that higher transformation temperatures cause the austenite/martensite morphology to become blocky instead of needle-like or film-like. To obtain a higher fraction of bainite, the T_0 curve must shift to the right-hand side on the Temperature vs Carbon Concentration diagram. This can be done by adding alloying elements and/or increasing the concentration of the elements that shift the T_0 curve to the right. For a constant concentration of alloying elements, a higher fraction of bainitic ferrite can be obtained by lowering the transformation temperature so that T_0 curve is reached at a later stage during transformation. Also, a lower transformation temperature will lead to thinner bainite sheaves, hence higher strength levels.

The transformation duration does not appear to have a significant effect on blocky M/A, indicating that the transformation stopped before the predicted time.

In most of the sample micrographs, elongated and sphere-like precipitates and inclusions can be observed (see Figure 4.3, Figure 4.5, Figure 4.6, Figure 4.7, Figure 4.12, Figure 4.18, and Figure 4.19). The inclusion morphology is indicative of forging process, and they are possibly MnS particles since the Mn and S content are high enough to form MnS inclusions.

The increase in the fraction of M/A islands can be explained by taking the T_0 curve into consideration. The T_0 curve for this alloy is plotted in Figure 4.2(c). For constant carbon concentration, as the transformation temperature increase, the bainite fraction will decrease. This can be visualized as such: if a tie line is drawn at the transformation temperature, the lever rule between the T_0 curve and the Ae1 line will

give the amount of bainite and untransformed austenite in the structure. Hence, higher transformation temperatures will result in less bainite transformation and transformation will stop sooner than predicted. If the temperature is increased further, the bainite transformation will not happen. This is visualized in Figure 5.1. The left-hand side of the T_0 curve is the region where bainite formation is thermodynamically feasible. As the transformation temperature increase, it becomes easier to meet the T_0 curve, on which the free energies of ferrite and austenite phases become equal, i.e., an equilibrium is reached. On the right-hand side of the T_0 curve, the bainite reaction is thermodynamically infeasible. If a higher fraction of bainite is desired, either the alloying concentrations must change so that T_0 shift to the right, or the transformation temperature should be lowered so that T_0 curve is met at a later stage.

Figure 5.2 shows 2 SEM images side by side, comparing the microstructures obtained by isothermal transformations at $360^{\circ}C$ and $420^{\circ}C$ for a duration of 24 hours. The comparison clearly demonstrates that a transformation at a higher temperature leads to retention of more M/A islands are formed.
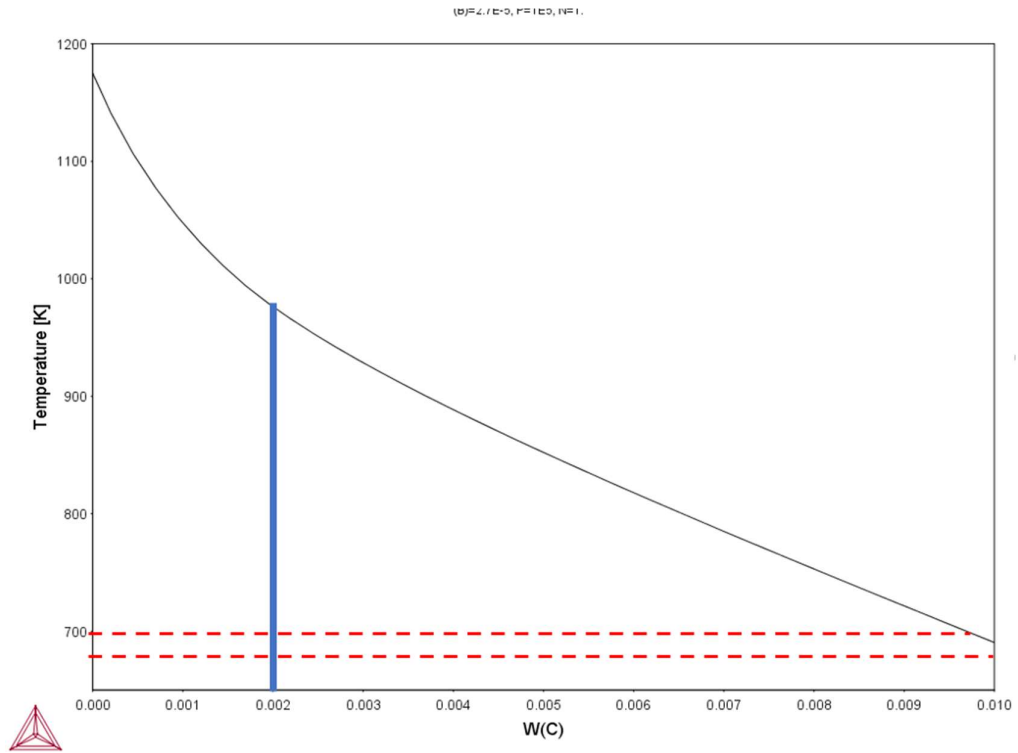
Figure 5.1. The T_0 curve and two tie lines for two different transformation temperatures. As the temperature is increased, the right hand side of the tie line gets shorter, indicating that bainite fraction decreases.
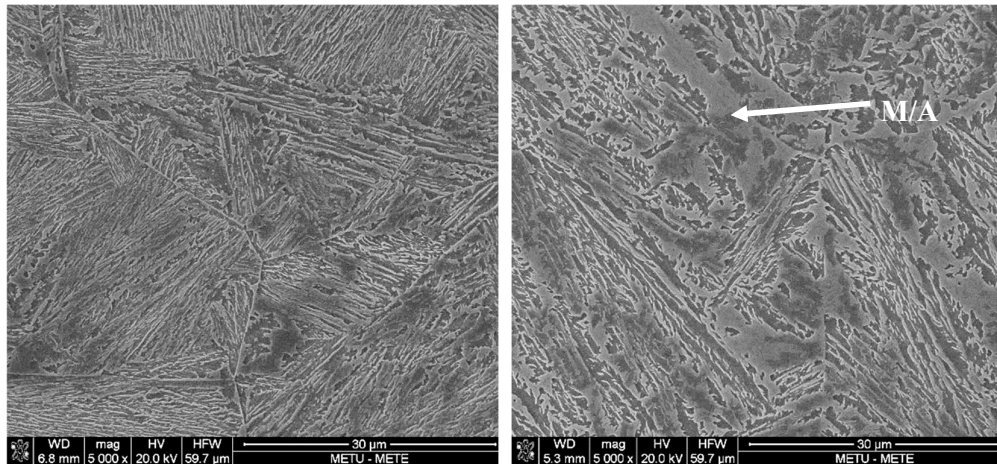
Figure 5.2. 360C-24h specimen (left) and 420C-24h specimen (right). The blocky M/A content is much higher at 420ºC.

5.2　Retained Austenite Measurements

Retained austenite measurements show that across all specimens, the amount of retained austenite in the system is similar. The lowest observation was for oil quenched specimen, which makes sense since oil quenching will produce only martensite and no bainite. The bainite transformation stabilizes some of the austenite in the system due to carbon rejection during transformation. However, martensite formation is purely displacive and carbon is trapped inside the structure.

As explained in the previous section, the bainite transformation stops earlier than expected due to T_0 phenomenon and if the temperature is increased, the transformation stops even earlier, with higher untransformed austenite levels. But this deduction cannot be made from the retained austenite data. The SEM image comparison is much more helpful to observe this phenomenon.

When the amount of M/A regions are taken into consideration, it seems safe to assume that the retained austenite peaks in the XRD patterns in Figure 4.37, Figure 4.38, Figure 4.39, Figure 4.40, and Figure 4.41 belong to the retained austenite films between bainite sheaves. Moreover, within several M/A islands, the presence of martensite has been demonstrated (see Figure 4.22(b), Figure 4.24(b), Figure 4.27(b), Figure 4.29(b), Figure 4.30(b), Figure 4.35(b), and Figure 4.36(b)). It is proven both by microscopy and XRD, that bainite reaction is incomplete for this alloy, under given conditions. If the carbon content of this alloy had been higher, higher retained austenite values would have been obtained from XRD analysis.

5.3   Mechanical Characterization

The hardness values are similar in terms of magnitude for isothermally transformed specimens. The highest hardness value belongs to martensite as expected. However, the hardness values for bainite fluctuate ever so slightly, depending on isothermal transformation temperature and holding time. At 360°C, the hardness values are around 400 HV and for 380°C, it is around 390 HV. For 400°C, we have the lowest hardness values observed for bainite, going as low as 378 HV. Finally, at 420°C, the hardness values increase to 410 HV. The normalized and as received specimens have similar hardness but both are lower than some of the isothermally transformed specimens. From experimental observations and literature survey, it is known that as the transformation temperature is decreased, the bainite sheave thickness decreases and a finer microstructure form. This decrease in sheave thickness results in a harder bainite due to higher dislocation density. As the temperature is increased, the sheave thickness increases and dislocation density decreases, resulting in a softer bainite. The trend that was expected from the results was that at higher transformation temperatures, hardness values should have been lower. However, the hardness values are around the same levels. This can be explained in terms of martensite and retained austenite contents. Although the bainite at higher transformation temperatures is softer, the presence of martensite in the microstructure may increase the hardness levels, offsetting the softness of the bainite. Combined with the SEM images, image analysis for M/A area fraction in Table 4.6, and XRD analysis, it becomes apparent that at transformations of 400 °C and 420 °C, higher levels of martensite are present. The low values of hardness for normalized specimens cannot be explained from the retained austenite levels. However, the microstructure of normalized specimen contains more granular bainite, hence the decrease in hardness when the steel is air cooled could be due to formation of granular bainite.

If the tensile test results are analyzed, increase in the transformation temperature increased the UTS but decreased the yield strength and ductility parameters such as

percent elongation and reduction in area. This behavior can also be explained from microstructural differences arising from transformation temperature.

The microstructure of 360C-24h sample is mostly needle-like lower bainite with few M/A islands. Since this temperature is the closest to M_s, the microstructure results in the smallest bainite sheave thickness. The reduction in bainite lath size leads to higher dislocation density, which leads to higher yield strength levels. However according to Long et al., low carbon low temperature bainite shows lower work hardening, which explains the lower UTS levels. As the transformation temperature is increased, the strength levels are expected to decrease and the yield strength indeed decreases. However, the UTS levels increase significantly, from 1250 MPa at 360 ^{o}C, to 1370 MPa at 400 ^{o}C and 1412 MPa at 420 ^{o}C. The bainite thickness increase leading to lower strength values cannot explain this behavior. But the formation of martensite can. Again, at higher transformation temperatures, the bainite transformation stops and remaining austenite transforms to martensite upon quenching. Higher levels of martensite in the structure will lead to higher strength values. Since martensite is a strong but brittle phase, it is also expected that specimens with high martensite levels will have lower ductility values and indeed they do. The percent elongation values measured for 400C-24h and 420C-24h are among the lowest, with only 12.3%. Whereas 360C-24h has an elongation of 17.6%. In the light of these facts, it can be concluded that transformation at 360 ^{o}C yields the highest fraction of bainite with superior mechanical properties and ductility. The decrease in yield strength can also be explained from the presence of granular bainite at 400 ^{o}C and 420 ^{o}C. The normalized specimen shows the same behavior with 360C-24h in terms of strength. However, the ductility is lower than 360C-24h.

Another point of comparison can be made with tensile ductility. Tensile toughness refers to multiplication of UTS and percent elongation and it is usually used as a measure of toughness. The tensile ductility of the specimens is listed below in Table 5.1. Again, it is proven that 360C-24h possesses superior properties and hence performance.

Table 5.1 Tensile toughness of the specimens tested

Sample ID	UTS (MPa)	%EL	Tensile Toughness (UTS×%EL) (GPa)
360C-24h	1255-1264	16.7-17.6	21.1-22.1
400C-24h	1364-1375	11.4-13.1	15.5-18.0
420C-24h	1412	11.4-13.1	16.3-18.3
Normalized	1264	13.2	16.7

CHAPTER 6

CONCLUSION

In this work, isothermal heat treatments and continuous cooling were used to produce bainitic and bainitic-martensitic combinations from a microalloyed bainitic forging steel. To establish the optimal processing procedure, microstructural characterisation, quantitative phase analysis, and mechanical testing were used. In this study, it is demonstrated that not only microstructure can be controlled with isothermal transformation, but the mechanical properties are also improved.

The following conclusions are drawn from this study:

1. Microstructural studies show that continuous cooling gives a heterogenous microstructure, a mixture of granular bainite and blocky M/A whereas isothermal transformation yields a more homogeneous microstructure. Lower transformation temperatures yield in much finer bainite microstructure with minimal martensite formation.

2. As the isothermal transformation temperature is increased, the bainite reaction halts at an earlier stage, leading to higher amounts of M/A islands in the microstructure. Although the retained austenite measurements do not indicate this, the SEM images combined with hardness values and the quantitative image analysis of optical micrographs point towards this conclusion.

3. Continuously cooled specimens gave poorer mechanical properties due to their heterogenous microstructure. The control of the microstructure is difficult in air cooling and relatively easy in isothermal transformation.

4. Isothermal transformation gives the best mechanical properties in terms of strength and ductility, with 360C-24h specimen.

5. If a process is to be designed, then it is suggested that an isothermal heat treatment should be employed, whether with salt baths or tunnel furnaces.

6. As future work, the influence of two-step isothermal treatments and quench and partitioning behavior of the steel studied in this work can be investigated.

REFERENCES

[1] Wang, Z., Hui, W., Xie, Z., Zhang, Y., & Zhao, X. (2020). Enhancing mechanical properties of a V + Ti microalloyed bainitic forging steel via tailoring microstructure through controlled forging. *Journal of Materials Science*, *55*(24), 10849–10862. https://doi.org/10.1007/s10853-020-04695-3

[2] Matlock, D. K., Krauss, G., & Speer, J. G. (2001). Microstructures and properties of direct-cooled microalloy forging steels. *Journal of Materials Processing Technology*, *117*(3), 324–328. https://doi.org/https://doi.org/10.1016/S0924-0136(01)00792-0

[3] Keul, C., Wirths, V., & Bleck, W. (2012). New bainitic steels for forgings. *Archives of Civil and Mechanical Engineering*, *12*(2), 119–125. https://doi.org/10.1016/j.acme.2012.04.012

[4] Buchmayr, B. (2016). Critical Assessment 22: bainitic forging steels. *Materials Science and Technology*, *32*(6), 517–522. https://doi.org/10.1080/02670836.2015.1114272

[5] Kesti, V., Kaijalainen, A., Väisänen, A., Järvenpää, A., Määttä, A., Arola, A. M., Mäntyjärvi, K., & Ruoppa, R. (2014). Bendability and Microstructure of Direct Quenched Optim® 960QC. *Materials Science Forum*, *783–786*, 818–824. https://doi.org/10.4028/www.scientific.net/MSF.783-786.818

[6] Sourmail, T., Maminska, Dipl.-I., Roth, Dipl.-I., D'eramo, Dipl.-I., & Galtier, Dipl.-I. (2017). *30 years of bainitic forging steels*.

[7] Sharma, S., Sangal, S., & Mondal, K. (2011). Development of New High-Strength Carbide-Free Bainitic Steels. *Metallurgical and Materials Transactions A*, *42*, 3921–3933. https://doi.org/10.1007/s11661-011-0797-6

[8] Bhadeshia, H. K. D. H. (2005). High Performance Bainitic Steels. *Materials Science Forum*, *500–501*, 63–74. https://doi.org/10.4028/www.scientific.net/MSF.500-501.63

[9] Adamczyk-Cieślak, B., Koralnik, M., Kuziak, R., Majchrowicz, K., Zygmunt, T., & Mizera, J. (2022). The Impact of Retained Austenite on the Mechanical Properties of Bainitic and Dual Phase Steels. *Journal of Materials Engineering and Performance*. https://doi.org/10.1007/s11665-021-06547-w

[10] Bhadeshia, H. K. D. H. (2019). *Bainite in Steels: Theory and Practice, Third Edition*. CRC Press. https://books.google.com.tr/books?id=SwqWDwAAQBAJ

[11] Yin, J., (2017). Formation of Bainite in Steels [Doctoral Thesis, KTH Royal Institute of Technology]. KTH Publication Database DiVA. https://www.diva-portal.org/smash/get/diva2:1097218/FULLTEXT01.pdf

[12] Garcia-Mateo, C., Paul, G., Somani, M. C., Porter, D. A., Bracke, L., Latz, A., Garcia De Andres, C., & Caballero, F. G. (2017). Transferring Nanoscale Bainite Concept to Lower C Contents: A Perspective. *Metals*, *7*(5). https://doi.org/10.3390/met7050159

[13] Pandit, A. S., & Bhadeshia, H. K. D. H. (2011). Diffusion-controlled growth of pearlite in ternary steels. *Proceedings: Mathematical, Physical and Engineering Sciences*, *467*(2134), 2948–2961. http://www.jstor.org/stable/23058917

[14] Kelly, P. M. (2012). 1 - Crystallography of martensite transformations in steels. In E. Pereloma & D. v Edmonds (Eds.), *Phase Transformations in Steels* (Vol. 2, pp. 3–33). Woodhead Publishing. https://doi.org/https://doi.org/10.1533/9780857096111.1.3

[15] Callister, W. D., & Rethwisch, D. G. (2018). *Materials Science and Engineering: An Introduction*. Wiley. https://books.google.com.tr/books?id=ZdVSDwAAQBAJ

[16] Yang, Z.-G., & Fang, H.-S. (2005). An overview on bainite formation in steels. *Current Opinion in Solid State and Materials Science*, *9*(6), 277–286. https://doi.org/https://doi.org/10.1016/j.cossms.2006.06.005

[17] Abbaszadeh, K., Saghafian, H., & Kheirandish, S. (2012). Effect of Bainite Morphology on Mechanical Properties of the Mixed Bainite-martensite Microstructure in D6AC Steel. *Journal of Materials Science & Technology*, *28*(4), 336–342. https://doi.org/https://doi.org/10.1016/S1005-0302(12)60065-6

[18] Campbell, F. C. (2008). *Elements of Metallurgy and Engineering Alloys*. ASM International. https://books.google.com.tr/books?id=6VdROgeQ5M8C

[19] Huang, Y., Zhao, A., He, J., Wang, X., Wang, Z., & Qi, L. (2013). Microstructure, crystallography and nucleation mechanism of NANOBAIN steel. *International Journal of Minerals, Metallurgy, and Materials*, *20*, 1155–1163. https://doi.org/10.1007/s12613-013-0849-6

[20] Yoozbashi, M. N., & Yazdani, S. (2015). XRD and TEM study of bainitic ferrite plate thickness in nanostructured, carbide free bainitic steels. *Materials Chemistry and Physics*, *160*, 148–154. https://doi.org/https://doi.org/10.1016/j.matchemphys.2015.03.071

[21] Cornide, J., Garcia-Mateo, C., Capdevila, C., & Caballero, F. G. (2013). An assessment of the contributing factors to the nanoscale structural refinement of advanced bainitic steels. *Journal of Alloys and Compounds*, *577*, S43–S47. https://doi.org/https://doi.org/10.1016/j.jallcom.2011.11.066

[22] Long, X. Y., Kang, J., Lv, B., & Zhang, F. C. (2014). Carbide-free bainite in medium carbon steel. *Materials & Design*, *64*, 237–245. https://doi.org/https://doi.org/10.1016/j.matdes.2014.07.055

[23] Caballero, F. G. (2012). 12 - Carbide-free bainite in steels. In E. Pereloma & D. v Edmonds (Eds.), *Phase Transformations in Steels* (Vol. 1, pp. 436–467). Woodhead Publishing. https://doi.org/https://doi.org/10.1533/9780857096104.3.436

[24] Rampelberg, C., Allain, S. Y. P., Geandier, G., Teixeira, J., Lebel, F., & Sourmail, T. (2021). Carbide-Free Bainite Transformations Above and Below

Martensite Start Temperature Investigated by In-Situ High-Energy X-Ray Diffraction. *JOM*, *73*(11), 3181–3194. https://doi.org/10.1007/s11837-021-04903-8

[25] Furuhara, T. (2012). 11 - Carbide-containing bainite in steels. In E. Pereloma & D. v Edmonds (Eds.), *Phase Transformations in Steels* (Vol. 1, pp. 417–435). Woodhead Publishing. https://doi.org/https://doi.org/10.1533/9780857096104.3.417

[26] Samanta, S., Biswas, P., Giri, S., Singh, S. B., & Kundu, S. (2016). Formation of bainite below the MS temperature: Kinetics and crystallography. *Acta Materialia*, *105*, 390–403. https://doi.org/https://doi.org/10.1016/j.actamat.2015.12.027

[27] Fielding, L. (2013). The Bainite Controversy. *Materials Science and Technology*, *29*, 383–399. https://doi.org/10.1179/1743284712Y.0000000157

[28] Singh, S. B. (2012). 10 - Mechanisms of bainite transformation in steels. In E. Pereloma & D. v Edmonds (Eds.), *Phase Transformations in Steels* (Vol. 1, pp. 385–416). Woodhead Publishing. https://doi.org/https://doi.org/10.1533/9780857096104.3.385

[29] Goulas, C., Kumar, A., Mecozzi, M.-G., Castro-Cerda, F. M., Herbig, M., Petrov, R. H., & Sietsma, J. (2019). Atomic-scale investigations of isothermally formed bainite microstructures in 51CrV4 spring steel. *Materials Characterization*, *152*, 67–75. https://doi.org/https://doi.org/10.1016/j.matchar.2019.03.038

[30] Hillert, M. (1994). Diffusion in growth of bainite. *Metallurgical and Materials Transactions A*, *25*(9), 1957–1966. https://doi.org/10.1007/BF02649044

[31] Hillert, M. (2002). Paradigm shift for bainite. *Scripta Materialia*, *47*, 175–180. https://doi.org/10.1016/S1359-6462(02)00125-2

[32] Caballero, F. G., & Bhadeshia, H. K. D. H. (2004). Very strong bainite. *Current Opinion in Solid State and Materials Science*, *8*(3), 251–257. https://doi.org/https://doi.org/10.1016/j.cossms.2004.09.005

[33] Huang, H., Sherif, M. Y., & Rivera-Díaz-del-Castillo, P. E. J. (2013). Combinatorial optimization of carbide-free bainitic nanostructures. *Acta Materialia*, *61*(5), 1639–1647. https://doi.org/https://doi.org/10.1016/j.actamat.2012.11.040

[34] Wei, W., Retzl, P., Kozeschnik, E., & Erwin Povoden-Karadeniz. (2021). A semi-physical α-β model on bainite transformation kinetics and carbon partitioning. *Acta Materialia*, *207*, 116701. https://doi.org/https://doi.org/10.1016/j.actamat.2021.116701

[35] Ravi, A. M., Sietsma, J., & Santofimia, M. J. (2016). Exploring bainite formation kinetics distinguishing grain-boundary and autocatalytic nucleation in high and low-Si steels. *Acta Materialia*, *105*, 155–164. https://doi.org/https://doi.org/10.1016/j.actamat.2015.11.044

[36] Ravi, A. M., Sietsma, J., & Santofimia, M. J. (2017). Bainite formation kinetics in steels and the dynamic nature of the autocatalytic nucleation process. *Scripta Materialia*, *140*, 82–86. https://doi.org/https://doi.org/10.1016/j.scriptamat.2017.06.051

[37] Shah, M., Das, S., & Ghosh Chowdhury, S. (2019). Effect of Alloying Elements on Microstructure and Mechanical Properties of Air-Cooled Bainitic Steel. *Metallurgical and Materials Transactions A*, *50*. https://doi.org/10.1007/s11661-019-05177-1

[38] Dikić, S., Glišić, D., Fadel, A., Jovanović, G., & Radović, N. (2021). Structure and Strength of Isothermally Heat-Treated Medium Carbon Ti-V Microalloyed Steel. *Metals*, *11*(7). https://doi.org/10.3390/met11071011

[39] Xiao, F., Liao, B., Shan, Y., & Yang, K. (2005). Isothermal transformation of low-carbon microalloyed steels. *Materials Characterization*, *54*(4), 417–422. https://doi.org/https://doi.org/10.1016/j.matchar.2005.01.007

[40] Kumar, A., & Singh, A. (2021). Mechanical properties of nanostructured bainitic steels. *Materialia*, *15*, 101034. https://doi.org/https://doi.org/10.1016/j.mtla.2021.101034

[41] Garcia-Mateo, C., & Caballero, F. (2005). The Role of Retained Austenite on Tensile Properties of Steels with Bainitic Microstructures. *MATERIALS TRANSACTIONS*, *46*. https://doi.org/10.2320/matertrans.46.1839

[42] Tsai, Y. T., Chang, H. T., Huang, B. M., Huang, C. Y., & Yang, J. R. (2015). Microstructural characterization of Charpy-impact-tested nanostructured bainite. *Materials Characterization*, *107*, 63–69. https://doi.org/https://doi.org/10.1016/j.matchar.2015.06.037

[43] Timokhina, I. B., Beladi, H., Xiong, X., Adachi, Y., & Hodgson, P. (2011). Nanoscale microstructural characterization of a nanobainitic steel. *Acta Materialia*, *59*, 5511–5522. https://doi.org/10.1016/j.actamat.2011.05.024

[44] Long, X. Y., Zhang, F. C., Kang, J., Lv, B., & Shi, X. B. (2014). Low-temperature bainite in low-carbon steel. *Materials Science and Engineering: A*, *594*, 344–351. https://doi.org/https://doi.org/10.1016/j.msea.2013.11.089

[45] Garcia-Mateo, C., Caballero, F. G., & Bhadeshia, H. K. D. H. (2005). Mechanical Properties of Low-Temperature Bainite. *Materials Science Forum*, *500–501*, 495–502. https://doi.org/10.4028/www.scientific.net/MSF.500-501.495

[46] Soliman, M., & Palkowski, H. (2016). Development of the low temperature bainite. *Archives of Civil and Mechanical Engineering*, *16*(3), 403–412. https://doi.org/https://doi.org/10.1016/j.acme.2016.02.007

[47] Liu, B., Li, W., Lu, X., Jia, X., & Jin, X. (2019). The effect of retained austenite stability on impact-abrasion wear resistance in carbide-free bainitic steels. *Wear*, *428–429*, 127–136. https://doi.org/https://doi.org/10.1016/j.wear.2019.02.032

[48] Chen, J., Lv, M., Tang, S., Liu, Z., & Wang, G. (2015). Correlation between mechanical properties and retained austenite characteristics in a low-carbon medium manganese alloyed steel plate. *Materials Characterization*, *106*, 108–111. https://doi.org/https://doi.org/10.1016/j.matchar.2015.05.026

[49] Wu, R., Li, W., Zhou, S., Zhong, Y., Wang, L., & Jin, X. (2014). Effect of Retained Austenite on the Fracture Toughness of Quenching and Partitioning (Q&P)-Treated Sheet Steels. *Metallurgical and Materials Transactions A*, *45*(4), 1892–1902. https://doi.org/10.1007/s11661-013-2113-0

[50] Sugimoto, K., Sato, S., Kobayashi, J., & Srivastava, A. K. (2019). Effects of Cr and Mo on Mechanical Properties of Hot-Forged Medium Carbon TRIP-Aided Bainitic Ferrite Steels. *Metals*, *9*(10). https://doi.org/10.3390/met9101066

[51] Grajcar, A., Skrzypczyk, P., & Kozłowska, A. (2018). Effects of Temperature and Time of Isothermal Holding on Retained Austenite Stability in Medium-Mn Steels. *Applied Sciences*, *8*(11). https://doi.org/10.3390/app8112156

[52] Girault, E., Mertens, A., Jacques, P., Houbaert, Y., Verlinden, B., & van Humbeeck, J. (2001). Comparison of the effects of silicon and aluminium on the tensile behaviour of multiphase TRIP-assisted steels. *Scripta Materialia*, *44*(6), 885–892. https://doi.org/https://doi.org/10.1016/S1359-6462(00)00697-7

[53] Sugimoto, K., Iida, T., Sakaguchi, J., & Kashima, T. (2000). Retained Austenite Characteristics and Tensile Properties in a TRIP Type Bainitic Sheet Steel. *Isij International - ISIJ INT*, *40*, 902–908. https://doi.org/10.2355/isijinternational.40.902

[54] SUGIMOTO, K., YU, B., MUKAI, Y., & IKEDA, S. (2005). Microstructure and Formability of Aluminum Bearing TRIP-Aided Steels with Annealed Martensite Matrix. *ISIJ International*, *45*(8), 1194–1200. https://doi.org/10.2355/isijinternational.45.1194

[55] Kozłowska, A., Grajcar, A., Janik, A., Radwański, K., Krupp, U., Matus, K., & Morawiec, M. (2021). Mechanical and thermal stability of retained austenite in plastically deformed bainite-based TRIP-aided medium-Mn steels. *Archives of Civil and Mechanical Engineering*, *21*(3), 133. https://doi.org/10.1007/s43452-021-00284-6

[56] de Cooman, B. C. (2004). Structure–properties relationship in TRIP steels containing carbide-free bainite. *Current Opinion in Solid State and Materials Science*, *8*(3), 285–303. https://doi.org/https://doi.org/10.1016/j.cossms.2004.10.002

[57] Hillert, M., Höglund, L., & Ågren, J. (2004). Role of carbon and alloying elements in the formation of bainitic ferrite. *Metallurgical and Materials Transactions A*, *35*(12), 3693–3700. https://doi.org/10.1007/s11661-004-0275-5

[58] Bhadeshia, H. (2009). Nanostructured bainite. *Proceedings of The Royal Society A: Mathematical, Physical and Engineering Sciences*, *466*, 3–18. https://doi.org/10.1098/rspa.2009.0407

[59] Grajcar, A., Kuziak, R., & Zalecki, W. (2012). Third generation of AHSS with increased fraction of retained austenite for the automotive industry. *Archives of Civil and Mechanical Engineering*, *12*(3), 334–341. https://doi.org/https://doi.org/10.1016/j.acme.2012.06.011

[60] Sourmail, T., Garcia-Mateo, C., Caballero, F. G., Cazottes, S., Epicier, T., Danoix, F., & Milbourn, D. (2017). The Influence of Vanadium on Ferrite and Bainite Formation in a Medium Carbon Steel. *Metallurgical and Materials Transactions A*, *48*(9), 3985–3996. https://doi.org/10.1007/s11661-017-4188-5

[61] Garcia-Mateo, C., Morales-Rivas, L., Caballero, F. G., Milbourn, D., & Sourmail, T. (2016). Vanadium Effect on a Medium Carbon Forging Steel. *Metals*, *6*(6). https://doi.org/10.3390/met6060130

[62] Kammouni, A., Saikaly, W., Dumont, M., Marteau, C., Bano, X., & Charaï, A. (2009). Effect of the bainitic transformation temperature on retained austenite fraction and stability in Ti microalloyed TRIP steels. *Materials Science and Engineering A-Structural Materials Properties Microstructure and Processing - MATER SCI ENG A-STRUCT MATER*, *518*, 89–96. https://doi.org/10.1016/j.msea.2009.05.015

[63] Cochrane, R. C. (2012). 6 - Phase transformations in microalloyed high strength low alloy (HSLA) steels. In E. Pereloma & D. v Edmonds (Eds.), *Phase Transformations in Steels* (Vol. 2, pp. 153–212). Woodhead Publishing. https://doi.org/https://doi.org/10.1533/9780857096111.2.153

[64] Liu, W., Liang, J., Jiang, Y., Zhang, B., & Zhao, A. (2019). A study of blocky retained austenite and properties under variously heat-treated ultra-fine bainitic steel. *Materials Research Express*, *6*(10), 105607. https://doi.org/10.1088/2053-1591/ab3937

[65] Lee, Y. K., Shin, H. C., Jang, Y. C., Kim, S. H., & Choi, C. S. (2002). Effect of isothermal transformation temperature on amount of retained austenite and its thermal stability in a bainitic Fe–3%Si–0.45%C–X steel. *Scripta Materialia*, *47*(12), 805–809. https://doi.org/https://doi.org/10.1016/S1359-6462(02)00303-2

[66] Sugimoto, K., Tsunezawa, M., Hojo, T., & Ikeda, S. (2004). Ductility of 0.1-0.6C-1.5Si1.5Mn Ultra High-strength TRIP-aided Sheet Steels with Bainitic Ferrite Matrix. *Isij International - ISIJ INT*, *44*, 1608–1614. https://doi.org/10.2355/isijinternational.44.1608

[67] Saleh, M. H., & Priestner, R. (2001). Retained austenite in dual-phase silicon steels and its effect on mechanical properties. *Journal of Materials Processing Technology*, *113*(1), 587–593. https://doi.org/https://doi.org/10.1016/S0924-0136(01)00638-0

[68] Wang, Z., Hui, W., Chen, Z., Zhang, Y., & Zhao, X. (2020). Effect of vanadium on microstructure and mechanical properties of bainitic forging steel. *Materials Science and Engineering: A*, *771*, 138653. https://doi.org/https://doi.org/10.1016/j.msea.2019.138653

[69] Park, J. S., & Lee, Y. K. (2007). Nb(C,N) precipitation kinetics in the bainite region of a low-carbon Nb-microalloyed steel. *Scripta Materialia*, *57*(2), 109–112. https://doi.org/https://doi.org/10.1016/j.scriptamat.2007.03.041

[70] Xie, Z. J., Liu, Z. F., Misra, R. D. K., Shang, C. J., Han, G., & Wang, X. L. (2019). Retained austenite stabilisation in low carbon high silicon steel during isothermal holding. *Materials Science and Technology*, *35*(1), 45–54. https://doi.org/10.1080/02670836.2018.1537224

[71] Grajcar, A., & Krztoń, H. (2011). Effect of isothermal holding temperature on retained austenite fraction in medium-carbon Nb/Ti-microalloyed TRIP steel. *Journal of Achievements in Materials and Manufacturing Engineering*, *49*, 391–399.

[72] Yu, H., Cai, Z., Ryom, K., Fu, G., & Zhu, M. (2019). Behavior of V-Ti Elements in Warm-Rolled Transformation-Induced Plasticity Steel with Medium Manganese Content. *ISIJ International*, *60*. https://doi.org/10.2355/isijinternational.ISIJINT-2019-329

[73] Ceschini, L., Marconi, A., Martini, C., Morri, A., & di Schino, A. (2013). Tensile and impact behaviour of a microalloyed medium carbon steel: Effect of the cooling condition and corresponding microstructure. *Materials & Design*, *45*, 171–178. https://doi.org/https://doi.org/10.1016/j.matdes.2012.08.063

[74] Zhao, X., Han, L., Li, C., & Gu, J. (2019). The effect of preexisting VC carbides on the bainite transformation in medium-carbon high-alloy steel. *Journal of Materials Research*, *34*(15), 2695–2704. https://doi.org/DOI: 10.1557/jmr.2019.14

[75] Xu, Z., Hui, W., Wang, Z., Zhang, Y., Zhao, X., & Zhao, X. (2017). Mechanical properties of a microalloyed bainitic steel after hot forging and tempering. *Journal of Iron and Steel Research, International*, *24*, 1085–1094. https://doi.org/10.1016/S1006-706X(17)30158-9

[76] Zhao, F., He, G., Liu, Y., Zhang, Z., & Xie, J. (2022). Effect of titanium microalloying on microstructure and mechanical properties of vanadium microalloyed steels for hot forging. *Journal of Iron and Steel Research International*, *29*(2), 295–306. https://doi.org/10.1007/s42243-021-00629-8

[77] ASTM Standard E3-11 Standard Guide for Preparation of Metallographic Specimens (2017). https://doi.org/10.1520/E0003-11R17

[78] ASTM Standard E975-13 Standard Practice for X-Ray Determination of Retained Austenite in Steel with Near Random Crystallographic Orientation (2013). https://doi.org/10.1520/E0975-13

[79] Toby, B. H., & Von Dreele, R. B. (2013). "GSAS-II: the genesis of a modern open-source all purpose crystallography software package". Journal of Applied Crystallography, 46(2), 544-549. doi:10.1107/S0021889813003531

[80] ASTM Standard E92-17 Standard Test Methods for Vickers Hardness and Knoop Hardness of Metallic Materials (2017). https://doi.org/10.1520/E0092-17

[81] ASTM Standard E8/E8M − 21 Standard Test Methods for Tension Testing of Metallic Materials (2021). https://doi.org/10.1520/E0008_E0008M-21

[82] Kohlhaas, R., Dunner, P., Schmits-Pranghe, N. Z. Angew. Phys. 23, 245 (1967)